

**A theoretical study of formation of clusters at nanoscale
using reaction-diffusion models in one and two dimensions**

By

TRILOCHAN BAGARTI

PHYS07200604031

Institute of Physics, Bhubaneswar

*A thesis submitted to the
Board of Studies in Physical Sciences*

*In partial fulfillment of requirements
For the Degree of*

**DOCTOR OF PHILOSOPHY
of**

HOMI BHABHA NATIONAL INSTITUTE



June, 2013

STATEMENT BY AUTHOR

This dissertation has been submitted in partial fulfillment of requirements for an advanced degree at Homi Bhabha National Institute (HBNI) and is deposited in the Library to be made available to borrowers under rules of the HBNI.

Brief quotations from this dissertation are allowable without special permission, provided that accurate acknowledgment of source is made. Requests for permission for extended quotation from or reproduction of this manuscript in whole or in part may be granted by the Competent Authority of HBNI when in his or her judgment the proposed use of the material is in the interests of scholarship. In all other instances, however, permission must be obtained from the author.

Trilochan Bagarti

DECLARATION

I, hereby declare that the investigation presented in the thesis has been carried out by me. The work is original and has not been submitted earlier as a whole or in part for a degree/diploma at this or any other Institution/University.

Trilochan Bagarti

Acknowledgments

I take this opportunity to thank my supervisor Prof. Kalyan Kundu for his guidance and continuous support during all these long years. I also thank him for giving me enormous freedom to carry out my research.

I am indebted to all my teachers for all I could learn from them and for all the inspiration they have given.

I sincerely thank my collaborators Prof. B.N. Dev and his group at IACS, Kolkata and Dr. Anupam Roy for the work we did together. I thank Prof. P. V. Satyam and his group and specially thank Dr. J. K. Dash for the work we had done together. I wish to thank Prof. T. P. Pareek for introducing me to a number of interesting problems during my visit to HRI, Allahabad. His encouragement and support has been invaluable.

I would like to express my sincere gratitude to my teacher and friend Prof. A. M. Jayannavar for all the time we have spent together not only for discussing physics but also for all the ordinary discussions that has enriched me both intellectually and spiritually. I would also like to thank Mrs. Maya Jayannavar for being so kind to me and sharing with me a world of numerous unforgettable stories which will remain forever in my memory.

I thank all my friends for their continuous support and encouragement during all these years. I'm grateful to my dearest friends Saumia P. S., Sourbh Lahiri, Ambaresh Shivaji, Jim Chacko, Subhashis Rana, Sankhadeep Chakrabarty, Ranjita Mohapatra, Ritu Sharma and Anurag Sahay for being so close to me all the time and for the time we have spent in IOP together; the memory of which I will cherish for many years to come.

I thank my friends Manoj Kashyap, Harshad Khaladkar and Vinit Kulkarni who despite being so far away has given me their continuous encouragement and support.

I wish to thank my childhood friend Omkar Pattnaik, Aftab Alam and Dinabandhu Bagarty for their kind help and support during all these years.

I wish to thank my parents, my brothers Laxmikant and Abinash and sister Varsha for all their patience and love. It would have been impossible to complete this work without their support. I would like to specially thank Dinabandhu and his family for their love and support.

Finally, I thank members of IOP for all their cooperation.

Trilochan Bagarti

List of publications

1. Patterns in Ge cluster growth on clean and oxidized Si(111)-(7×7) surfaces
Anupam Roy, Trilochan Bagarti, K. Bhattacharjee, K. Kundu, B.N.Dev,
Surf. Sci. 606, 777 (2012).
2. A reaction diffusion model of pattern formation in clustering of adatoms on silicon surfaces
Trilochan Bagarti, Anupam Roy, K. Kundu, B.N. Dev,
AIP Advances **2**, 042101 (2012).
3. The effect of exclusion on nonlinear reaction diffusion system in inhomogeneous media
Trilochan Bagarti, Anupam Roy, K. Kundu and B. N. Dev,
(to be submitted)
4. Universality in shape evolution of $\text{Si}_{1-x}\text{Ge}_x$ structures on high index Silicon surfaces
J. K. Dash, T. Bagarti, A. Rath, R. R. Juluri and P. V. Satyam,
EPL **99** 66004 (2012).¹

¹This thesis is based on (1-3).

Contents

Table of Contents	vi
Synopsis	viii
1 Introduction to pattern formation and reaction-diffusion systems with disorder	1
1.1 Introduction	1
1.1.1 Experimental motivation	2
1.2 Pattern formation in nature	5
1.3 Pattern formation in reaction-diffusion systems	7
1.4 Reaction-diffusion systems in disordered media	8
1.4.1 Trapping reaction-diffusion process: Green's function methods	13
1.4.2 Perfect traps and the law of stretched-exponential	20
1.5 The concept of the first passage time	22
1.6 Summary	24
1.7 Plan of the thesis	25
2 Reaction diffusion model for the formation of clusters on a surface with defects	26
2.1 Introduction	26
2.2 Formulation of the model	27
2.2.1 The ring model	29
2.2.2 The point model	31
2.3 Asymptotic large time limit	33
2.4 Simulations and numerical results	33
3 The effect of exclusion on nonlinear reaction-diffusion system with disorder	39
3.1 Introduction	39
3.2 Theoretical model	41

3.3	Trapping reaction with self-exclusion	47
3.3.1	Survival probability	48
3.4	Numerical results	51
4	Conclusion	55
A	Green's function	57
A.1	Green's functions-I	57
A.2	Green's functions-II	57
B	The Talbot Method	59
C	Derivation of the kinetic equations	61
C.1	Kinetic equation for linear model	61
C.2	Kinetic equations for nonlinear model	62
D	Derivation of exclusion term from master equation	64
E	Monte Carlo Algorithm	66
E.1	Stochastic simulation algorithm based on Smoluchowski equation:	66
F	Numerical Codes	68
F.1	Numerical solution of the trapping problem	68
F.2	Numerical solution of the ring defect model	70
F.3	Numerical solution of the point defect model	72
	Bibliography	74

Synopsis

Pattern formation at nanoscale is currently an active field of research. It is important for a growing number of technological applications such as fabrication of nano-devices, designing of materials with desired electrical, optical and mechanical properties [1]. Nanopatterning on surfaces can be achieved by many ways, for example by self-organization and artificially by direct atom manipulation, to name a few [2–4]. It is also important from a theoretical point of view as it presents a considerable amount of challenge for a theoretical understanding of the processes at nanoscale. In the pattern formation at nanoscales, it is experimentally found that clusters are formed and are distributed on the surface, leading to interesting types of nanopatterns. So, it is important to model and study theoretically cluster formation and its dynamics over a time period.

The surface plays a very crucial role in deciding the properties of the nanostructure. It has been observed that preferential nucleation of self-organized nanostructures takes place on the surface along step edges [5, 6], dislocations [7–10] and domain boundaries [11, 12]. We have proposed a two dimensional reaction-diffusion mechanism for the formation of clusters in the presence of surface defects such as point defects, ring defects and extended island like defects [13]. But, the model is general enough to implement in arbitrary dimensions.

Reaction-diffusion models have been used to model pattern formation in physics, chemistry and biology [14]. In a seminal paper by Alan Turing, it was shown for the first time that, a variety of pattern can emerge from a spatially homogeneous state due to diffusion driven instabilities [15]. This instability, called the Turing instability, was originally proposed to explain morphogenesis. Reaction-diffusion models in disordered media have been studied extensively in the past [16] for various physical and chemical processes. Disordered media has been modeled through fractals, percolation clusters, hierarchical lattice or quenched disorder. Various aspects of reaction-diffusion processes in disordered media such as self-segregation of diffusing particles [17, 18], long time behavior of the decay of particle density [19–21], the kinetics of diffusion limited coalescence and annihilation in random media [22–25], have been studied. Recently, the effect of quenched disorder and internal noise on the transport properties in a reaction-diffusion model has been studied for the 'birth-death' process in a real world situation [26]. Reaction-diffusion in disordered systems is also used to model the decay and preservation of marine organic carbon [27]. It is generally found that reaction-diffusion processes in

random media show anomalous behavior [28].

In this thesis we present a theoretical study of reaction-diffusion models in the presence of disorder. The motivation of this work comes from experiments in which Ge is deposited on Si surfaces. From the experiments it was found that clusters were preferentially formed at the locations of surface defects on Si surfaces [13]. Through these reaction-diffusion models the growth process of Ge clusters on Si surfaces are studied. It is found that patterns formed are qualitatively similar to those observed in the experiments. So, we establish through this work that these patterns are primarily induced by surface defects and domain boundaries.

In the first part of the thesis we study the cluster formation by linear reaction-diffusion model. The cluster formation process is approximated by a first order reaction of the form $S \rightleftharpoons P$. Here S denotes the deposited Ge ad-atom and P denotes the Ge-cluster. This simplified reaction scheme arises, due to the fact that we do not distinguish between different sizes of clusters as different species of product. The origin of the assumption is as follows. Since the diffusion coefficients of these clusters are almost same, we therefore denote all clusters by a single species P . The surface defects are assumed as isolated regions on the Si surface where the reactions take place. However, away from the defects there is only diffusion and no reactions can occur. Diffusion takes place on the surface with constant diffusion coefficients. The coupled reaction-diffusion equations are solved by Green's functions and regular perturbation technique in the abstract vector space [29,30]. In this case, the natural vector space is a Hilbert space [31]. It is to be noted that when the problem is cast with respect to its natural Hilbert space, remarkable similarities with related quantum mechanical scattering processes are nicely revealed [30].

It can be shown that for N_d surface defects the coupled reaction-diffusion equations in the Laplace domain forms a set of $2N_d$ linear equations. Solving $2N_d$ linear equations gives the solution at each defect position. Furthermore, the solution at an arbitrary position can then be expressed as a linear combination of the all the solutions at defect positions. We have obtained the concentrations by implementing Talbot method for numerical inverse Laplace transformation [32]. From our numerical calculations we have found that clusters start emerging at the location of the surface defects and grows with time. In the long time limit the profile becomes flat as more Ge is deposited. This is also true in the experimental case. We have explored numerically the sizes of these cluster as a function of the reaction rates and the diffusion constants. Furthermore, we have studied the cluster formation in the presence of large number of

defects by Monte Carlo simulations. The first passage time statistics is studied and we have obtained empirically the first passage time probability density.

In the second part of the thesis we consider the formation of cluster in the presence of exclusion. The origin of exclusion is related to non-bonding interactions between the particles. In any volume element only a finite number of particles can be accommodated. So, when the number of cluster particles in the volume element increases, adatoms and/or cluster particles repel one another. This in turn, prevents packing of uncountable number of particles in a given volume. The non-bonding interaction is an effective force of repulsive nature between the diffusing particles. Diffusion coefficients of the reacting species are determined experimentally. In the reaction-diffusion equations, adatom-adatom and cluster-cluster exclusion effect are absorbed in the mean field way in their diffusion coefficients respectively. So, in the zeroth order approximation this self exclusion contribution can be assumed to be negligible. The adatom-cluster exclusion is incorporated into the reaction-diffusion equations through a repelling force proportional to the gradient of the concentrations. This type of approach has been taken to understand chemotaxis in biological problems [33, 34].

It is found that the exclusion terms can be derived from the microscopic principle using master equation. Nonlinear term appears in the reaction-diffusion equations which consists of coupling of the concentration of one species with the gradient of the other species. We assume that the medium is inhomogeneous and consists of point defects. For the cluster formation in the vicinity of a surface defects, we further consider an algebraic nonlinear reaction process in which η number of adatoms react to form a cluster.

Clearly the problem becomes too difficult to be tractable analytically. However, in the limit when exclusion effect is weak we find a linearized reaction-diffusion equation. The linear equation gives us very important insight into the process. We find that due to the presence of exclusion an extra drift term appears in the reaction-diffusion equations. For the adatoms the drift velocity is outward from the location of the point defect where as for the cluster particles it is directed into the defect site. Furthermore, it also breaks the symmetry of the reaction terms by effectively modifying the reaction rates. These linearized equations are solved in the Laplace domain using the Green's function method. The solution is obtained by Talbot numerical inverse Laplace transform. Numerical investigation using finite difference methods is further conducted in one and two dimensions for varying exclusion strength ϵ and nonlinearity η . From our numerics, we confirm that, the predictions of the modified linear equations

qualitatively agrees with the original equations. The width of the cluster concentration profile is found to be decreasing with increasing exclusion strength and decreasing nonlinearity. In two dimension it is found that the mean concentration decreases with nonlinearity and exclusion. The most interesting conclusion that we can draw from this model is that, exclusion and algebraic nonlinearity both suppress the formation of clusters.

We have further studied the effect of self-exclusion in reaction-diffusion process. In this model we consider a single static trap (T) at the origin where a diffusing adatom (S) get adsorbed at a constant rate i.e. $S + T \rightarrow T$. Self-exclusion however has the opposite effect on the reaction-diffusion process as compared to the exclusion of adatoms due to the cluster and vice versa. We note that the self exclusion can also described through a concentration dependent diffusion coefficient. Perturbative solution to the reaction-diffusion is calculated upto second order in reaction rate. It is found that the width of the depletion zone increases and is proportional to exclusion strength ϵ . The concentration at a the trapping site is more as compared to the case when exclusion process is absent.

We finally conclude that reaction-diffusion models in inhomogeneous media can be used successfully to describe the formation of clusters at nanoscales in the presence of surface defects of any topology, step edges and domain boundaries. The surface defects are modeled as reaction centers in the reaction-diffusion model having various topologies. We find that models considered, albeit minimal in nature, are quite good in explaining qualitatively the formation of clusters. In the nonlinear model we have investigated the effect of exclusion and nonlinearity in the cluster formation process. We draw the most important conclusion that exclusion and nonlinearity both have a suppressing effect in the formation of clusters.

Chapter 1

Introduction to pattern formation and reaction-diffusion systems with disorder

1.1 Introduction

Since ancient times pattern formation in nature has been a great source of curiosity and fascination to mankind mostly due to their aesthetic values. Everything that we see around us possesses some kind of pattern. A beautiful pattern that can be observed in objects like snowflakes, crystal structure, hexagonal convection cells, pattern on the wings of a butterfly, sunflower, etc is usually identified by a high degree of symmetry. These beautiful structure are mostly ordered geometrical objects or fractal structure with certain symmetries. However, there are other patterns in nature which are equally fascinating but, which appears not so beautiful. These patterns are mostly random patterns with no specific order or length scales. Some common examples of random patterns are turbulence, diffusion limited aggregation clusters, fracture, percolation, etc. When we look at these patterns we can observe that nature repeats certain kind of similarities in a large number of seemingly unrelated patterns. It may also happen that similar kinds of pattern found at widely separated length scales have a common mechanism by which they are formed.

At nanoscales a large variety of pattern can be seen. In a number of cases formation of pattern at nanoscale can also be modeled by the same equations that describe macroscopic pattern formation. In the following we shall discuss the experimental motivation of the present work on cluster formation at nanoscale.

1.1.1 Experimental motivation

In the recent years there has been a tremendous amount of research devoted to understand physics at nanoscale. The formation of patterns at nanoscale has been studied extensively. Patterns at nanoscale is achieved both by self-organization [1–3] as well as artificially [4]. Self-organized alignment of island has been studied by a number of author [6, 11, 35, 36]. It has been found that the variation of strain field over the surface has significant effect on surface diffusion and nucleation of islands [7]. Also the presence of disorder on the surface plays a very important role in the formation of the nanopattern. Self-organized nanostructures is observed to favor nucleation along step edges [6, 13, 37, 38], dislocations [7, 39–41] or domain boundaries [11, 13, 42].

Epitaxial growth of Ge on a clean, defect-free Si surfaces, proceeds through the completion of a wetting layer, grown in the layer-by-layer mode [43] via either 2D island nucleation or step flow [44–46]. However, in the presence of defects such as domain boundaries, Ge adatoms deposited on the surface follow the preferential nucleation and growth at domain boundaries [13].

Various types of defects are formed on Si(111)-(7×7) surface [11, 47–55]. From our experiments we have observed the presence of bilayer steps and terraces with domain boundaries formed on clean Si(111)-(7×7) surface. Growth processes on these surfaces are strongly influenced by the presence these defects. In Fig. (1.1)(a) we can see a $1000 \times 1000 \text{ nm}^2$ area which shows bilayer steps along the vertical direction (dashed line) and terraces with domain boundaries along the horizontal direction (solid line) on the clean Si(111)-(7×7) surface. These defect may have been formed due to a short annealing period or from the presence of contaminants on the surface [50]. Irregularity in these structures makes it difficult to understand these defects [53]. The strong interaction between dimer and adatoms, changed electronic configuration between faulted and unfaulted halves of the unit cells and other metastable triangular subunits (i.e. 5×5 unit cell) play a key role in the formation of these structures. We have observed that a prolonged flash (~ 5 min) at $\sim 1200^\circ\text{C}$ followed by controlled cooling to room temperature produces such domains.

In Fig. (1.1)(b) we can see a high resolution STM image which shows the atomic arrangements of 7×7 surface reconstruction. *Furthermore, due to missing atoms at isolated points from the surface layer, defects are formed at random positions.* The height profiles are shown

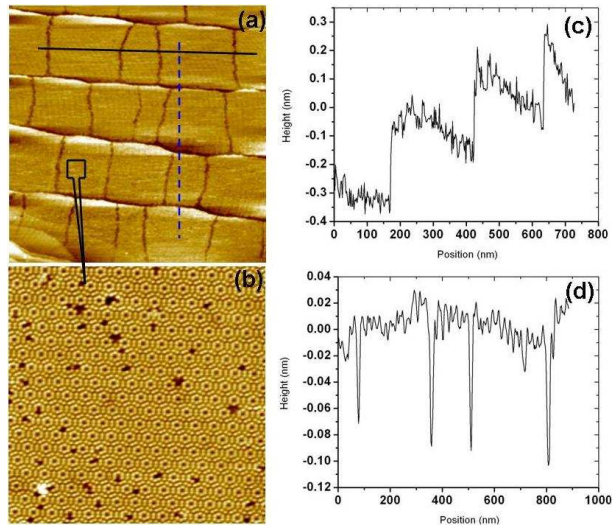


Figure 1.1: STM images of Si(111)-(7 \times 7) surface: (a) steps and domain boundaries on terraces are seen (scan area 1000 \times 1000 nm², bias voltage -2 V, tunneling current 0.18 nA), (b) a high resolution STM image (scan area 40 \times 40 nm², bias voltage 2.3 V, tunneling current 0.19 nA) - a part of the image in (a) - shows (7 \times 7) surface reconstruction. The depth of the dark regions and the height of the bright spot in (b) are ~ 0.1 nm. Height profiles from the image in (a) are shown - (c) along the vertical dashed line and (d) along the horizontal line. The step heights [seen in (c)] correspond to a bilayer height (0.31 nm) or a (111) planar spacing.

in Fig. (1.1)(c) and (d). A height scan across the step edges show that the steps are bilayer steps Fig. (1.1)(c). A scan on the terrace shows that the domain boundaries are trenches of depth ~ 0.1 nm and width ~ 0.2 nm. The domain boundaries appear almost straight and perpendicular to the terrace.

From the deposition of Ge on these surfaces we observed that Ge adatoms nucleate first at the domain boundaries and the step edges and subsequently on the flat terraces. Similar growth processes has been reported earlier by a number of authors [6, 11, 56]. Sgarlata et. al. have shown that, after formation of wetting layer, the Ge islands grow preferentially along the step edges [6]. In our experiment we have found that preferential growth of Ge within the wetting layer (0.5 bilayer). Similar growth processes have also been reported [57, 58]. *In Fig. (1.2) we see a dense decoration of domain boundaries with Ge islands and smaller density of islands within the domains.* Due to the missing adatoms at the domain boundaries, a large number of broken bonds are present there. The adsorption of Ge adatoms reduces the number of broken bonds which is thermodynamically favorable as it lowers the free energy of the system. The stability of the structure has been tested experimentally by annealing the sample for 30 min at the same temperature. Once the Ge clusters are formed, the cluster diffusion would be

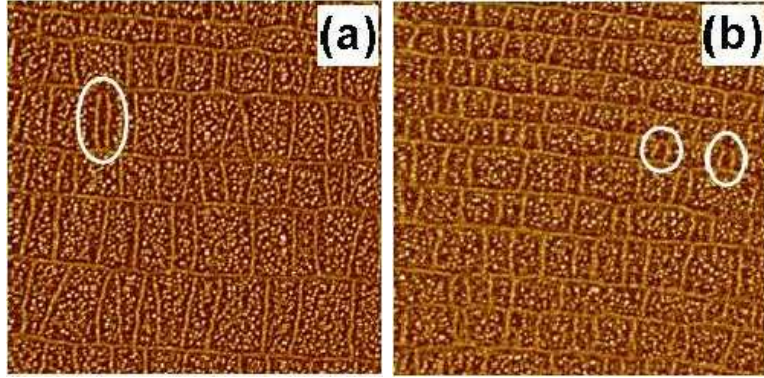


Figure 1.2: STM images (bias voltage 2.2 V and tunneling current 0.2 nA) from a 0.5 BL Ge grown a Si(111)-(7×7) surface at elevated substrate temperature ($\sim 550^\circ\text{C}$) showing pattern formation: (a) scan area $2500 \times 2500 \text{ nm}^2$ (b) scan area $2000 \times 2000 \text{ nm}^2$ at different positions on the surface. Three denuded regions are marked in (a) and (b). Ge clustering is dominant at domain boundaries and step edges.

negligible compared to adatom diffusion. Smallest domain has Ge cluster only at the step edges and domain boundaries, the domains themselves are denuded (marked by circles in Fig. (1.2)). The largest such domain is $\sim 80\text{nm}$ which gives an estimate of the effective diffusion length. Diffusion lengths of the same order has been observed in Ref. [11] (90 nm) and [58] (70 nm).

We propose a reaction-diffusion model of cluster formation observed in these experiments. We assume that clusters are formed in localized areas where the defects are located. Since the structure appears first at the domain boundaries and the step edges, it indicates that the reaction rate at the boundary is higher from the rate at the defects inside the domains.

In the following section we present a brief review of some of the key concepts and some important results in pattern formation. The theory of pattern formation in reaction-diffusion systems is discussed in Sec. 1.3. Here we will discuss the Turing mechanism of pattern formation. In Sec. 1.4 we review reaction-diffusion processes in disordered media. We will discuss using a simple example of trapping reaction-diffusion problem how anomalous behavior arises due to the presence of disorder. Through this example we shall also illustrate the mathematical techniques we shall be using in studying our reaction-diffusion models. The law of stretched exponential is re-derived. The plan of the thesis is discussed in Sec. 1.7.

1.2 Pattern formation in nature

The study of pattern formation is a vast subject that has grown out of centuries of human inquiry. A mathematical understanding of some aspects of pattern formation had been achieved only in the recent times. The key ingredient necessary for the emergence of pattern from a uniform structureless state is “instability” that leads to a spontaneous breaking of symmetry. Instability sets in when a system is driven away from equilibrium and various types of pattern can be categorized according to the instabilities [14]. The earliest studies were performed on fluid mechanical systems. In 1900 Benard demonstrated successfully that a layer of liquid between two flat plates when heated from below evolves into an unstable state of convective roll patterns. Rayleigh later showed that the onset of these convective rolls depends on a dimensionless number R which is the ratio between the buoyancy force and the viscous force. This number R is called the Rayleigh number. He showed that when R exceeds a critical value $R_c \simeq 1708$, instability sets in. This number is universal to different fluids used in the experiment. From the conducting state the fluid evolves into stationary hexagonal cell pattern which further bifurcate into convective roll patterns [59]. The roll pattern is the only pattern predicted by the Bossinesq approximation. Hexagonal cells pattern is a consequence of non-Bossinesq approximation. It has been reported that there is a possibility that during the transition from the hexagonal to the convective roll state the fluid has a tendency to spontaneously form rotating spiral state [60]. Furthermore, it has been found that roll pattern evolves into “target” patterns that arises due to the defect core instability mechanism [61]. Transition from a many “target” to spiral state and target to spiral turbulence has also been observed [62]. Similarly in fluid flow problems there is a transition from laminar to turbulent flow when the dimensionless Reynolds number exceeds a critical value. A complete understanding of turbulence has still not been achieved to this day. Turbulent flow is very common in nature and can be seen everywhere around us. Cumulus clouds, plume of smokestack, flowing water in rivers, wakes of ship etc. are some common examples of turbulence. Although there is no precise definition of turbulence it can be characterized by the irregularity in the flow pattern, diffusivity which causes rapid mixing, very high rate of mass, momentum and heat transport, vorticity fluctuations and dissipation etc [63].

One can see the most beautiful patterns in snowflakes. Snowflakes are found naturally in a wide variety of patterns. They all possess hexagonal symmetry, which arises due to the molec-

ular structure of the water molecule. The snowflakes grow on seed particles in an environment of supersaturated water vapor. The growth takes place with a front moving outward with the seed at the center. It is found that the surface tension at the liquid-solid interface provides the stabilizing force responsible for pattern formation [64]. The boundary condition has to include the effect of curvature in order to form the patterns by anisotropic growth. The ratio of the surface tension at the liquid-solid interface to the latent heat per unit volume provides the length scale of the pattern formation. There are also random crystal growth which produces dendritic structures. The diffusion limited aggregates(DLA) model was introduced by Witten and Sanders to describe the formation of random dendritic-crystal growth [65]. These random aggregates grows from a seed particle forming dendritic branches in all direction in a random fashion. The dynamics involve solving the Laplace equation with moving boundary condition. Random dendritic growth is seen in many cases such as electrodeposition [66, 67], dendritic solidification [68], viscous fingering [69], electric discharge and bacterial colony growth [70] to name a few. It is found that the clusters are scale invariant i.e. there is no natural length scale that can be identified in these objects. The density-density correlation has a power law behavior $\langle \rho(r')\rho(r' + r) \rangle \sim r^{-A}$, where the exponent A is related to the dimension of the space d and Hausdorff dimension D_f by $D_f = d - A$. Instabilities of the Mullins and Sekerka type is attributed to the unstable growth of the clusters [71, 72]. Furthermore Tamas Vicsek had shown that both ordered as well as disordered structure can be generated by assuming that the sticking probability of the particle arriving at the surface depends on the local curvature of the cluster and a particle on the cluster is allowed to relax to a neighboring site [73]. Two dimensional growth of bacterial colony through diffusion-limited process has been observed. It has been found that the bacterial colony resembles the DLA pattern with a fractal dimension $D_f \simeq 1.73$ [70].

Pattern formation in chemical and biological systems is even more complex. Alan Turing in his seminal paper in 1952 proposed that, reaction-diffusion systems consisting of chemical species (*morphogen*) can give rise to pattern formation by diffusion driven instabilities (cf. Sec. 1.3). Latter Gierer and Meinhardt generalized Turing's idea into patterning principle of short-range activation, long-range inhibition or local activation, lateral inhibition [74]. These ideas have been used to explain a large number of pattern formation in biology such as the development of organs in various organism, animal coat patterns etc [75]. We do not wish to pursue going further in this direction as we shall be discussing pattern formation in reaction-

diffusion system in Sec. 1.3.

1.3 Pattern formation in reaction-diffusion systems

A reaction-diffusion system consists of a system of chemical species undergoing a reactions and diffusion process. The reaction-diffusion models can also describe processes other than chemical systems such as population models [75]. The general reaction-diffusion equations for a system of n species in d dimensional space is given by the following

$$\partial_t \mathbf{u} = \hat{\mathcal{L}}\mathbf{u} + \boldsymbol{\rho}(\mathbf{u}, \mathbf{x}, t), \mathbf{x} \in \Omega, t > 0, \quad (1.1a)$$

$$\mathbf{u}(\mathbf{x}, 0) = \mathbf{u}_0(\mathbf{x}), \quad (1.1b)$$

where $\Omega \subset \mathbb{R}^d$ and the boundary conditions are specified on the surface $\partial\Omega$. The vector $\mathbf{u} = (u_1, u_2, \dots, u_n)^T \in \mathbb{R}_+^n$ represents the concentration of the n species, $\hat{\mathcal{L}}$ is a differential operator which describes the diffusive part and $\boldsymbol{\rho}(\mathbf{u}, \mathbf{x}, t) \in \mathbb{R}^n$ is a smooth function which denotes the reaction part. Let the differential operator be of the form $\hat{\mathcal{L}} = \mathbf{D}\partial_{\mathbf{x}}^2$ where \mathbf{D} is a $n \times n$ diffusion matrix and $\partial_{\mathbf{x}}^2 = \sum_{i=1}^d \partial_{x_i}^2$ is the Laplacian operator in d dimension. These n coupled partial differential equation describes the evolution of the reacting species. It is natural to ask, how does the above set of coupled equations generate patterns. The mechanism for the formation of patterns in homogeneous reaction-diffusion system was discovered by A. M. Turing in 1952 [15]. He showed that diffusion driven instabilities can give rise to the formation of a wide variety of patterns. The experimental verification of Turing mechanism was found by Belousov and Zhabotinskii [75]. However, the conditions needed for Turing instability in a general reaction-diffusion system was found only recently [76]. Let us assume that diffusion matrix \mathbf{D} is constant and the reaction term $\boldsymbol{\rho}$ does not depend explicitly on \mathbf{x} and t . Suppose that $\mathbf{u}(t) = \mathbf{u}_s$ is a locally stable homogeneous steady state solution of the kinetic equation

$$\dot{\mathbf{u}}(t) = \boldsymbol{\rho}(\mathbf{u}(t)), \mathbf{u}(0) = \mathbf{u}_0 \quad (1.2)$$

Linearizing around the solution \mathbf{u}_s the Eq. (1.1) can be written as

$$\partial_t \delta \mathbf{u} = \hat{\mathcal{L}}\delta \mathbf{u} + \mathbf{J}(\mathbf{u}_s)\delta \mathbf{u}, \mathbf{x} \in \Omega, t > 0, \quad (1.3)$$

where $\mathbf{u} = \mathbf{u}_s + \delta \mathbf{u}$ and $\mathbf{J}(\mathbf{u}_s) = [\partial_{u_i} \rho_j(\mathbf{u}(t))], i, j = 1, 2, \dots, n$ is the Jacobian matrix. Let $\delta \mathbf{u} \sim \exp(\omega t + i\mathbf{k}\mathbf{x})$, so that the characteristic equation become

$$\det \{ \omega \mathbf{I} + |\mathbf{k}|^2 \mathbf{D} - \mathbf{J} \} = 0 \quad (1.4)$$

If all the roots of Eq. (1.4) have negative real part then Eq. (1.1) is linearly stable. Turing instability sets in when the control parameters are varied and we have a situation when for the first time a single root crosses the imaginary axis while all eigenvalues of \mathbf{J} has negative real parts [77]. The change in control parameters makes the uniform steady state \mathbf{u}_s unstable to perturbations with a nonzero wave number. When ω is zero there are some modes that grow into spatially inhomogeneous steady states giving rise to Turing pattern.

Let us consider the activator-inhibitor model introduced by Turing [15]. We have \mathbf{D} is 2×2 diagonal matrix with components $D_{ij} = \delta_{ij}D_i, i, j = 1, 2$ where D_1 and D_2 are positive constants, $\mathbf{u} = (u_1, u_2)^T$, $\boldsymbol{\rho}(\mathbf{u}(t)) = (f(u_1, u_2), g(u_1, u_2))^T$. The homogeneous steady state solution of the kinetic equation Eq. (1.2) is linearly stable therefore from the linearized equation we should have

$$\begin{aligned} \partial_{u_1}f + \partial_{u_2}g &< 0, \\ \partial_{u_1}f\partial_{u_2}g - \partial_{u_2}f\partial_{u_1}g &> 0. \end{aligned} \quad (1.5)$$

Substituting $\delta\mathbf{u} \sim \exp(\omega t - ikx)$ in Eq. (1.3) we obtain the following dispersion relation

$$\det \begin{pmatrix} \omega + k^2D_1 - \partial_{u_1}f & -\partial_{u_2}f \\ -\partial_{u_1}g & \omega + k^2D_2 - \partial_{u_2}g \end{pmatrix} = 0. \quad (1.6)$$

The solution of the above equation is given by $\omega_{1,2} = (-b \pm \sqrt{b^2 - 4c})/2$ where $b = k^2(D_1 + D_2) - (\partial_{u_1}f + \partial_{u_2}g)$ and $c = (k^2D_1 - \partial_{u_1}f)(k^2D_2 - \partial_{u_2}g) - \partial_{u_2}f\partial_{u_1}g$. Using Eq. (1.5) we see that $b > 0$ for all $k \in \mathbb{R}$. For instability the two roots should have alternate signs. We therefore have $\omega_1\omega_2 < 0$ which results in the following inequality.

$$k^4 - k^2 \left(\frac{\partial_{u_1}f}{D_1} + \frac{\partial_{u_2}g}{D_2} \right) + \frac{\partial_{u_1}f\partial_{u_2}g - \partial_{u_2}f\partial_{u_1}g}{D_1D_2} < 0. \quad (1.7)$$

From Eq. (1.7) we obtain

$$\begin{aligned} \frac{\partial_{u_1}f}{D_1} + \frac{\partial_{u_2}g}{D_2} &> 0, \\ \left(\frac{\partial_{u_1}f}{D_1} + \frac{\partial_{u_2}g}{D_2} \right)^2 - 4 \left(\frac{\partial_{u_1}f\partial_{u_2}g - \partial_{u_2}f\partial_{u_1}g}{D_1D_2} \right) &> 0. \end{aligned} \quad (1.8)$$

The conditions Eq. (1.5) and (1.8) define the Turing space.

1.4 Reaction-diffusion systems in disordered media

It is interesting to study reaction-diffusion processes with disorder because in real systems we always see disorder. The existence of defects and impurities are examples of disorder in

crystals. The occurrence of defects becomes more prominent at higher temperature. There are various kinds of defect in crystals i.e. point defects such as vacancies, interstitials, interstitial impurities; line defects such as dislocations, grain boundaries etc. Disorder in materials is very crucial in determining the electrical, optical and mechanical properties. For example, impurities can be doped into material to increase its tensile strength. The dc conductivity of amorphous germanium show $\sigma(T) \sim \exp(-(T_0/T)^{0.25})$, $T_0 \simeq 7 \times 10^7 K$ due to the tunneling of localized state of electron from one domain to other in the material [78].

Reaction-diffusion processes in disordered media has been studied extensively in the past [16, 28, 79]. In this section we review some of the work on reaction-diffusion models in disordered media and we hope that it will give a general idea of the various interesting properties of these processes. Using a trapping reaction problem we shall be illustrating how we can use the abstract vector space notations and the Green's function methods to formulate the problem in a very elegant way and calculate various quantities.

There are various models of disordered media that has been used to study these diffusion processes. Fractals, percolation cluster, DLA cluster, quenched disorder etc has been used as models of disorder. Random walk on Seirpinski gasket [80] was studied and it was found that it shows anomalous behavior. The mean square displacement is $\langle R_N^2 \rangle \sim N^{2/d_w}$, $d_w \simeq 2.32 \pm 0.01$. The anomalous diffusion-exponent is related to the fractal dimension of the structure. Here we have $d_w = 2 - d + d_f + \tilde{\mu} = \ln(d+3)/\ln 2$ where d is the space dimension on which the structure is embedded and d_f is the fractal dimension. Similarly diffusion on percolation cluster have been studied for various types of lattices. It is known that for a two dimensional square lattice there exist an infinite percolation cluster just above the critical concentration $p = p_c = 0.592745$ (p is the fraction of occupied lattice sites) [16]. The probability P_∞ that a site belongs to the incipient infinite cluster is $P_\infty \sim (p - p_c)^\beta$ for $p > p_c$. For $p < p_c$ the diameter of the cluster is characterized by a correlation length $\xi(p) \sim (p_c - p)^{-\nu}$. The exponents β and ν are universal and depends only on the spatial dimension but not on the type of the lattice. Three characteristic regimes for diffusion on percolation cluster are found. For $p > p_c$ the infinite cluster is homogeneous for length scale greater than the correlation length ($R > \xi(p)$) the diffusion is regular with diffusion exponent $d_w = 2$. At the critical point $p = p_c$ the incipient infinite cluster is self similar and the diffusion is anomalous with $d_w > 2$. For $p < p_c$ the largest cluster has a typical size $\xi(p)$ and we have $\langle R(t)^2 \rangle \sim \xi^2(p)$ for large time [16].

Disorder can also be introduced in diffusion problems even on a regular lattices by introducing a random waiting time in the random walk. A particle performing a random walk on a lattice spends a random waiting time $\tau > 0$ at each site before every hopping [28]. The step lengths could also be a random variable. This type of random walks are called continuous time random walk. The properties of the continuous time random walk depends on the distribution of the random waiting time $\psi(\tau)$. Suppose that the mean of the waiting time $\langle \tau \rangle$ is finite, then we have in the large time limit a normal diffusion with the mean space displacement $\langle X^2 \rangle \sim 2Dt$, where $D = \langle l^2 \rangle / 2\langle \tau \rangle$, l is a random step length and t is the total waiting time. However, if $\psi(\tau)$ is a “broad” distribution such that $\langle \tau \rangle$ is not finite (i.e for $\psi(\tau) \sim \tau_0^\mu \tau^{-(1+\mu)}$, ($\tau \rightarrow \infty$) and $\mu \in (0, 1]$ such that $t \sim \tau_0 N^{1/\mu}$) we find that diffusion is sub-diffusive with

$$\langle X^2 \rangle \sim \begin{cases} \langle l^2 \rangle \left(\frac{t}{\tau_0} \right)^\mu & \text{if } \mu \in (0, 1), \\ \frac{\langle l^2 \rangle t / \tau_0}{\ln(t/\tau_0)} & \text{if } \mu = 1. \end{cases} \quad (1.9)$$

When $\mu \in (1, 2]$ anomalous correction appears with the mean square displacement becoming

$$\langle X^2 \rangle \sim \begin{cases} 2Dt + ct^{1/2} & \text{if } \mu \in (1, 2), \\ 2Dt + ct \ln t & \text{if } \mu = 2, \end{cases}, \quad (1.10)$$

and $\langle X^2 \rangle \sim Dt + ct^{1/2}$ for $\mu > 2$ [28]. In these models the disorder is time varying as the waiting time at a site for different visits can be different. Disorder can also be frozen into the lattice and for all visits by the particle it spends the same random waiting time. This type of disorder do not vary with time and are called quenched disorder. Reaction-diffusion processes in media with quenched disorder has been studied by a number of authors [16–26, 28, 79, 81–83].

Quenched disorder model has been used to study diffusion controlled reaction processes in disordered media. Diffusion on comb like structures where the teeth of the comb act as traps where the particle stay for longer time. With a waiting time distribution $\psi(\tau) \sim \tau^{-3/1}$ (i.e. taken as the first time return to the origin) show anomalous diffusion with $\langle X^2 \rangle \sim t^{1/2}$ [28, 84, 85]. Anomalous diffusion in an array of convective roll could be a possible physical realization of the diffusion on comb like structures [84]. Random barrier models has been studied in which the transition rate are random variable show anomalous properties [82, 83, 86–89]. It has been shown through real-space renormalization group calculations, that one dimensional random walks with static disorder (i.e. disorder in hopping rates and step lengths) leads to a non-Markovian diffusion with generalized diffusion constant $D(t) \sim t^{-3/2}$ as $t \rightarrow \infty$ [90]. In a recent study of diffusion processes in the presence of membranes, it was shown that correlated

spatial disorder gives rise to long term memory effect and through renormalization group technique it was shown that there is a slow decrease of the diffusion constant $D(t) \simeq D_\infty + t^{-1/2}$. The mean square displacement $\langle x^2 \rangle \simeq 2D_\infty t + \text{const.}\sqrt{t}$ [91].

Another class of problem with quenched disorder consists of “the trapping reaction-diffusion” models in which the number of particles is not conserved. These models consists of diffusing particles on a lattice (continuous space) which contains isolated sites (regions) called traps. The traps can be assumed static or mobile which depends on the problem one wish to study. When a diffusing particle (A) arrive at a trap (T) the reaction $A + T \rightarrow (1 - \epsilon)A + T$, $\epsilon \in [0, 1]$ takes place. If $\epsilon < 1$ we know that only a portion of the particle get trapped and we call it a partial trap. When $\epsilon = 1$ we have a perfect trap [92]. The problem of trapping reaction-diffusion processes has been studied for almost a hundred years [93]. Various aspects of trapping reaction-diffusion processes has been studied since then. Reaction occurring at the traps create depletion zones that induces self-segregation of the diffusing particles. This self-segregation affects the global reaction kinetics [18, 19, 94, 95]. Therefore, in diffusion-controlled reaction processes the rate equation solution may not always be accurate. Hence for more realistic situations the kinetic law needs to be modified.

Long time behavior in trapping reaction-diffusion processes show that the survival probability in the asymptotic time limit follow a stretched exponential law for both static [19, 96, 97] and mobile [98–103] traps. For static traps in d dimension distributed randomly with uniformly probability density, the survival probability is given by

$$P(t) \sim \exp(-\alpha_d \rho^{2/(d+2)} t^{d/d+2}), \quad (1.11)$$

where α_d is a constant which depends on the dimensionality of the space, ρ is the trap density. Similarly for the case of mobile traps the survival probability is given by

$$P(t) \sim \begin{cases} \exp(-\alpha_1 \rho t^{1/2}) & d = 1, \\ \exp(-\alpha_2 \rho t / \ln t) & d = 2, \\ \exp(-\alpha_d \rho t) & d = 3, \end{cases} \quad (1.12)$$

where the traps are undergoing normal diffusion and the constants α_d depends also on the diffusion constant of the traps.

So far, we have discussed diffusion phenomena in disordered media which can be categorized according to the type of diffusion. The diffusion processes on fractal structures, percolation cluster, Brownian motion and other processes modeled through random walks are entirely

different from the reaction-diffusion processes modeled through macroscopic equation involving concentrations of the chemical species. The former is the case of “self diffusion” where as the latter is “collective diffusion” [104]. In the random walk models (or Brownian motion) the stochasticity in the dynamics arises due to the thermal fluctuation of the surrounding media (e.g. a pollen grain in water or diffusing impurity atom in a crystal). Here we are concerned with the motion of a single diffusing particle. The probability density of finding the Brownian particle is described by the Fokker-Planck equation. In the over damped limit with no external forces acting on the particle the equation reduces to a simple diffusion equation. The diffusion constant D_s can be expressed through the velocity auto-correlation function.

$$D_s = \frac{1}{Nd} \sum_{i=1}^N \int_0^{\infty} dt \langle \mathbf{v}_i(t) \mathbf{v}_i(0) \rangle \quad (1.13)$$

where N is the total number of particles, $\mathbf{v}_i(t)$ is the velocity of the i -th particle and d dimension of space [105].

Collective diffusion on the other hand takes into account the interaction between particles. A system of particles in equilibrium has a uniform concentration and for a any perturbation from the equilibrium value there is a corresponding current given by the Fick’s first law

$$\mathbf{J}(\mathbf{x}, t) = -D_c \partial_{\mathbf{x}} c(\mathbf{x}, t), \quad (1.14)$$

where D_c is the collective diffusion constant and $c(\mathbf{x}, t)$ is the concentration at position \mathbf{x} at time t . The diffusion constant can be expressed by the total flux correlation function

$$D_c = \frac{1}{Nd} \sum_{i=1}^N \int_0^{\infty} dt \langle \mathbf{J}_T(t) \mathbf{J}_T(0) \rangle, \quad (1.15)$$

where $\mathbf{J}_T(t) = \sum_{i=1}^N \mathbf{v}_i(t)$ in the total velocity flux, $1/S_0$ is the thermodynamic factor which is related to the isothermal compressibility $\chi_T = S_0 / (\langle c \rangle k_B T)$. For surface diffusion it can also be expressed in terms of the derivative of the chemical potential μ . We have $1/S_0 = (k_b T)^{-1} \partial \mu / \partial \log \theta$ where θ is the surface coverage. Although there is no general expression that related D_c to D_s and approximate relationship is given by the so-called Darken equation $D_c = D_s / S_0$ [105].

The two diffusion constants are same for dilute system where density of particle is low. Self-diffusion constant D_s can simply be determined by observing a single Brownian particle under the microscope. It can also be determined by “forced Rayleigh” scattering or neutron

scattering experiment. The collective diffusion constant D_c on the other hand can be determined from the density correlation function using inelastic light scattering techniques [104]. We note here that the effect of particle-particle interaction is already included in the collective diffusion constant D_c when we are concerned only about the diffusion. However, when particles of many species are involved and reactions between different species can give rise to large concentration gradients the interaction between particles of different species has to be introduced by hand. This interaction is the non-bonding interaction between particles which is called volume exclusion (cf. Chapter 3).

1.4.1 Trapping reaction-diffusion process: Green's function methods

In this subsection we will illustrate the use of Green's function in reaction-diffusion equations and formulate the trapping reaction-diffusion problem in an abstract vector space notations. We will obtain the perturbation solution for the partial traps problem. Expressions for the survival probabilities and the anomalous characteristics are re-derived and their implications are discussed.

Let us consider the case of trapping reaction in one dimension. Suppose that, we have traps uniformly distributed on the x-axis with ρ traps per unit length on an average. For all $x_i \in \mathbb{R}, i = 1, 2, \dots$ real numbers, the set $\mathbb{S} = \{x_1, x_2, \dots, x_k, \dots\}$ denote the positions of the trapping sites on the x-axis. The reaction-diffusion equation is given by

$$\begin{aligned} \partial_t u(x, t) &= D \partial_x^2 u(x, t) - \kappa \sum_{x_i \in \mathbb{S}} \delta(x - x_i) u(x, t), \quad x \in \mathbb{R}, t > 0, \\ u(x, 0) &= f(x), \end{aligned} \quad (1.16)$$

where D is the diffusion coefficient and $\kappa > 0$ is the trapping rate. Taking Laplace transform of Eq. (1.16) we obtain

$$(s - D \partial_x^2 - K(x)) \tilde{u}(x, s) = f(x), \quad x \in \mathbb{R}, \quad (1.17)$$

where $K(x) = -\kappa \sum_{x_i \in \mathbb{S}} \delta(x - x_i)$ and $\tilde{u}(x, s)$ is the Laplace transform of the density $u(x, t)$. We can use the Green's function method to solve Eq. (1.17). The Green's function $G(x|x')$ is defined by

$$(s - D \partial_x^2 - K(x)) G(x|x') = \delta(x - x'), \quad (1.18)$$

with $G(x|x')$ satisfying the same boundary conditions.

We cast the problem in an abstract vector space [30]. Let $\hat{L}(x)$ be a hermitian differential operator. There is a complete set of eigenfunctions $\{\tilde{u}_n(x)\}$ such that

$$\hat{L}(x)\tilde{u}_n(x) = \lambda_n\tilde{u}_n(x), \quad x \in \Omega. \quad (1.19)$$

subject to boundary conditions on $\partial\Omega$. The set $\{\tilde{u}_n(x)\}$ can be assumed orthonormal. We can use the Dirac's bra and ket notation so that we have

$$\tilde{u}_n(x) = \langle x|\tilde{u}_n\rangle, \quad \tilde{u}_n^*(x) = \langle \tilde{u}_n|x\rangle, \quad (1.20a)$$

$$\delta(x-x')\hat{L}(x) = \langle x|\hat{L}|x'\rangle, \quad (1.20b)$$

$$\langle x|x'\rangle = \delta(x-x'), \quad (1.20c)$$

$$\int dx|x\rangle\langle x| = \mathbf{1}, \quad (1.20d)$$

where $|x\rangle$ is the eigenvector of the position operator. The eigenvalue equation in Eq. (1.19) becomes

$$\hat{L}|\hat{u}_n\rangle = \lambda_n|\hat{u}_n\rangle. \quad (1.21)$$

Orthonormality and the completeness conditions are given by

$$\langle \tilde{u}_n|\tilde{u}_m\rangle = \delta_{n,m}, \quad (1.22a)$$

$$\sum_n |\tilde{u}_n\rangle\langle \tilde{u}_n| = \mathbf{1} \quad (1.22b)$$

respectively. The above Eq. (1.17) and Eq. (1.18) can be rewritten in abstract notation as the following

$$(s - D\partial_x^2 - \hat{K})|\tilde{u}\rangle = |f\rangle \quad (1.23)$$

$$(s - D\partial_x^2 - \hat{K})\hat{G} = \mathbf{1}, \quad (1.24a)$$

$$\text{or } \hat{G} = (s - D\partial_x^2 - \hat{K})^{-1}, \quad (1.24b)$$

where $\langle x|\tilde{u}\rangle = \tilde{u}(x)$, $\langle x|f\rangle = f(x)$, $\langle x|(s - D\partial_x^2 - \hat{K})|\tilde{u}\rangle = (s - D\partial_x^2 - K(x))\tilde{u}(x)$ and $\langle x'|\hat{G}|x\rangle = G(x'|x)$. In the abstract notation the reaction term $K(x)$ becomes the reaction operator $\hat{K} = -\kappa \sum_{x_i \in \mathbb{S}} |x_i\rangle\langle x_i|$. From Eq. (1.23) the solution can be written in terms of the Green's function as $\tilde{u}(x, s) = \langle x|\tilde{u}\rangle = \langle x|\hat{G}|f\rangle$. The calculation of Green's function $G(x|x')$

$$\begin{aligned}
\Rightarrow &= \longrightarrow + \sum_i \overset{\bullet}{\longrightarrow} + \sum_{i,j} \overset{\bullet}{\longrightarrow} \overset{\bullet}{\longrightarrow} \\
\Rightarrow &= G(x|x'), \quad \bullet = -\kappa, \\
\longrightarrow &= G^{(0)}(x|x'),
\end{aligned}$$

Figure 1.3: Feynman diagrams for Eq. (1.26).

should give the solution for any given initial condition $f(x)$. Consider the expression in Eq. (1.24b)

$$\begin{aligned}
\hat{G} &= (s - D\partial_x^2 - \hat{K})^{-1}, \\
&= \left[(s - D\partial_x^2)(\mathbf{1} - (s - D\partial_x^2)^{-1}\hat{K}) \right]^{-1}, \\
&= (\mathbf{1} - (s - D\partial_x^2)^{-1}\hat{K})^{-1}(s - D\partial_x^2)^{-1}, \\
&= (\mathbf{1} - \hat{G}^{(0)}\hat{K})^{-1}\hat{G}^{(0)}, \\
&= \hat{G}^{(0)} + \hat{G}^{(0)}\hat{K}\hat{G}^{(0)} + \hat{G}^{(0)}\hat{K}\hat{G}^{(0)}\hat{K}\hat{G}^{(0)} + \dots,
\end{aligned} \tag{1.25}$$

where $\hat{G}^{(0)} = (s - D\partial_x^2)^{-1}$ is the bare Green's function. Eq. (1.25) can also be written as

$$\begin{aligned}
\langle x | \hat{G} | x' \rangle &= \langle x | (\hat{G}^{(0)} + \hat{G}^{(0)}\hat{K}\hat{G}^{(0)} + \hat{G}^{(0)}\hat{K}\hat{G}^{(0)}\hat{K}\hat{G}^{(0)} + \dots) | x' \rangle, \\
\text{or } G(x|x') &= G^{(0)}(x|x') - \kappa \sum_{x_i \in \mathbb{S}} G^{(0)}(x|x_i)G^{(0)}(x_i|x') \\
&\quad + \kappa^2 \sum_{x_i, x_j \in \mathbb{S}} G^{(0)}(x|x_i)G^{(0)}(x_i|x_j)G^{(0)}(x_j|x') + \dots,
\end{aligned} \tag{1.26}$$

The expression Eq. (1.26) is represented by Feynman diagrams in Fig. (1.3) Rearranging the terms in the right hand side of Eq. (1.25) gives

$$\hat{G} = \hat{G}^{(0)} + \hat{G}\hat{K}\hat{G}^{(0)} = \hat{G}^{(0)} + \hat{G}^{(0)}\hat{K}\hat{G}. \tag{1.27}$$

The last equation Eq. (1.27) is called the Dyson equation. From Eq. (1.25) we obtain the following solution

$$\begin{aligned}
\tilde{u}(x, s) &= \langle x | \hat{G} | f \rangle \\
&= \langle x | (\hat{G}^{(0)} + \hat{G}^{(0)}\hat{K}\hat{G}^{(0)} + \hat{G}^{(0)}\hat{K}\hat{G}^{(0)}\hat{K}\hat{G}^{(0)} + \dots) | f \rangle,
\end{aligned} \tag{1.28}$$

Suppose that we have $f(x) = \delta(x) = \langle x|0 \rangle$ then Eq. (1.28) becomes

$$\begin{aligned}\tilde{u}(x, s) &= G^{(0)}(x|0) - \kappa \sum_{x_i \in \mathbb{S}} G^{(0)}(x|x_i)G^{(0)}(x_i|0) \\ &+ \kappa^2 \sum_{x_i, x_j \in \mathbb{S}} G^{(0)}(x|x_i)G^{(0)}(x_i|x_j)G^{(0)}(x_j|0) + \dots,\end{aligned}\quad (1.29)$$

where

$$\begin{aligned}\langle x|\hat{G}^{(0)}|0 \rangle &= G^{(0)}(x|0), \\ \langle x|\hat{G}^{(0)}\hat{K}\hat{G}^{(0)}|0 \rangle &= -\kappa \sum_{x_i \in \mathbb{S}} \langle x|\hat{G}^{(0)}|x_i \rangle \langle x_i|\hat{G}^{(0)}|0 \rangle, \\ &= -\kappa \sum_{x_i \in \mathbb{S}} G^{(0)}(x|x_i)G^{(0)}(x_i|0)\end{aligned}$$

etc. The bare Green's function is $G^{(0)}(x|x') = \exp(-\sqrt{s/D}|x - x'|)/(2\sqrt{Ds})$. A straight forward inverse Laplace transform yields

$$\begin{aligned}u(x, t) &= \frac{1}{\sqrt{4\pi Dt}} \exp\left(\frac{-|x|^2}{4Dt}\right) - \frac{\kappa}{4D} \sum_{x_i \in \mathbb{S}} \operatorname{erfc}\left(\frac{|x - x_i| + |x_i|}{2\sqrt{Dt}}\right) \\ &+ \frac{\kappa^2}{8D^2} \sum_{x_i, x_j \in \mathbb{S}} \left\{ 2\sqrt{\frac{Dt}{\pi}} \exp\left(\frac{-z(x, x_i, x_j)^2}{4Dt}\right) \right. \\ &\quad \left. - z(x, x_i, x_j) \operatorname{erfc}\left(\frac{z(x, x_i, x_j)}{2\sqrt{Dt}}\right) \right\} + \dots,\end{aligned}\quad (1.30)$$

where $z(x, x_i, x_j) = |x - x_i| + |x_i - x_j| + |x_j|$. This expression in Eq. (1.30) agrees well only when time t is small. Due to the secular term at the second order the solution will diverge for large time. Let us assume that the traps are sparsely distributed so that contribution from terms $G^{(0)}(x_i|x_j)$ for $i \neq j$ in Eq. (1.29) can be ignored. This is decided by the diffusion constant for the following reason a particle which diffuses faster will contribute more as it can move from one trap to other easily. With this approximation Eq. (1.29) can be written as

$$\begin{aligned}\tilde{u}(x, s) &= G^{(0)}(x|0) - \kappa \sum_{x_i \in \mathbb{S}} G^{(0)}(x|x_i)G^{(0)}(x_i|0) \\ &+ \kappa^2 \sum_{x_i \in \mathbb{S}} G^{(0)}(x|x_i)G^{(0)}(x_i|x_i)G^{(0)}(x_i|0) + \dots, \\ &= G^{(0)}(x|0) - \kappa \sum_{x_i \in \mathbb{S}} G^{(0)}(x|x_i) \\ &\quad \times \{1 - \kappa G^{(0)}(x_i|x_i) + \kappa^2 G^{(0)}(x_i|x_i)^2 \dots\} G^{(0)}(x_i|0) \\ &+ \dots, \\ &\simeq G^{(0)}(x|0) - \kappa \sum_{x_i \in \mathbb{S}} \frac{G^{(0)}(x|x_i)G^{(0)}(x_i|0)}{1 + \kappa G^{(0)}(x_i|x_i)}\end{aligned}\quad (1.31)$$

The Feynman diagrams for the Greens function $G(x|x')$ with the approximation in Eq. (1.31) can be written by choosing appropriate diagrams from Fig. (1.3)(cf. Fig. (1.4)). Taking Laplace

$$\begin{aligned}
\text{(a)} \quad \Rightarrow \Rightarrow &\simeq \longrightarrow + \sum_i \longrightarrow \overset{i}{\bullet} \longrightarrow + \longrightarrow \overset{i}{\circlearrowleft} \longrightarrow \\
&+ \longrightarrow \overset{i}{\circlearrowleft} \overset{i}{\circlearrowleft} \longrightarrow + \dots, \\
&= \longrightarrow + \sum_i \longrightarrow \overset{i}{\bullet} \longrightarrow (1 + \overset{i}{\circlearrowleft} \\
&\quad + \overset{i}{\circlearrowleft} \overset{i}{\circlearrowleft} + \dots), \\
&= \longrightarrow + \sum_i \longrightarrow \overset{i}{\bullet} \longrightarrow (1 - \overset{i}{\circlearrowleft})^{-1}, \\
\text{(b)} \quad \Rightarrow \Rightarrow &= G(x|x'), \quad \longrightarrow = G^{(0)}(x|x'), \\
\bullet &= -\kappa, \quad \overset{i}{\circlearrowleft} = -\kappa G^{(0)}(x_i|x_i),
\end{aligned}$$

Figure 1.4: (a) Feynman diagrams, (b) Notations. Setting $x' = 0$ gives us the solution Eq. (1.31).

transform of Eq. (1.31) we obtain

$$\begin{aligned}
u(x, t) &\simeq \frac{1}{\sqrt{4\pi Dt}} \exp\left(\frac{-|x|^2}{4Dt}\right) \\
&- \frac{\kappa}{4D} \sum_{x_i \in \mathbb{S}} \exp\left(\frac{(|x - x_i| + |x_i|)\kappa}{2D} + \frac{\kappa^2 t}{4D}\right) \operatorname{erfc}\left(\frac{|x - x_i| + |x_i|}{2\sqrt{Dt}} + \frac{\kappa\sqrt{t}}{2\sqrt{D}}\right)
\end{aligned} \tag{1.32}$$

Note that the approximate solution given in Eq. (1.32) is valid for a sparsely distributed traps. We can immediately recognize from Eq. (1.32) that this solution is the sum of solutions of Eq. (1.16) with a single trap located at $x = x_i$ for $i = 1, 2, \dots, N_D$, with initial condition $\delta(x)/N_D$ where N_D is the total number of traps in \mathbb{S} . In Fig. (1.5) we have plotted the solution $u(x, t)$ for the case when there are no traps. Without trap there is a pure diffusive process and the delta function evolves into a Gaussian (see Fig. (1.5) curve (A)). The curve (B) and (C) represent the numerical and the perturbation solution Eq. (1.32) respectively. It can be seen that the approximate solution agrees quite well.

Using the Eq. (1.29) the concentration averaged over disorder can be calculated order by

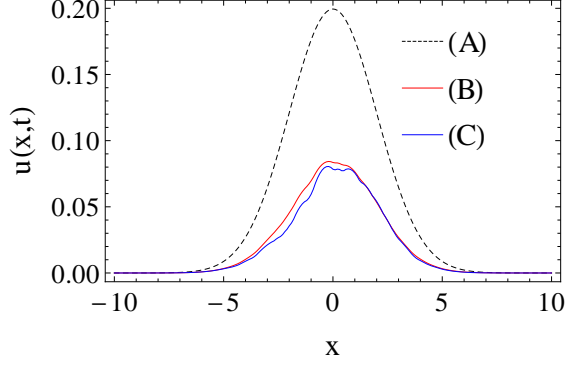


Figure 1.5: The curve (A) shows the concentration $u(x, t)$ when there is no trap. A comparison of the numerical solution in (B) with the perturbation solution (C) obtained from Eq. (1.32) is shown. Number of traps is 80 randomly distributed in $(-10, 10)$, diffusion constant $D = 1.0$, trapping rate $\kappa = 0.1$ and time $t = 2.0$.

order. We have

$$\begin{aligned} \langle \tilde{u}(x, s) \rangle &= \langle G^{(0)}(x|0) \rangle - \langle \kappa \sum_{x_i \in \mathbb{S}} G^{(0)}(x|x_i) G^{(0)}(x_i|0) \rangle \\ &+ \langle \kappa^2 \sum_{x_i, x_j \in \mathbb{S}} G^{(0)}(x|x_i) G^{(0)}(x_i|x_j) G^{(0)}(x_j|0) \rangle + \dots, \end{aligned} \quad (1.33)$$

where $\langle \cdot \rangle$ denotes the mean taken over the disorder. The first term on the right hand side of Eq. (1.33) is $\langle G^{(0)}(x|0) \rangle = G^{(0)}(x|0)$. The higher order terms can be calculated in the following way. Let $[-L, L]$ on the x-axis contain N trapping sites with random variables $x_i \in \mathbb{S}_N$, $i = 1, 2, \dots, N$ being uniformly distributed with probability density $P(x_1, x_2, \dots, x_N) = 1/(2L)^N$. Note that, in the limit $N, L \rightarrow \infty$ we have $N/L \rightarrow \rho$ and the set $\mathbb{S}_N = \mathbb{S}$. The second term on the right had side becomes

$$\begin{aligned} I_1(x) &= \left\langle \sum_{x_i \in \mathbb{S}_N} G^{(0)}(x|x_i) G^{(0)}(x_i|0) \right\rangle, \\ &= \frac{1}{4sD} \sum_{x_i \in \mathbb{S}_N} \left\langle \exp \left(-\sqrt{\frac{s}{D}} (|x - x_i| + |x_i|) \right) \right\rangle, \\ &\stackrel{L, N \rightarrow \infty}{=} \frac{\rho}{4sD} e^{-\sqrt{\frac{s}{D}} |x|} \left(|x| + \sqrt{\frac{D}{s}} \right). \end{aligned} \quad (1.34)$$

To calculate the third term we can use $I_1(x_i)$ and assume total randomness [95] where the correlation can be neglected. The mean of product can be replaced by the product of means so

that we obtain

$$\begin{aligned}
I_2(x) &= \left\langle \sum_{x_i, x_j \in \mathbb{S}_N} G^{(0)}(x|x_i)G^{(0)}(x_i|x_j)G^{(0)}(x_j|0) \right\rangle, \\
&= \left\langle \sum_{x_i \in \mathbb{S}_N} G^{(0)}(x|x_i)I_1(x_i) \right\rangle, \\
&\stackrel{L, N \rightarrow \infty}{=} \frac{\rho^2}{8(Ds)^{3/2}} e^{-\sqrt{\frac{s}{D}}|x|} \left(\frac{|x|^2}{2} + \frac{3|x|}{2} \sqrt{\frac{D}{s}} + \frac{3D}{2s} \right).
\end{aligned} \tag{1.35}$$

Similarly,

$$I_3(x) = \frac{\rho^3}{96D^{1/2}s^{5/2}} e^{-\sqrt{\frac{s}{D}}|x|} \left(|x|^3 \left(\frac{s}{D} \right)^{3/2} + 6|x|^2 \frac{s}{D} + 15|x| \sqrt{\frac{s}{D}} + 15 \right). \tag{1.36}$$

Continuing in the same way we can calculate higher order terms $I_n(x)$ for $n = 4, 5, \dots$. The mean concentration $\langle u(x, t) \rangle$ can then be calculated by taking the inverse Laplace transform of Eq. (1.33) after substituting $I_n(x)$ for $n = 1, 2, \dots$. We obtain

$$\begin{aligned}
\langle u(x, t) \rangle &\simeq \left(1 - \kappa\rho t + \frac{(\kappa\rho t)^2}{2} - \frac{(\kappa\rho t)^3}{6} \pm \dots \right) \frac{1}{\sqrt{4\pi Dt}} \exp\left(\frac{-|x|^2}{4Dt}\right), \\
&= \exp(-\kappa\rho t) \frac{1}{\sqrt{4\pi Dt}} \exp\left(\frac{-|x|^2}{4Dt}\right)
\end{aligned} \tag{1.37}$$

The result obtained in Eq. (1.37) can be understood by simple intuitive reasoning. The number of traps in an unit length is ρ . At each trap a particle can get trapped at a rate κ . If the number of particle per unit length at some instant of time t is $n(t)$, then the number of particle getting trapped will be proportional to $n(t)$ with each particle getting trapped at a rate $\kappa\rho$. The trapping reaction, $A + T \xrightarrow{\kappa} T$ for each trap is transformed into the reaction $A \xrightarrow{\kappa\rho} \phi$. Thus the trapping reaction-diffusion problem is transformed into that of a ‘‘pure death process’’ with rate $\kappa\rho$. We can write $dn(t)/dt = -\kappa\rho n(t)$. Eq. (1.37) therefore suggests that the density falls of exponentially at a rate $\kappa\rho$ at each point x . This is valid for all κ with sufficiently large ρ . Note also that, when limit $\kappa \rightarrow 0$ the mean concentration $\langle u(x, t) \rangle$ evolves into a Gaussian due to pure diffusion. In this limit we can therefore write an effective reaction-diffusion equation of the form $\partial_t u = D\partial_x^2 u - \kappa\rho u$. The mean survival probability is $P(t) := \int \langle u(x, t) \rangle dx = \exp(-\kappa\rho t)$. However, for perfect traps we shall see that this is not the case (cf. Sec. 1.4.2).

The diffusive and the trapping reaction processes have also become independent in this limit ($0 < \kappa \ll 1$) when we are concerned only about the mean concentrations.

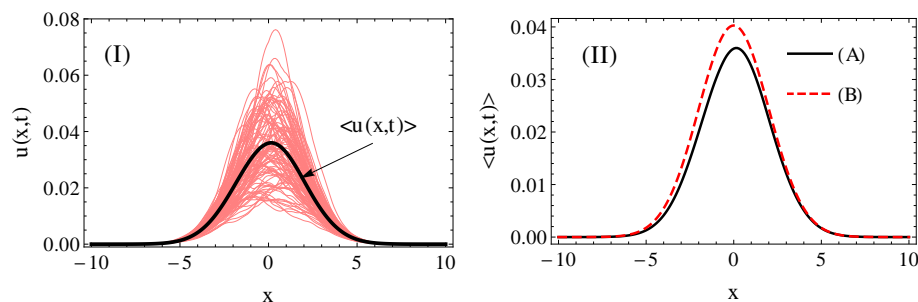


Figure 1.6: (I) Concentration $u(x, t)$ (100 realizations in pink) and the concentration averaged over disorder, $\langle u(x, t) \rangle$ (in thick black). (II) The mean concentration $\langle u(x, t) \rangle$ from numerical calculations (A) and the approximate solution Eq. (1.37) (B) are compared. The number of traps is 80 randomly distributed in $(-10, 10)$, diffusion constant $D = 1.0$, trapping rate $\kappa = 0.2$, $\rho = 4.0$ and time $t = 2.0$.

In Fig. (1.6)(I) we have plotted the numerical solution for 100 different realizations (in pink) of the trapping reaction-diffusion process and the mean concentration $\langle u(x, t) \rangle$ is calculated from 1000 realizations. The number of traps is taken 80 which are chosen from a uniform distribution in $(-10, 10)$, $D = 1$, $\kappa = 0.2$ and $t = 2.0$. In Fig. (1.6)(II) the solution Eq. (1.37) is compared with the corresponding numerical values of the mean concentration. From Fig. (1.6)(I) the spread in the individual curves $u(x, t)$ also indicates the non-selfaveraging characteristics of the mean concentration.

1.4.2 Perfect traps and the law of stretched-exponential

Perfect traps are those which traps particles with unit probability. Here we will consider the case of perfect traps distributed uniformly along the x -axis. Unlike the case of partial traps where only a fraction of the particles get trapped, in this case we will see that the survival probability decays slower than exponential. We call this the law of stretched exponential (i.e. $P(t) \sim \exp(-\alpha t^{1/3})$ in one dimension).

For all finite reaction rates ($\kappa < \infty$) the probability of getting trapped at a trapping site is less than unity hence making it a partial trap. We have already discussed this case in Sec. 1.4.1 and found that the survival probability decays exponentially in time (with the assumption of complete randomness). In the limit $\kappa \rightarrow \infty$ we have “perfect traps” (i.e. $A + T \xrightarrow{\infty} T$). Since every particle arriving at a trap vanishes, the distribution of perfect traps, partition the x -axis into a collection of disjoint intervals. In each interval the concentration $u(x, t)$ evolve independently, hence if we consider the dynamics in one such interval we should be able to

study the whole system. Consider the trapping reaction-diffusion Eq. (1.16)

$$\partial_t u(x, t) = D\partial_x^2 u(x, t) - \kappa \sum_{x_i \in \mathbb{S}} \delta(x - x_i) u(x, t), x \in \mathbb{R}, t > 0,$$

with the initial condition $f(x) = 1$. Consider a particular interval of length $2a$ so that we have $K(x) = -\kappa(\delta(x - a) + \delta(x + a))$ (i.e. after a linear transformation $x \rightarrow x + \text{const.}$). Using Eq. (1.23) and Eq. (1.27) we have can be written write as following integral equation

$$\begin{aligned} |\tilde{u}\rangle &= \hat{G}^{(0)}|f\rangle + \hat{G}^{(0)}\hat{K}|\tilde{u}\rangle, \\ &= \hat{G}^{(0)}|f\rangle + \kappa(\hat{G}^{(0)}|a\rangle\langle a|\tilde{u}\rangle + \hat{G}^{(0)}|-a\rangle\langle -a|\tilde{u}\rangle). \end{aligned} \quad (1.38)$$

Now closing from the left with $\langle x|$ and substituting $\langle x|\hat{G}^{(0)}|f\rangle = \int G^{(0)}(x|x')dx' = 1/s$ and $\kappa\langle x|\hat{G}^{(0)}|\pm a\rangle\langle \pm a|\tilde{u}\rangle = G^{(0)}(x|\pm a)\tilde{u}(\pm a, s)$ we have

$$\tilde{u}(x, s) = \frac{1}{s} - \kappa [G^{(0)}(x|a)\tilde{u}(a, s) + G^{(0)}(x|-a)\tilde{u}(-a, s)]. \quad (1.39)$$

Setting $x = \pm a$ in the left hand side of Eq. (1.39) and solving for $\tilde{u}(\pm a, s)$ we obtain

$$\tilde{u}(\pm a, s) = \frac{1}{s \left(1 + \frac{\kappa}{2\sqrt{Ds}} + \frac{\kappa \exp(-2a\sqrt{s/D})}{2\sqrt{Ds}} \right)}. \quad (1.40)$$

We have

$$\begin{aligned} \tilde{u}(x, s) &= \frac{1}{s} - \frac{\kappa (G^{(0)}(x|a) + G^{(0)}(x|-a))}{s \left(1 + \frac{\kappa}{2\sqrt{Ds}} + \frac{\kappa \exp(-2a\sqrt{s/D})}{2\sqrt{Ds}} \right)}, \\ &= \frac{1}{s} - \frac{G^{(0)}(x|a) + G^{(0)}(x|-a)}{s \left(1 + \exp(-2a\sqrt{s/D}) \right) / (2\sqrt{Ds})}. \end{aligned} \quad (1.41)$$

For κ finite, the Eq. (1.41) leads to a power law decay of the survival probability of a particle $P(t) \sim 2a^2 t^{-1/2}$, ($t \rightarrow \infty$) in $(-a, a)$. Also, for a periodic distribution of traps gives exponential decay $P(t) \sim \exp(-\kappa t/a)$ [21]. In the limit $\kappa \rightarrow \infty$ we have

$$\tilde{u}(x, s) = \frac{1}{s} - \frac{\cosh(x\sqrt{s/D})}{s \cosh(a\sqrt{s/D})}. \quad (1.42)$$

Inverse Laplace transform of Eq. (1.42) (cf. Ref. [106]) gives

$$u(x, t) = \frac{4}{\pi} \sum_{n=0}^{\infty} \frac{1}{2n+1} \exp\left(\frac{-\pi^2(2n+1)^2 Dt}{4a^2}\right) \sin\left(\frac{(2n+1)\pi(a+x)}{2a}\right). \quad (1.43)$$

Expression Eq. (1.43) can also be obtained by solving the diffusion equation with absorbing boundary conditions at the boundaries. We note here that, we have incorporated this in the reaction operator. The survival probability in the interval $(-a, a)$ is

$$\begin{aligned} p(a, t) &= \frac{1}{2a} \int_{-a}^a u(x, t) dx, \\ &= \frac{8}{\pi^2} \sum_{n=0}^{\infty} \frac{1}{(2n+1)^2} \exp\left(\frac{-\pi^2(2n+1)^2 Dt}{4a^2}\right). \end{aligned} \quad (1.44)$$

As the traps are uniformly distributed on the x-axis, the disjoint intervals has a Poisson distribution $p(x) = \rho \exp(-\rho x)$ where x is the length of an interval and ρ is the density of traps (i.e. number of traps per unit length). The probability that a particle occur in an interval of length x is proportional to the length x . The probability of a particle occurring in an interval of length x is therefore $\rho^2 x \exp(-\rho x) dx$. The survival probability becomes

$$\begin{aligned} P(t) &= \int_0^{\infty} p(x, t) \rho^2 4x \exp(-\rho 2x) dx, \\ &= \frac{8\rho^2}{\pi^2} \sum_{n=0}^{\infty} \frac{1}{(2n+1)^2} \int_0^{\infty} \exp(-\alpha_n/x^2 - \rho x) x dx, \\ &= \frac{16}{\pi^{5/2}} \sum_{n=0}^{\infty} \frac{1}{(2n+1)^2} G_{0,3}^{3,0} \left(\frac{\alpha_n \rho^2}{4} \mid 0, 1, \frac{3}{2} \right), \end{aligned} \quad (1.45)$$

where $\alpha_n = (2n+1)^2 \pi^2 Dt$ and $G_{0,3}^{3,0} \left(\frac{\alpha_n \rho^2}{4} \mid 0, 1, \frac{3}{2} \right)$ is the Meijer G-function [107]. In the asymptotic limit $t \rightarrow \infty$ taking the $n = 0$ term only, we have from Eq. (1.45)

$$P(t) = \frac{16}{\pi^{3/2}} \exp\left(\frac{-3(\rho^2 \pi^2 Dt)^{1/3}}{2^{2/3}}\right) \left\{ \frac{2\pi\rho}{\sqrt{3}} \sqrt{Dt} + \frac{17\pi^{1/3} \rho^{1/3}}{2^{1/3} \cdot 3^{1/2} \cdot 9} (Dt)^{1/6} + O((Dt)^{-1/6}) \right\} \quad (1.46)$$

This is the required stretched exponential behavior. This stretched exponential behavior arises due to the contribution from large trap free regions in the distribution of traps which is in contrast with the exponential decay when κ is finite and ρ is large.

1.5 The concept of the first passage time

The calculation of first passage time is very useful in the study of stochastic processes that are triggered by first passage processes e.g. the Kramer's escape problem. In chapter 2 we have studied the first passage time statistics for our reaction-diffusion model using Monte Carlo simulations. Here we discuss the concept of first passage in a pure diffusion process.

Let us consider a particle at the origin $\mathbf{0}$ at time $t = 0$. The particle performs a random walk in d dimensional space. What is the probability $F(\mathbf{x}, t|\mathbf{0}, 0)$ that the particle reaches the point \mathbf{x} at time t for the first time [108]. The probability $P(\mathbf{x}, t|\mathbf{0}, 0)$ of finding the particle at \mathbf{x} at time t given that it started from the origin $\mathbf{0}$ at time $t = 0$ can be written as

$$P(\mathbf{x}, t|\mathbf{0}, 0) = \delta_{\mathbf{x},\mathbf{0}}\delta_{t,0} + \sum_{t' \leq t} F(\mathbf{x}, t'|\mathbf{0}, 0)P(\mathbf{x}, t|\mathbf{x}, t'). \quad (1.47)$$

The expression Eq. (1.47) says that, for a particle starting at the origin at time $t = 0$ the probability of finding the particle at \mathbf{x} at time t equals the sum of all probabilities of finding the particle for the first time at \mathbf{x} at a time $t' \leq t$ given that the particle is again found at \mathbf{x} at time t . Using generating functions

$$\begin{aligned} \tilde{P}(\mathbf{x}, z) &= \sum_{t=0}^{\infty} P(\mathbf{x}, t|\mathbf{0}, 0)z^t, \\ \tilde{F}(\mathbf{x}, z) &= \sum_{t=0}^{\infty} F(\mathbf{x}, t|\mathbf{0}, 0)z^t \end{aligned} \quad (1.48)$$

we obtain

$$\tilde{P}(\mathbf{x}, z) = \delta_{\mathbf{x},\mathbf{0}} + \tilde{F}(\mathbf{x}, z)\tilde{P}(\mathbf{0}, z). \quad (1.49)$$

In Eq. (1.49) we have used the fact that $P(\mathbf{x}, t|\mathbf{x}, t') = P(\mathbf{x}, t - t'|\mathbf{0}, 0)$. In the continuous time limit the sum in Eq. (1.47) should be replaced by an integral over 0 to t and the generating function by the corresponding Laplace transforms. The mean first passage time and the higher moments can be calculated by

$$\langle t^n \rangle = \int t^n F(\mathbf{x}, t|\mathbf{0}, 0)dt, \quad n = 1, 2, \dots \quad (1.50)$$

The probability of first return time to the origin tells us interesting properties of the diffusion process. In the large time limit $t \rightarrow \infty$ we have (for derivation see Ref. [108])

$$F(\mathbf{0}, t|\mathbf{0}, 0) \sim \begin{cases} t^{d/2-2}, & d < 2 \\ 1/(t \ln^2 t), & d = 2. \\ t^{-d/2}, & d > 2 \end{cases} \quad (1.51)$$

The probability of return to the origin $F(\mathbf{0}, t|\mathbf{0}, 0)$ is approximately related to the survival probability $S(t)$ by $1 - S(t) \sim \int^t F(\mathbf{0}, t'|\mathbf{0}, 0)dt'$. The above expression Eq. (1.51) indicates a change in behavior with change in dimension of space. For $d \leq 2$ the survival probability $S(t)$ vanishes as $t \rightarrow \infty$ which implies that the diffusive motion is *recurrent* i.e. the particle

will return to the starting point with unit probability. However, for $d > 2$ there is a nonzero probability that the particle will never return. In this case the diffusion is called *transient*.

In the conventional method the first-passage probability can be calculated from the diffusion equation. Consider the diffusion equation

$$\partial_t u = D \partial_{\mathbf{x}}^2 u, \quad \mathbf{x} \in \Omega, t > 0. \quad (1.52)$$

We have a single particle at the origin so we set the initial concentration $u(\mathbf{x}, 0) = \delta(\mathbf{x})$. We want to compute the probability of hitting the boundary $\partial\Omega$. Also, there should be no contribution from the exterior of the boundary so we need to impose absorbing boundary condition $u(\mathbf{x}, t) = 0$ for all $\mathbf{x} \in \partial\Omega$. The outgoing flux $j(\mathbf{y}, t)$ at the boundary is given by

$$j(\mathbf{y}, t) = -D \partial_{\hat{\mathbf{n}}} u(\mathbf{x}, t)|_{\mathbf{x}=\mathbf{y}}, \quad \mathbf{y} \in \partial\Omega, \quad (1.53)$$

where $\hat{\mathbf{n}}$ is the outward normal to the boundary $\partial\Omega$. The eventual hitting probability is given by

$$P_{\text{hitting}}(\mathbf{y}) = \int_0^\infty j(\mathbf{y}, t) dt, \quad \mathbf{y} \in \partial\Omega. \quad (1.54)$$

The hitting probability in Eq. (1.54) can be calculated by first solving the diffusion equation Eq. (1.52) in Ω with the absorbing boundary conditions and then computing the outward flux at the boundary $\partial\Omega$. Finally, evaluating the integral in Eq. (1.54) gives $P_{\text{hitting}}(\mathbf{y})$.

1.6 Summary

In this chapter we discussed the experimental motivation of the present work. We saw that defects on Si(111)7×7 surface plays a very crucial role in cluster formation processes at nanoscales. We discussed pattern formation in nature with a number of well known problems. It seems that pattern formation arises due to instabilities that give rise to spontaneous symmetry breaking. Turing instability in reaction-diffusion problems is discussed. Furthermore, we discussed reaction-diffusion systems in disordered medium. Anomalous behavior is seen due to the presence of disorder in a number of models.

Using trapping problems in one dimension we illustrated the method of Green's function techniques in reaction-diffusion systems. We showed that the reaction term appears as a reaction operator in the abstract vector space formulation. We shall be using these techniques to study our models of cluster formation. Further the law of stretched exponential was re-derived

where we found the exact expression for the survival probability. In the large time limit we found the $\exp(-\alpha t^{1/3})$ behavior from this expression. In addition to a factor $t^{1/2}$ as obtained in Ref. [96] the next order term is $t^{1/6}$. The first passage time probability was discussed.

1.7 Plan of the thesis

The plan of the thesis is the following. In chapter 2, we propose a reaction-diffusion model that describes the formation of Ge clusters on Si(111)7×7 surface we have discussed above. In our model we introduce a simple reaction scheme to describe the reaction process for the formation of clusters. The reactions are assumed to occur only at the location of the defects, step edges and domain boundaries which we call reaction centers. As from our experiments the step edges and domain boundaries for a single domain form a closed geometry, we take a circular boundary in our model. Under certain approximation we show that the reaction-diffusion process turns out to be a set coupled linear partial differential equations. We shall use the method of Green's function and regular perturbation theory to solve the coupled equations. We will show that, through this minimal model we can form patterns which is qualitatively similar to the patterns we have observed in our experiments. Monte Carlo simulation have been used to show similar pattern for a large number of defects. The mean first passage time to exit from the domain is calculated from the simulation. The probability density of the first passage time is obtained and its properties are discussed.

In chapter 3, we investigate the effect of exclusion in the formation of Ge clusters. The origin of exclusion is related to the non-bonding interaction between particles. The exclusion terms are derived from the microscopic principle using master equations in which we assume a concentration dependent hopping rate. The cluster formation reaction occurs in the vicinity of the reaction centers. We assume an algebraic nonlinear reaction process to account for multiple number of adatoms reacting simultaneously. For the case of weak exclusion we will show that the reaction-diffusion equations can be reduced to a set of coupled linear partial differential equations with drifts. These drift diffusion equations are exactly solvable and show the qualitative behavior of our original equations. For the case of self exclusion we study trapping problem where will show that the effect is opposite. We will then discuss survival probability in the presence of exclusion. Finally, numerical investigation are presented.

In chapter 4, we conclude with future extensions of the work and possible applications.

Chapter 2

Reaction diffusion model for the formation of clusters on a surface with defects

2.1 Introduction

Growth processes on surfaces at nanoscales can show a countless varieties of patterns. Perfectly ordered geometrical structures, random patterns or both could arise in the growth processes depending on the experimental conditions. Formation of self-organized nanostructures has been extensively studied in the past [1–3]. Preferential nucleation of the self-organized nanostructures along step edges [5, 6, 109], dislocations [7–10] or domain boundaries [12, 110] has been observed. It has been observed that for the Ge adatoms deposited on the Si surface there is a preferential growth at the domain boundaries [13]. Also random clusters are formed at the location of surface defects present inside the domain boundary. These domain boundaries and surface defects act as traps for the deposited adatoms. We present here a reaction diffusion model for these growth processes and pattern formation. This work has been motivated by experimental work on pattern formation in the deposition of Ge on Si(111)-(7 × 7) surfaces [13] as well as several other previous investigations [5–10, 12, 109, 110]. We note that ours is a case of reaction-diffusion process in random media.

Reaction diffusion processes in random media has been extensively studied in the past. The models that are considered consist of diffusion limited reactions of a single species in the presence of static and moving traps. The traps are the sites where the reactant species get partially or completely adsorbed. These models have been used to explain various processes such as trapping of exciton in a crystal at a defect, electron-hole and soliton-antisoliton recombination, chemical binding of interstitial hydrogen atoms by impurities [16]. Various aspects of reaction-diffusion processes in disordered media such as self-segregation of diffusing particles [17, 18],

long time behavior of decay of particle density [19–21], the kinetics of diffusion limited coalescence and annihilation in random media [22–25], have been studied. Recently, the effect of quenched disorder and internal noise on the transport properties in a reaction diffusion model has been studied for 'birth-death' process in a real world situation [26]. Fertile patches called oasis lay randomly in the desert where the population can multiply by birth process and in the desert the population decays due to death processes. Reaction-diffusion in disordered systems is also used to model the decay and preservation of marine organic carbon [27].

The model that we study here consists of two species linear reaction diffusion processes in the presence of reaction centers (surface defects). Our primary interest is to describe the reaction-diffusion of Ge adatoms on the Si surface. However, this model can be used in cases where the process is occurring on a two dimensional surface. Reactions take place only in a small neighborhood of the defects present on the Si surface. Some results of a two species reaction diffusion process in the presence of ring defects can be found in Ref. [13, 111, 112].

In section 2.2 we describe theoretical models. The ring and the point models are discussed. Greens function method is used for the solution of our reaction diffusion equation. In section 2.4 we will describe the Monte Carlo simulations and discuss the numerical results for the point defect model. Time evolution of the growth processes is studied from the obtained solutions. We will show that this reaction diffusion model shows the pattern formation that were experimentally reported earlier. Through the MC simulations we investigate the first passage statistics. The first passage time studied here gives us an estimate of the time a particle takes from the origin to reach the domain boundary. This provide us the time scale for the growth process at the domain boundary. The mean first passage time and the first passage time probability density are calculated numerically. The large time asymptotic is discussed in section 2.3.

2.2 Formulation of the model

The model consist of the reaction-diffusion processes of two species S and P on a two dimensional flat surface. Here S denotes the Ge adatoms and P denotes the sum total of possible Ge-clusters. The reaction $S \rightleftharpoons P$ occurs at the location of the defects present on the surface. We call these defects as reaction centers. The reaction scheme is chosen here to describe the clusterization process (see Appendix C.1). We are considering a sequential clusterization pro-

cess in this model, however, the actual clusterization process could be quite complicated. The coupled reaction diffusion equations are given by

$$\begin{aligned}\partial_t S(\mathbf{r}, t) &= D_s \mathcal{L} S(\mathbf{r}, t) - K_f(\mathbf{r}) S(\mathbf{r}, t) - K_R(\mathbf{r}) S(\mathbf{r}, t) + K_b P(\mathbf{r}, t) + J(\mathbf{r}, t), \\ \partial_t P(\mathbf{r}, t) &= D_p \mathcal{L} P(\mathbf{r}, t) - K_b(\mathbf{r}) P(\mathbf{r}, t) + K_f(\mathbf{r}) S(\mathbf{r}, t),\end{aligned}\quad (2.1)$$

where $S(\mathbf{r}, t)$ and $P(\mathbf{r}, t)$ are the concentrations at position \mathbf{r} and time t , D_s and D_p are the diffusion coefficients and $K_f(\mathbf{r})$ and $K_b(\mathbf{r})$ are the reaction rates. The reaction rates are given by $K_\alpha(\mathbf{r}) = k_\alpha \delta(\mathbf{r} - \boldsymbol{\rho})$, for $\boldsymbol{\rho} \in \Omega$. The set Ω denotes the regions on the Si surface where defects are located. The domain boundary is modeled as a ring of radius R and is given by $K_R(\mathbf{r}) = k_R \delta(|\mathbf{r}| - R)/|\mathbf{r}|$. This is no restriction of the proposed model. Any type of boundary can be considered. Then the model will require a full-scale numerical approach. $J(\mathbf{r}, t)$ is an external flux. Equation (2.1) is subject to the boundary conditions $S(\mathbf{r}, t)$, $P(\mathbf{r}, t)$ are finite at the origin and vanishes at infinity. The initial conditions are $S(\mathbf{r}, 0) = P(\mathbf{r}, 0) = 0$. Let $\phi(\mathbf{r}, s)$, $\psi(\mathbf{r}, s)$ and $\hat{J}(\mathbf{r}, s)$ be the Laplace transform of $S(\mathbf{r}, t)$, $P(\mathbf{r}, t)$ and $J(\mathbf{r}, t)$ respectively. From Eq. (2.1) we have

$$\begin{aligned}|\phi(s)\rangle &= G_s^{(1)}(s) D_s^{-1} (-K_f |\phi(s)\rangle + K_b |\psi(s)\rangle + |\hat{J}(s)\rangle), \\ |\psi(s)\rangle &= G_p^{(0)}(s) D_p^{-1} (-K_b |\psi(s)\rangle + K_f |\phi(s)\rangle).\end{aligned}\quad (2.2)$$

where $\langle \mathbf{r} | \phi(s) \rangle = \phi(\mathbf{r}, s)$, $\langle \mathbf{r} | \psi(s) \rangle = \psi(\mathbf{r}, s)$, $\langle \mathbf{r} | \hat{J}(s) \rangle = \hat{J}(\mathbf{r}, s)$, $\delta(\mathbf{r} - \mathbf{r}') K_j(\mathbf{r}) = \langle \mathbf{r} | K_j | \mathbf{r}' \rangle$ for $j = f, b, R$, $\langle \mathbf{r} | (sD_s^{-1} - \mathcal{L}) | \phi(s) \rangle = (sD_s^{-1} - \mathcal{L})\phi(\mathbf{r}, s)$ and $\langle \mathbf{r} | (sD_p^{-1} - \mathcal{L}) | \psi(s) \rangle = (sD_p^{-1} - \mathcal{L})\psi(\mathbf{r}, s)$. [30] The orthogonality and the completeness relations are given as $\langle \mathbf{r} | \mathbf{r}' \rangle = \delta(\mathbf{r} - \mathbf{r}')$ and $\int |\mathbf{r}\rangle \langle \mathbf{r}| d\mathbf{r} = 1$. [30] The operator \mathcal{L} is the Laplacian in polar coordinate system [113]. The Green's function are defined by

$$\begin{aligned}G_p^{(0)}(s) &= [sD_p^{-1} - \mathcal{L}]^{-1}, \\ G_s^{(0)}(s) &= [sD_s^{-1} - \mathcal{L}]^{-1}, \\ G_s^{(1)}(s) &= [sD_s^{-1} - \mathcal{L} + D_s^{-1} K_R]^{-1}.\end{aligned}\quad (2.3)$$

The domain boundary is a circle of radius R so that we can write $K_R = |R\rangle k_R \langle R|$. Expression for $G_s^{(1)}(s)$ can be written in terms of the t-matrix as

$$G_s^{(1)}(s) = G_s^{(0)}(s) + G_s^{(0)}(s) T_R(s) G_s^{(0)}(s) \quad (2.4)$$

where the t-matrix $T_R(s)$ [30] is given by

$$\begin{aligned} T_R(s) &= -(D_s^{-1}K_R - D_s^{-1}K_R G_s^0(s)D_s^{-1}K_R + D_s^{-1}K_R G_s^0(s)D_s^{-1}K_R G_s^0(s)D_s^{-1}K_R \dots) \\ &= \frac{|R\rangle(-k_R/D_s)\langle R|}{1 + (k_R/D_s) \int G_s^{(0)}(R, \theta|R, \theta)d\theta} \end{aligned} \quad (2.5)$$

The Green's function in the limit $k_R \rightarrow \infty$ is

$$G_s^{(1)}(s) = G_s^{(0)}(s) - \frac{G_s^{(0)}(s)|R\rangle\langle R|G_s^{(0)}(s)}{\int G_s^{(0)}(R, \theta|R, \theta)d\theta} \quad (2.6)$$

The expressions for $G_\alpha^{(0)}(s)$ and $G_\alpha^{(1)}(s)$ are given in Appendix A.1. Equation (2.4) and (2.5) can also be written in terms of Feynman diagrams (cf. Fig. 2.1). Using these expression in Eq. (2.2), $|\phi(s)\rangle$ and $|\psi(s)\rangle$ can be written in terms of the Green's functions. The concentrations can then be calculated by inverse Laplace transformation of $|\phi(s)\rangle$ and $|\psi(s)\rangle$. At the domain boundary the reaction $S \rightarrow S'$ takes place at a rate k_R which is sufficiently high. This implies that those particles that reaches the domain boundary get permanently trapped there.

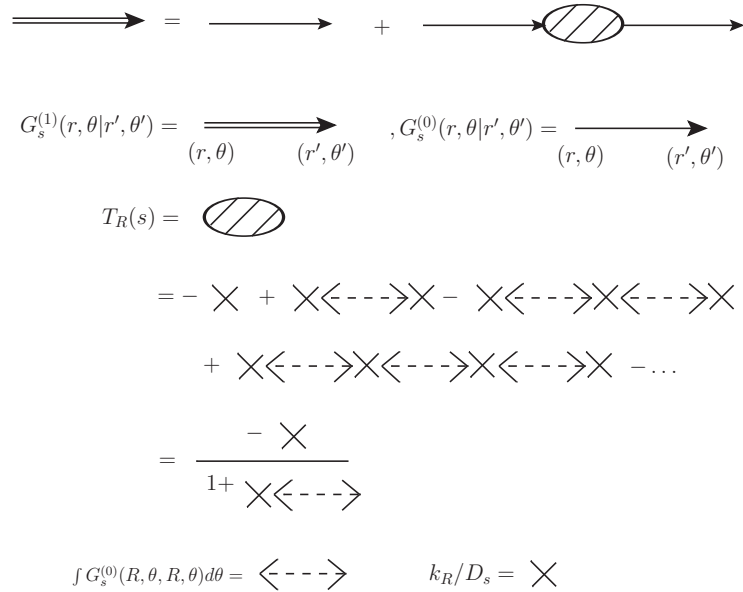


Figure 2.1: Green's function $G_s^{(1)}(r, \theta|r', \theta')$ expressed in Feynman diagrams.

2.2.1 The ring model

The reaction centers are modeled as concentric rings with center at the origin. Due to the circular symmetry we have $\mathcal{L} = \frac{1}{r} \frac{d}{dr} \left(r \frac{d}{dr} \right)$. The concentrations are given by $S(r, t)$ and $P(r, t)$.

The reaction rates are given by $K_\alpha(r) = k_\alpha \sum_{r_i} \delta(r - r_i)/r$, where index α is f or b and r_i denotes the collection of all random variable uniformly distributed in $(0, R)$. Thus Ω is defined by the collection of all these circles. A particle flux $J(\mathbf{r}, t)$ is incident normal to the surface. We assume $J(\mathbf{r}, t) = j_0 \exp(-\lambda r)$ to be exponentially decaying. Here the reaction $S \rightleftharpoons P$ occurs at the i -th ring and there is diffusion away from the ring. At the boundary $r = R$ the reaction $S \rightarrow S'$ takes place at a rate k_R . The diffusion constant of S' is assumed very low as compared to that of S and P . Let $\phi(r, s)$, $\psi(r, s)$ and $\hat{J}(r, s) = j_0 \exp(-\lambda r)/s$ be the Laplace

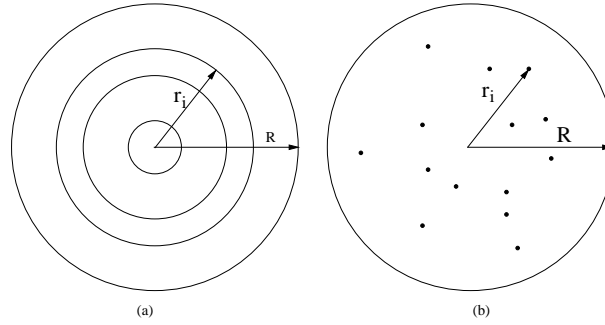


Figure 2.2: Geometry of the reaction diffusion process (a) the ring model: the largest ring of radius R denotes the domain boundary, other rings denote the ring defects, (b) the point model: the dots dispersed within the radius R denote the point defects on the surface.

transform of the concentrations $S(r, t)$, $P(r, t)$ and $J(r, t)$ respectively. We obtain $\phi(r, s)$ and $\psi(r, s)$ in terms of the Green's function $G_s^{(1)}(r|r')$ and $G_p^{(0)}(r|r')$.

$$\begin{aligned}
 \phi(r, s) &= \sum_{\{r_i\}} G_s^{(1)}(r|r_i) \rho_1(r_i, s) + Q(r, s), \\
 \psi(r, s) &= \sum_{\{r_i\}} G_p^{(0)}(r|r_i) \rho_2(r_i, s), \\
 \rho_1(r_i, s) &= \frac{k_b}{D_s} \psi(r_i, s) - \frac{k_f}{D_s} \phi(r_i, s), \\
 \rho_2(r_i, s) &= \frac{k_f}{D_p} \phi(r_i, s) - \frac{k_b}{D_p} \psi(r_i, s).
 \end{aligned} \tag{2.7}$$

where $Q(r, s) = (2\pi/D_s) \int G_s^{(1)}(r|r') \hat{J}(r', s) r' dr'$. Using Eqs. (2.3) the Green's function can be written as

$$G_\alpha^{(0)}(r|r') = \frac{1}{2\pi} I_0(\sqrt{s/D_\alpha} r) K_0(\sqrt{s/D_\alpha} r'), \tag{2.8}$$

where the index α is s or p and $r < r'$. When $r > r'$ replace r by r' and vice versa in Eq. (2.8). In $G_\alpha^{(0)}(r|r')$ the Laplace variable s has been kept implicit for clarity. It will be explicitly

written as $G_\alpha^{(0)}(r, r', s)$ whenever required. The presence of the domain boundary $K_R(r)$ acts as a defect. So, we can write the Green's function in the presence of single defect as

$$G_s^{(1)}(r|r') = G_s^{(0)}(r|r') - \frac{G_s^{(0)}(r|R)G_s^{(0)}(R|r')}{G_s^{(0)}(R|R)}. \quad (2.9)$$

in the lim $k_R \rightarrow \infty$, which makes the domain boundary a perfect sink at $r = R$. Now, suppose there are N_D number of defects. Setting $r = r_j$ for all $j = 1, 2, \dots, N_D$ in Eq. (2.2) we obtain $2N_D$ linear equations which can be solved to obtain $\phi(r_j, s)$ and $\psi(r_j, s)$ for all $j = 1, 2, \dots, N_D$. From Eq.(2.7) $S(r, t)$ and $P(r, t)$ can then be obtained using Inverse Laplace transform. Let us now consider the case of a single defect. From Eq.(2.7) we have

$$\phi(r, s) = Q(r, s) - \frac{k_f}{D_s} \frac{G_s^{(1)}(r|r_1)Q(r_1, s)}{\Delta(r_1)}, \quad (2.10)$$

$$\psi(r, s) = \frac{k_f}{D_p} \frac{G_p^{(0)}(r|r_1)Q(r_1, s)}{\Delta(r_1)}, \quad (2.11)$$

where $\Delta(r_1) = 1 + (k_f/D_s)G_s^{(1)}(r_1|r_1) + (k_b/D_p)G_p^{(0)}(r_1|r_1)$. We notice from Eq. (2.10) that, the inverse Laplace transform of the first part $Q(r, s)$ gives the solution of the diffusion equation with a sink at $r = R$ in the presence of external flux. The second part involves a convolution in time the effect of which is to decrease the concentration near the reaction center. Similarly from Eq. (2.11) we can see the converse. For large number of defects $\phi(r, s)$ and $\psi(r, s)$ will be too complicated, but the concentrations will show the same behavior close to the defect centers. We have implemented the Talbot Inverse Laplace transformation method [32] in our numerical computations. In Fig. 2.3 we use the domain boundary as the unit circle so that $0 \leq r \leq 1 (= R)$. In Fig. 2.3 we plot the concentrations $S(r, t)$ and $P(r, t)$ at time $t = 1.0$ for $D_s = 0.1$, $D_p = 0.01$, $k_f = k_p = 0.1$. There are four ring defects with radius randomly chosen in $(0, 1)$. The concentration for P shows peaks of decreasing heights at those radii. This happens due to the exponentially decaying incident flux. We will discuss next in the point model how point defect gives rise to similar peaks. We will see that both models differs only in their geometrical aspects.

2.2.2 The point model

In this model, we consider point reaction centers spread uniformly over the surface. Let \mathbf{r}_i be the position of the i -th reaction center where $1 \leq i \leq N_D$ and N_D is the total number of reaction centers (see Fig. 2.2(b)). So we have $\Omega = \{\mathbf{r}_1, \dots, \mathbf{r}_{N_D}\}$ the set of position vectors of

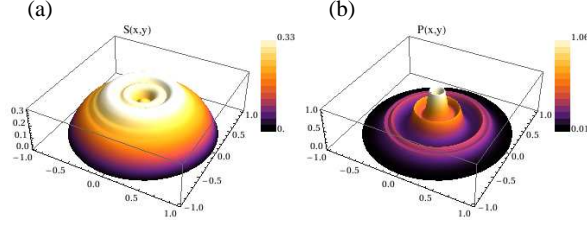


Figure 2.3: Concentrations (a) $S(\mathbf{r}, t)$ and (b) $P(\mathbf{r}, t)$ at time $t = 1.0$ where $\mathbf{r} = (x, y)$, $D_s = 0.1$, $D_p = 0.01$, $k_f = 1.0$, $k_p = 0.1$ in the presence of four ring defects in $0 \leq r \leq 1$. Incident flux in exponentially decaying with $\lambda = 1.0$.

reaction centers. The reaction rates are given by $K_\alpha(\mathbf{r}) = k_\alpha \sum_{i=1}^n \delta(\mathbf{r} - \mathbf{r}_i)$, where $\alpha = f, b$. The Laplace transform of the concentrations $S(\mathbf{r}, t)$, $P(\mathbf{r}, t)$ are given by

$$\begin{aligned}
 \phi(r, \theta) &= \sum_{(r_i, \theta_i) \in \Omega} G_s^{(1)}(r, \theta | r_i, \theta_i) \rho_1(r_i, \theta_i) + Q(r, \theta), \\
 \psi(r, \theta) &= \sum_{(r_i, \theta_i) \in \Omega} G_p^{(0)}(r, \theta | r_i, \theta_i) \rho_2(r_i, \theta_i), \\
 Q(r, \theta) &= \frac{1}{sD_s} \int G_s^{(1)}(r, \theta | r', \theta') J(r', \theta') r' dr' d\theta', \\
 \rho_1(r_i, \theta_i) &= \frac{-k_f}{D_s} \phi(r_i, \theta_i) + \frac{k_b}{D_s} \psi(r_i, \theta_i), \\
 \rho_2(r_i, \theta_i) &= \frac{-k_b}{D_p} \psi(r_i, \theta_i) + \frac{k_f}{D_p} \phi(r_i, \theta_i), \tag{2.12}
 \end{aligned}$$

Here we have $\mathbf{r} = (r, \theta)$ and $\mathbf{r}_i = (r_i, \theta_i)$ as we are using polar coordinate system. The values of $\phi(r_i, \theta_i)$ and $\psi(r_i, \theta_i)$ can be obtained by solving the following linear equations

$$\begin{aligned}
 \phi_i &= \sum_{j=1}^{N_D} (G_s^{(1)})_{i,j} (-k_f \phi_j + k_b \psi_j) / D_s + Q_i, \\
 \psi_i &= \sum_{j=1}^{N_D} (G_p^{(0)})_{i,j} (-k_b \psi_j + k_f \phi_j) / D_p. \tag{2.13}
 \end{aligned}$$

where $(G_s^{(1)})_{i,j} = G_s^{(1)}(r_i, \theta_i | r_j, \theta_j)$, $\phi_j = \phi(r_j, \theta_j)$, $\psi_j = \psi(r_j, \theta_j)$ and $Q_i = 1/(sD_s) \int G_s^{(1)}(r_i, \theta_i | r', \theta') J(r', \theta') r' dr' d\theta'$ for all $i = 1, 2, \dots, N_D$. Inverting the Eq.(2.13 and 2.12) to the time domain will give us the concentrations $S(\mathbf{r}, t)$ and $P(\mathbf{r}, t)$.

2.3 Asymptotic large time limit

Consider the ring model with one ring defect. The Green's function in Eq.(2.10) and(2.11) when expanded in Taylor series near $s = 0$ can be written as

$$\begin{aligned} G_s^{(1)}(r|r') &\simeq -\frac{1}{2\pi} \left(1 + \frac{sr^2}{4D_s}\right) \left(1 + \frac{sr'^2}{4D_s}\right) \ln(r'/R) + \dots, \\ G_p^{(0)}(r|r') &\simeq -\frac{1}{2\pi} \left(1 + \frac{sr^2}{4D_s}\right) \left(1 + \frac{sr'^2}{4D_s}\right) \left(\ln \frac{s^{1/2}r'}{2D_s^{1/2}} + \gamma\right) + \dots, \end{aligned}$$

where $r < r'$. For $r > r'$ replace r by r' and vice versa. For $k_f/D_s \ll 1$ and $k_b/D_p \ll 1$ denominator can be approximated as unity. Using the above expressions we have $Q(r, s) \sim s^{-1}$ so that $Q(r, t)$ in the long time asymptotic limit becomes

$$Q^*(r) \simeq \frac{-j_0}{D_s \lambda^2} \{Ei(-\lambda R) - Ei(-\lambda r) + e^{-\lambda r} - e^{\lambda R} + \ln(r/R)\} \quad (2.14)$$

The concentration $S(r, t)$ and $P(r, t)$ in the asymptotic limit $t \rightarrow \infty$ [114] can be written as

$$\begin{aligned} S(r) &\simeq Q^*(r) + \frac{k_f}{2\pi D_s} Q^*(r_1) F_1(r), \\ P(r) &\simeq \frac{-k_b}{2\pi D_p} Q^*(r_1) F_2(r), \end{aligned} \quad (2.15)$$

where

$$\begin{aligned} F_1(r) &= \begin{cases} \ln \frac{r_1}{R} & \text{if } r \leq r_1, \\ \ln \frac{r}{R} & \text{if } r > r_1. \end{cases} \\ F_2(r) &= \begin{cases} \gamma - \frac{1}{2} \ln \frac{4D_p Ct}{r_1^2} - \frac{r}{8D_p t} & \text{if } r \leq r_1, \\ \gamma - \frac{1}{2} \ln \frac{4D_p Ct}{r^2} - \frac{r_1}{8D_p t} & \text{if } r > r_1. \end{cases} \end{aligned} \quad (2.16)$$

and $\gamma = \ln C = 0.5772\dots$. The function $Q^*(r)$ is a monotonically decreasing function with maximum at the origin $r \rightarrow 0$ and zero at the domain boundary $r = R$. From the expression obtained in Eq.(2.15 and 2.16) we find that in the presence of a single ring defect the concentration $S(r)$ and $P(r)$ varies logarithmically as one move away from the ring defect.

2.4 Simulations and numerical results

We saw earlier that the solution $S(\mathbf{r}, t), P(\mathbf{r}, t)$ can be calculated by using the Green's functions. However for a large number of defects it becomes difficult to evaluate it numerically. We explore numerically the results we have obtained in Eq.(2.12) for a small number of defect $N_D = 8$. In our computations we have implemented the fixed Talbot method for inverse

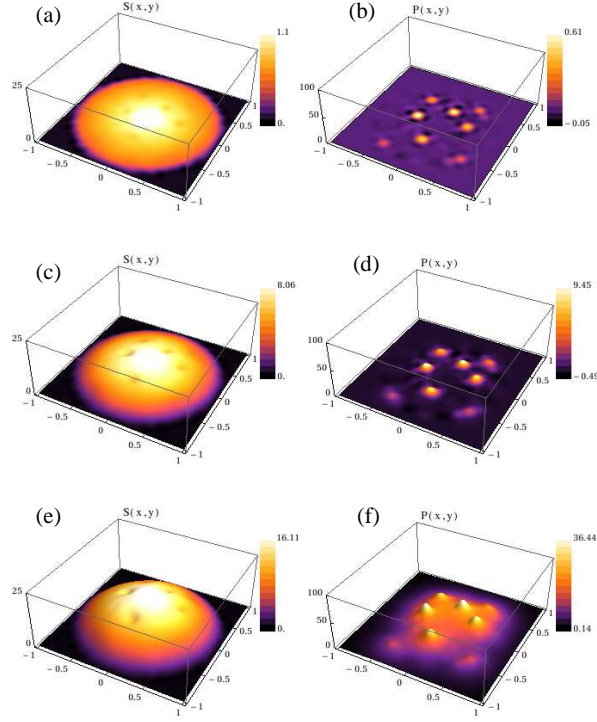


Figure 2.4: Concentration $S(\mathbf{r}, t)$ at time (a) $t = 0.01$, (c) $t = 0.1$, (e) $t = 1.0$ and concentration $P(\mathbf{r}, t)$ at time (b) $t = 0.01$, (d) $t = 0.1$, (f) $t = 1.0$ for $D_s = 1.0$ and $D_p = 0.1$.

Laplace transformations [32]. For large number of defects we have studied the system by Monte Carlo simulations. For our numerical computations we have scaled all relevant parameters of the model by the radius of the domain boundary R i.e. $D_\alpha \rightarrow \tau D_\alpha / R^2$, $k_\alpha \rightarrow \tau k_\alpha$ where the index α is s or p , $\tau = R^2 / D_s$ is the unit of time. The values of plots are obtained by setting flux $\tau j_0 \rightarrow 1$. The parameter λ is taken as $1/R$ with the assumption that the flux of particles falls off appreciably outside the domain boundary. In the plots in Fig. 2.4 we show the time evolution of the diffusion process. The following parameters, $D_s = 1.0$, $D_p = 0.1$, $k_f = 0.1$ and $k_b = 0.01$ were used. At $t = 0.01$ (Fig. 2.4 a and b) one can find that the reaction has just begun and thus the concentrations of P around the reaction centers can be seen. As we advance ahead in time the concentration of P becomes more prominent and the space between the reaction centers starts filling up due to the diffusion of P . Concentration of S show dips at the locations where the concentration of P peaks. We further note that peaks of P appearing nearer to the origin are higher than those closer to the periphery. This happens as we have chosen an exponentially decaying flux. Asymptotic results were obtained for the following set of parameters $D_s \gg D_p$ with $k_f = k_b = 0.1$ and time $t = 1.0$. Figure 2.5 (a,

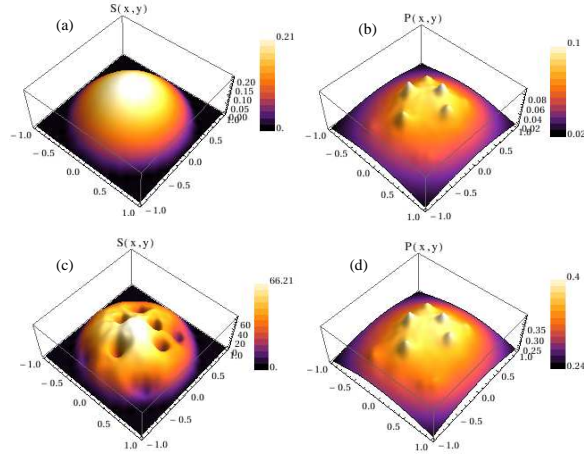


Figure 2.5: Concentrations $S(\mathbf{r}, t)$ and $P(\mathbf{r}, t)$: (a,b) for $D_s \gg D_p$ at $t = 1.0$, (c,d) for $D_s \ll D_p$ at $t = 1.0$.

b) shows the case for $D_s \gg D_p$. In this case the S species diffuses very fast compared to the P species. Consequently the concentration plot of S shows the expected smoothness. For the opposite case (i.e., $D_s \ll D_p$) we note that (Fig. 2.5 (c, d)) there are deep hole-like structures in S concentration plot. This means that more number of particles have undergone reactions near the reaction centers as this should be the case for $D_s \ll D_p$. Similarly, if we vary the reaction rate constants we find that the peaks of P grow and dips appear in S with increasing k_f , the rate constant for the conversion of S to P . The concentrations of S and P for $t = 1.0$, $(k_f, k_b) = (0.1, 0.1), (0.5, 0.1), (0.1, 0.5)$ and $D_s = D_p = 1.0$ are plotted in Fig. 2.6.

For a large number of reaction centers we performed Monte Carlo simulations to study the reaction diffusion process. We have used the stochastic simulation algorithm [115]. Reaction centers are uniformly distributed inside the circular domain of radius R . Each reaction center is a circular disk of radius $a \ll R$ centered at $\mathbf{r}_i, i = 1, 2, \dots, N_D$ where the reaction $S \rightleftharpoons P$ take place with rate $k_\alpha, \alpha = f, b$. Outside the circular region there is no reaction. Note that in this numerical approach we allow a definite area for the reaction center. The species S and P freely diffuse with diffusion constant D_s and D_p respectively. Whenever a particle of type S reaches the domain boundary $|\mathbf{r}| = R$ the reaction $S \rightarrow S_1$ occur with probability 1. This makes it a perfect sink (i.e. limit $k_R \rightarrow \infty$). We have taken a constant flux rate J . The simulation algorithm is discussed in Appendix E. A snapshot of the simulation with $N_D = 150$ is shown in Fig. 2.7. The following parameters were used $D_s = 1.0, D_p = 0.01, D_{S_1} = 0.001, k_f =$

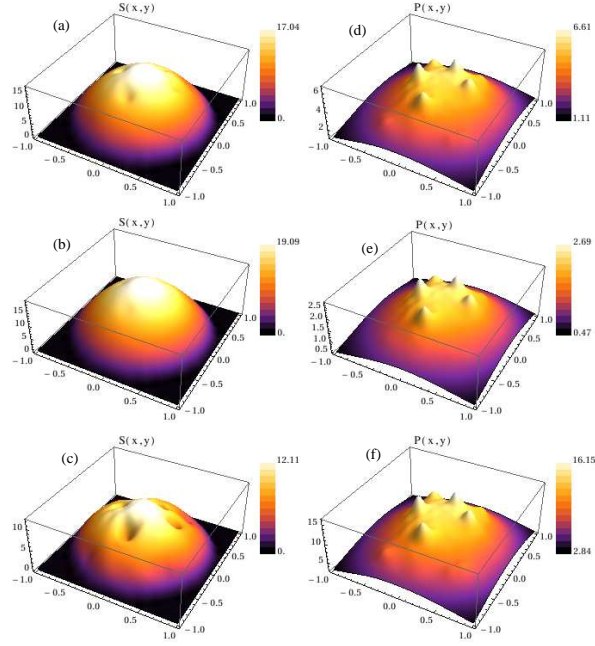


Figure 2.6: Concentrations of $S(\mathbf{r})$ (a, b, c) and $P(\mathbf{r})$ (d, e, f): (a, d) $k_f = 0.1, k_b = 0.1, t = 1.0$; (b, e) $k_f = 0.1, k_b = 0.5, t = 1.0$; (c, f) $k_f = 0.5, k_b = 0.1, t = 1.0$.

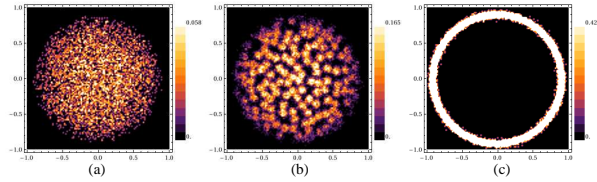


Figure 2.7: Snapshots of concentrations: (a) S , (b) P and (c) S_1 obtained from MC simulation after 5×10^4 MC steps.

1.0, $k_b = 0.1$. The plot shows the density of particles at 5×10^4 Monte Carlo steps. One MC step consist of one diffusive step of each particle on the surface followed by the corresponding reaction step which occurs at rate k_f or k_b depending on the type of particle.

We studied the first passage time statistics of the reaction diffusion process using MC simulations. In the previous chapter we discussed the first passage time probability. In our simulation an adatom starts diffusion from the origin at time $t = 0$. It undergoes a number of reactions along its path before it hits the domain boundary at R . The diffusion coefficient at a time t depends on whether it is of type S or P. The first passage time is defined as the time required for the particle to reach the domain boundary at R irrespective of its type when it reaches the domain boundary. From our MC simulations we have found that for a fixed N_D the

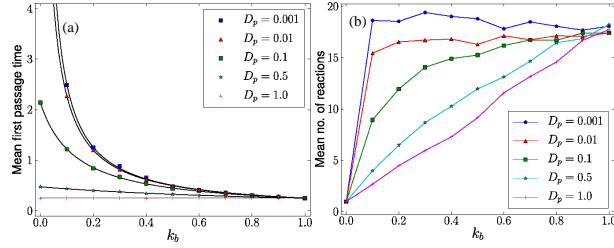


Figure 2.8: (a) Mean first passage time and (b) mean number of reaction as a function of k_b . Black lines in (a) is $P(\tau_f)$ that are fit to the MC results (points). $D_s = 1, k_f = 1$.

mean first passage time is correlated to the number of reactions the particle undergoes during the entire path. We calculated the mean first passage time and the mean number of reactions as a function of k_b for different values of D_p . The mean first passage time $\langle \tau_f \rangle$ is found to be a strictly decreasing function of k_b . We found that $\langle \tau_f \rangle \sim c_1 / (k_b + c_2)$ where c_1 and c_2 are positive constants that depends on D_p . To the best of our knowledge it is a new result.

Let us assume that the probability density of first passage time $P(\tau_f) = p(\tau_f) \exp(-A\tau_f)$ where $p(\tau_f)$ is a positive polynomial and $A > 0$ is a constant. For small values of D_p we have $\langle \tau_f \rangle \sim c_1 / k_b$ (see Fig. 2.8 (a) for $D_p < 0.5$). We can assume $p(\tau_f)$ linear which leads to $P(\tau_f) = A^2 \tau_f \exp(-A\tau_f)$ where A depends on D_p . This probability density agrees quite well with the results obtained from the MC simulations. The mean first passage time then gives $A = 2k_b / c_1$. In Fig. 2.9 we plotted the probability density $P(\tau_f)$ for $D_p = 0.1$ and $k_b = 0.1, 0.25, 0.5$ along with the densities obtained from the MC simulations. For small values of D_p we found that the function $P(\tau_f)$ fit very well with the MC results.

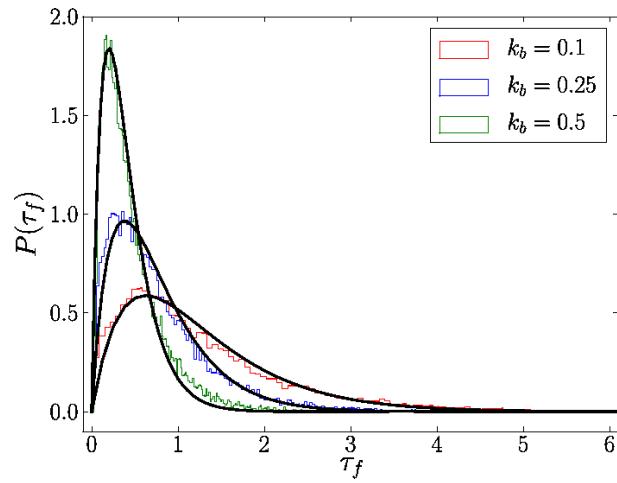


Figure 2.9: Comparison of probability densities obtained from MC simulations(thin colored lines) with $P(\tau_f)$ (thick solid lines). $D_s = 1, D_p = 0.1, k_f = 1.0$

Chapter 3

The effect of exclusion on nonlinear reaction-diffusion system with disorder

3.1 Introduction

Cluster formation at nanoscales induced by surface defects has been studied extensively in recent times ([5–10, 12, 13, 109, 110] and the references therein). It has been found that step edges [5, 6, 109], dislocations [7–10] and domain boundaries [12, 110] play a very crucial role in cluster formation. In a recent paper it is shown that when Ge is deposited on Si surfaces preferential growth occurs at surface defects and domain boundaries [13]. A reaction diffusion model is proposed which qualitatively explains the cluster formation [112]. Surface defects and domain boundaries are taken as localized reaction centers in the form of point defects and ring defects. Furthermore, simple linear form of the reaction is considered. This can be justified under certain approximation. In the studied model clusters and adatoms were allowed to diffuse normally with intrinsic diffusion coefficients [13, 112].

Reaction diffusion models in presence of defects has been studied earlier to model a number of phenomena such as trapping of exciton in a crystal at a defect, recombination of electron and hole and soliton and antisoliton [16]. In these works trapping reactions have been studied in which the reactants get absorbed completely or partially at trapping sites (i.e. reaction centers). The authors have focused primarily on the statistical properties such as long time behavior and self segregation [17–21]. Furthermore, these models describe a non-interacting system of particle undergoing reactions in a disordered media. Here we would like to emphasize that when we say an “interacting“ reaction diffusion system, we simply mean interaction between particles other than the reactive interactions (or simply reactions).

Our main aim in this chapter is two fold. In the first place, we plan to study the effect of

exclusion in the formation of cluster induced by surface defects. The effect of exclusion in a multispecies reaction-diffusion system in the presence of disorder has not been studied so widely. This exclusion effect arises due to repulsion among diffusing particles. For the same kind of particles, this repulsive effect is incorporated in a mean field way in their diffusion coefficients, which is an experimentally determined quantity [104]. But, there is also repulsion among dissimilar species. So, this must be taken into account at least in a mean field way in any reaction-diffusion system.

Exclusion effect in homogeneous reaction diffusion systems has been studied by a number of authors. In lattice models exclusion is incorporated by restricting the occupancy of a site strictly to a single particle. Recently, it is shown that in a lattice system with contact interactions there could be discrepancies between the lattice and their corresponding continuum model. This arises because in the continuum model the diffusion constant becomes dependent on the concentration which may take unphysical values for different lattice types and the chosen interaction neighborhood [116]. However, the continuum model agrees well for mild to moderate contact interaction strength.

If we look at normal diffusion the diffusivity is independent of the concentration of the diffusing particles. However, in a multiparticle system in which there is interaction between the diffusing particles the diffusivity can depend on the concentration. In such systems anomalous diffusion might be observed. It was shown that the critical behaviors of non-equilibrium absorbing phase transitions under particle conservation are affected when excluded volume interaction is incorporated [117]. Experimental observations have established that all concentration dependent diffusion process leads to anomalous diffusion [118,119]. In an interacting multiparticle system, concentration dependent diffusion coefficient appears naturally [120]. Nonlinear Fokker-Planck equation has been studied in the past that describes the stochastic motion of a particle in a media whose drift and diffusion terms depends on the probability density of the particle [120–124]. In the model considered here we have two coupled Smoluchosky equations [125] in which repulsive force on any one type of particles is generated by other species. In the developed Smoluchosky equations the repulsive force on a given type of particles is assumed to be generated by the concentration gradients of the other species. For a single species system, equation studied here is same in form , developed by other authors [122, 123].

On the same note repulsive interaction between particles can also be seen as an exclusion effect as the repulsive force originates from an effective field produced by other particles on a

tagged particle. Note that any two particles cannot occupy the same position at the same time. Hence, this effect can be introduced by a repulsive interaction between the particles (i.e. hard core repulsion) as it is done here. We would also like to emphasize here that this is an alternative way of incorporating exclusion effects in mean field equations. In this article we study a reaction diffusion system in the presence of exclusion and disorder. This type of approach has been taken to understand chemotaxis in biological problems [33, 34]. Furthermore, exclusion processes on lattice has been studied extensively in the past to model problems in physics, chemistry and biology. It is also shown how these reaction diffusion equation can be derived using microscopic principles from the master equation [125, 126].

Another important feature here is that the incorporation of nonlinear cluster formation reaction scheme. Since there is no proven reaction scheme for the formation of nanoclusters on Si surfaces, we use algebraic nonlinearity in the reaction scheme. The relevant chemical kinetic equations are derived in Appendix C.2.

In Sec. 3.2 we discuss the theoretical model. A perturbative analysis of one-dimensional system is also presented. In Sec. 3.3 we study the effect of exclusion in a simple diffusion process in the presence of a trap site at the origin. We show here that self-exclusion gives rise to concentration dependent diffusion coefficient. We draw important conclusions about the formation of clusters in the presence of exclusion from this simple set up. Numerical results for both one dimensional and the original model of two dimensions are discussed in Sec. 3.4.

3.2 Theoretical model

We consider a reaction diffusion process on a flat surface on which reaction occurs only in the neighborhood of reaction centers. Reaction centers are localized regions on the surface where we allow the reaction to take place. Away from the reaction centers there is only diffusion. At a reaction center we assume η adatom combine to form a cluster. The coupled reaction diffusion equation is given by

$$\begin{aligned} \partial_t S(\mathbf{x}, t) = & \partial_{\mathbf{x}}(D_s \partial_{\mathbf{x}} S(\mathbf{x}, t) + \epsilon S(\mathbf{x}, t) \partial_{\mathbf{x}} P(\mathbf{x}, t)) \\ & - K_f(\mathbf{x}) S(\mathbf{x}, t)^\eta + K_b(\mathbf{x}) P(\mathbf{x}, t) + J(\mathbf{x}, t), \end{aligned} \quad (3.1)$$

$$\begin{aligned} \partial_t P(\mathbf{x}, t) = & \partial_{\mathbf{x}}(D_p \partial_{\mathbf{x}} P(\mathbf{x}, t) + \epsilon P(\mathbf{x}, t) \partial_{\mathbf{x}} S(\mathbf{x}, t)) \\ & - K_b(\mathbf{x}) P(\mathbf{x}, t) + K_f(\mathbf{x}) S(\mathbf{x}, t)^\eta. \end{aligned} \quad (3.2)$$

We assume that there is no external flux, $J(\mathbf{x}, t) = 0$ and the initial conditions are given by $S(\mathbf{x}, 0) = 1$ and $P(\mathbf{x}, 0) = 0$. These equations are supplemented by appropriate boundary conditions. The diffusion and the drift terms in Eq. (3.1) and Eq. (3.2) can be derived from the master equation (see Eq. (D)). For $\epsilon = 0$ the process is purely diffusive and describes a noninteracting system of particles. When $\epsilon \neq 0$ it describes a system in which particles of different species interact via volume exclusion. We have modeled this through an additional drift term for each species that depends on the gradient of concentration of the other species. This can be pictured in the following manner. Consider an adatom in the vicinity of a cluster. Due to thermal noise the diffusion term can be clearly written as $D_s \partial_{\mathbf{x}}^2 S$. It is to be noted that in Fickian diffusion arising from the nonuniformity of the chemical potential the form of the diffusive term remains same, except that self-diffusion coefficient D_s is replaced by cooperative diffusion coefficient [104]. In addition to this the adatom experiences a repelling force ($\epsilon > 0$) $-\epsilon \partial_{\mathbf{x}} P$ which appears as an additional drift term in Eq. (3.1) and similarly in Eq. (3.2). We note here that the surface defects help reaction to occur forming clusters in its neighborhood. On the other hand the cluster repels adatoms, thereby preventing them to reach the defect site. So, clearly the formation of cluster involves a competition between these two counter processes. The exclusion of one species of particle by the other species of particles we call here as cross-exclusion. When exclusion of a particle by their own kind is involved we will call it self-exclusion. In our model we have not included the self-exclusion-terms as it will only make the diffusion coefficient dependent on concentrations. In Sec. 3.3 we will consider a trapping reaction at a static defect to examine the effect of self-exclusion.

Our next aim is to analyze the solution of these coupled equations for a perturbative exclusion effect with keeping the reaction scheme linear as it is done in our earlier work [112]. We further consider a single point defect at the origin. Note that if $\epsilon = 0$ and $\eta = 1$ the above equation becomes linear. We can write $K_f(\mathbf{x}) = k_f \delta(\mathbf{x})$ and $K_b(\mathbf{x}) = k_b \delta(\mathbf{x})$. The above equation for the linear case with a single defect is exactly solvable and we get.

$$S(\mathbf{x}, t) = 1 - \frac{k_f}{2\sqrt{D_s}k} H_s(\mathbf{x}, t), \quad (3.3)$$

$$P(\mathbf{x}, t) = \frac{k_f}{2\sqrt{D_p}k} H_p(\mathbf{x}, t), \quad (3.4)$$

where $k = (k_f/\sqrt{D_s} + k_b/\sqrt{D_p})/2$ and the function $H_\alpha(\mathbf{x}, t)$ is given by

$$H_\alpha(\mathbf{x}, t) = \operatorname{erfc}\left(\frac{|\mathbf{x}|}{2\sqrt{D_\alpha t}}\right) - \exp(|\mathbf{x}|k/D_\alpha + k^2 t) \operatorname{erfc}\left(\frac{|\mathbf{x}|}{2\sqrt{D_\alpha t}} + kt\right). \quad (3.5)$$

For the nonlinear case i.e. for finite value of ϵ an analytical solution to the above set of equations cannot be obtained in a straight forward way.

Let us consider the nonlinear case $\epsilon \neq 0$ and $\eta = 1$ in one dimension with a single defect at the origin. We want to see the effect of a small exclusion ($0 < \epsilon \ll 1$) term. We assume that the solution to Eq. (3.1) and Eq. (3.2) can be written as [127]

$$S = S_0 + \epsilon S_1 + \dots + \epsilon^{n-1} S_{n-1} + O(\epsilon^n), \quad (3.6)$$

$$P = P_0 + \epsilon P_1 + \dots + \epsilon^{n-1} P_{n-1} + O(\epsilon^n), \quad (3.7)$$

where S_0 and P_0 are solutions of Eq. (3.1) and Eq. (3.2) with $\epsilon = 0$ and is given by Eq. (3.3) and Eq. (3.4) in one dimension. We can expand the Eq. (3.1) and Eq. (3.2) in a regular perturbation series in powers of ϵ , the resulting equations of order n will be the reaction diffusion equation with $\epsilon = 0$ and a source (sink) terms centered at the defect sites that are functions of solution of order $(n - 1)$ equations. The general n order equation can be written as

$$\partial_t S_n(x, t) = D_s \partial_x^2 S_n(x, t) - K_f(x) S_n(x, t) + K_b(x) P_n(x, t) + J_{s,n}(x, t), \quad (3.8a)$$

$$\partial_t P_n(x, t) = D_p \partial_x^2 P_n(x, t) - K_b(x) P_n(x, t) + K_f(x) S_n(x, t) + J_{p,n}(x, t), \quad (3.8b)$$

where $J_{s,0} = 0$ and $J_{p,0} = 0$, $J_{s,n}(\mathbf{x}, t)$ and $J_{p,n}(\mathbf{x}, t)$ are source (sink) functions that are written in terms of S_{n-k} , P_{n-k} , $\partial_{\mathbf{x}} S_{n-k}$ and $\partial_{\mathbf{x}} P_{n-k}$ for $1 < k < n$. Although these equations are linear, solving order by order is still very difficult due to the complicated source (sink) terms on the right hand side. It is also not our aim to find a perturbative solution of the problem at this point. We can gain ample insight by replacing Eq. (3.1) and Eq. (3.2) by a simpler set of equations.

For small ϵ we can make the following approximation in Eq. (3.1) and Eq. (3.2)

$$\epsilon \partial_{\mathbf{x}} S \simeq \epsilon \partial_{\mathbf{x}} S_0, \quad \epsilon \partial_{\mathbf{x}} P \simeq \epsilon \partial_{\mathbf{x}} P_0. \quad (3.9)$$

The resulting equations are a set of linear equations with variable coefficients. However, these equations are still far from being solvable. To simplify it further we shall use the properties of the functions $S_0(x, t)$ and $P_0(x, t)$. The gradients, $\partial_x S_0(x, t)$ and $\partial_x P_0(x, t)$ are odd functions in x and have a finite discontinuity at the reaction center $x = 0$. So, we have $\partial_x S_0(0^-, t) = -\partial_x S_0(0^+, t)$ and $\partial_x P_0(0^-, t) = -\partial_x P_0(0^+, t)$. Also we have $|\partial_x S_0(x, t)|$ and $|\partial_x P_0(x, t)|$ monotonically decreasing for $x \in (0, -\infty)$ or $x \in (0, \infty)$ and as $x \rightarrow \pm\infty$, $\partial_x S_0(x, t) = \partial_x P_0(x, t) = 0$. Therefore there exist $x = x^*, y^* > 0$ such that $0 \leq |\partial_x S_0(x^*, t)| \leq |\partial_x S_0(0^+, t)|$ and $0 \leq |\partial_x P_0(y^*, t)| \leq |\partial_x P_0(0^+, t)|$ for all $t > 0$.

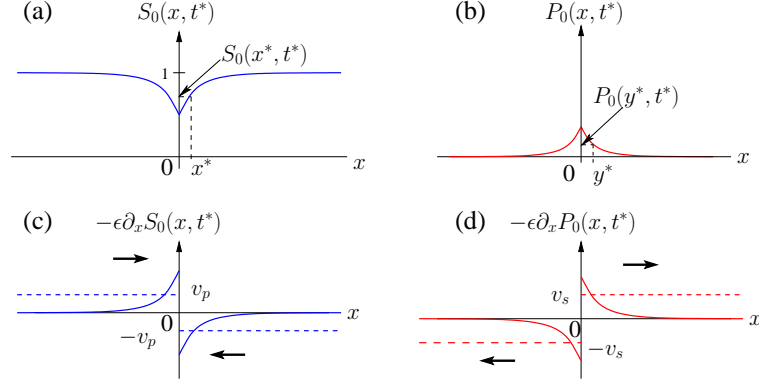


Figure 3.1: Schematic diagram: (a) adatom concentration $S_0(x, t^*)$, (b) cluster concentration $P_0(x, t^*)$, (c) exclusion term $-\epsilon \partial_x S_0(x, t^*)$ and (d) exclusion term $-\epsilon \partial_x P_0(x, t^*)$. Thick horizontal arrows in (c) denotes the direction of the repulsive force on the cluster particles P due to the adatoms. In (d) it denotes the direction of repulsive force on the adatoms S due to the clusters. $v_s = |\epsilon \partial_x P_0(y^*, t^*)|$ and $v_p = |\epsilon \partial_x S_0(x^*, t^*)|$ are drift speed of adatoms and cluster arising due to exclusion. Time $t^* \in [0, t]$ and $x = x^* > 0$ and $y^* > 0$ are points where the concentrations have the mean value.

We can make further approximations so that the gradients in Eq. (3.9) can be replaced by constants which is valid in some time interval $[0, t]$. Let us choose $x^*, y^* > 0$ and $t^* \in [0, t]$ such that it satisfies $H_s(x^*, t^*) = H_s(0, t^*)/2$ and $H_p(y^*, t^*) = H_p(0, t^*)/2$ (See Fig. 3.1). Solution of these equations give the values of x^* and y^* at which the concentrations has its mean value at some time t^* . In our calculations we have taken $t^* = t/2$. Equation Eq. (3.9) can now be written as

$$\epsilon \partial_x S \simeq v_p \text{sgn}(x), \epsilon \partial_x P \simeq -v_s \text{sgn}(x), \quad (3.10)$$

where $v_s = |\epsilon \partial_x P_0(y^*, t^*)|$ and $v_p = |\epsilon \partial_x S_0(x^*, t^*)|$ and $\text{sgn}(x) = 2(\theta(x) - 1/2)$ accounts for the discontinuity at the reaction center $x = 0$ ($\theta(x)$ is the Heaviside step function). Since we are replacing monotonically decreasing functions by constants the approximation Eq. (3.10) is valid in the neighborhood of the reaction center for a small time interval $[0, t]$. Note that in this approximation all the particles are moving into or away from the reaction center at constant speeds v_s and v_p but in the actual case this is not true when the gradients are monotonically decreasing. However, this overestimation of v_s and v_p will not alter the basic physics of the problem. We obtain the following simplified reaction diffusion equations

$$\begin{aligned} \partial_t S(x, t) &= D_s \partial_x^2 S(x, t) - v_s \text{sgn}(x) \partial_x S(x, t) \\ &\quad - (k_f + 2v_s) \delta(x) S(x, t) + k_b \delta(x) P(x, t), \end{aligned} \quad (3.11)$$

$$\begin{aligned}\partial_t P(x, t) &= D_p \partial_x^2 P(x, t) + v_p \text{sgn}(x) \partial_x P(x, t) \\ &\quad - (k_b - 2v_p) \delta(x) P(x, t) + k_f \delta(x) S(x, t).\end{aligned}\quad (3.12)$$

Here we note that, two very interesting features arise due to the effect of exclusion. First, it gives an extra drift term with velocity which is either into or away from the defect site. Secondly, it modifies the reaction rates and the reaction terms become different for two reacting species breaking constraints of our kinetic scheme (see Eq. (3.1) and Eq. (3.2)). Let us define $\tilde{k}_f = k_f + 2v_s$ and $\tilde{k}_b = k_b - 2v_p$. The Eq. (3.11) and Eq. (3.12) after Laplace transform can be written in an abstract notation [30] as the following

$$|\phi(s)\rangle = G_s(s) \left[-\tilde{K}_f |\phi(s)\rangle + K_b |\psi(s)\rangle + |J(s)\rangle \right], \quad (3.13)$$

$$|\psi(s)\rangle = G_p(s) \left[-\tilde{K}_b |\psi(s)\rangle + K_f |\phi(s)\rangle \right], \quad (3.14)$$

where $\langle x | \phi(s) \rangle = \phi(x, s)$ and $\langle x | \psi(s) \rangle = \psi(x, s)$ are the Laplace transform of $S(x, t)$ and $P(x, t)$ respectively. The flux term appears due to the initial condition $S(x, 0) = 1 = \langle x | J(s) \rangle$. The reaction operators are defined by $\delta(x - x') k_\alpha \delta(x) = \langle x | K_\alpha | x' \rangle$ and $\delta(x - x') \tilde{k}_\alpha \delta(x) = \langle x | \tilde{K}_\alpha | x' \rangle$. The Green's functions $G_s(s)$ and $G_p(s)$ are defined by

$$G_s(s) = [s - D_s \partial_x^2 + v_s \text{sgn}(x) \partial_x]^{-1}, \quad (3.15)$$

$$G_p(s) = [s - D_p \partial_x^2 - v_p \text{sgn}(x) \partial_x]^{-1}. \quad (3.16)$$

The expressions for the Green's functions in Eq. (3.15) and Eq. (3.16) are given in A.2. Next consider diffusion of adatoms on a surface without defects. If we choose the initial concentration $S(x, 0) = \delta(x)$, we know that it will evolve as Gaussian as there is no cluster formation. Now suppose that we introduce a force field at the origin such that it gives rise to a constant drift velocity v_s in the outward direction. The diffusion of adatoms can be described by the following equation

$$\partial_t S(x, t) = \partial_x [D_s \partial_x - v_s \text{sgn}(x) \partial_x] S(x, t) \quad (3.17)$$

In the Laplace domain we can write

$$\phi(x, s) = \frac{G_s(x|0)}{1 + 2v_s G_s(0|0)}. \quad (3.18)$$

Here $\phi(x, s)$ is the Laplace transform of $S(x, t)$. For brevity the Laplace variable s is kept implicit in $G_s(x|x')$. Using the expression for the Green's function Eq. (A.5) and Eq. (A.6) in

Eq. (3.18) and taking inverse Laplace transform, the solution of Eq. (3.17) can be written as

$$S(x, t) = \frac{1}{\sqrt{4\pi D_s t}} \exp\left(\frac{-(|x| - v_s t)^2}{4D_s t}\right) - \frac{v_s}{4D_s} e^{v_s|x|/D_s} \operatorname{erfc}\left(\frac{|x| + v_s t}{2\sqrt{D_s t}}\right). \quad (3.19)$$

Looking at Eq. (3.19) we note from the first term that adatoms are pushed away from the origin to a distance $v_s t$. The second term has a minimum at the origin and reduces the concentration by small amount which is of the order v_s .

Now returning to our reaction diffusion problem we should expect that, in the presence of exclusion, adatoms will experience an extra repulsive force which is directed outward from the center of the surface defect. From Eq. (3.13) and Eq. (3.14) we obtain

$$\phi(x, s) = Q(x) - \frac{\tilde{k}_f G_s(x|0)Q(0)}{\Delta} - \frac{(\tilde{k}_f \tilde{k}_b - k_f k_b) G_s(x|0) G_p(0|0) Q(0)}{\Delta}, \quad (3.20)$$

$$\psi(x, s) = \frac{k_f G_p(x|0)Q(0)}{\Delta}, \quad (3.21)$$

where

$$\Delta = 1 + \frac{\tilde{k}_f}{2D_s(-\rho_s + \gamma_s)} + \frac{\tilde{k}_b}{2D_p(-\rho_p + \gamma_p)} + \frac{\tilde{k}_f \tilde{k}_b - k_f k_b}{4D_s D_p (-\rho_s + \gamma_s)(-\rho_p + \gamma_p)}, \quad (3.22)$$

$\rho_s = v_s/(2D_s)$, $\rho_p = -v_p/(2D_p)$, $\gamma_s = \sqrt{\rho_s^2 + s/D_s}$ and $\gamma_p = \sqrt{\rho_p^2 + s/D_p}$. The function $Q(x) = \langle x|G_s(s)|J \rangle = 1/s$.

The inverse Laplace transformation of $\phi(x, s)$ and $\psi(x, s)$ is performed numerically by Talbot method [32] which we denote by $S_l(x, t)$ and $P_l(x, t)$ respectively. In Fig. 3.2 (a) and 3.2 (b) we have plotted the concentrations for the case $\epsilon = 0$ denoted by S_0, P_0 , actual numerical solution S, P of (3.1) and (3.2) obtained by finite difference method and the solution of the modified linear equations S_l, P_l . The parameters are $\epsilon = 0.1$, $D_s = 1$, $D_p = 0.25$, $k_f = 1.0$, $k_b = 0.1$ and $t = 1.0$. In Fig. 3.2(b), we note that the solution S_l and P_l and the numerical solution S and P at a point close to the defect site have reduced as compared to the bare case, i.e. $\epsilon = 0$ concentrations, S_0, P_0 . The current due to diffusion and the drift current are in opposite directions for both adatom and cluster which effectively reduces the number of particle at the origin. However, this is true only for small value of $0 < \epsilon \ll 1$. For higher values of ϵ the diffusion and the drift currents will be comparable and the higher order terms in ϵ will also have a significant contribution (see Fig. 3.4).

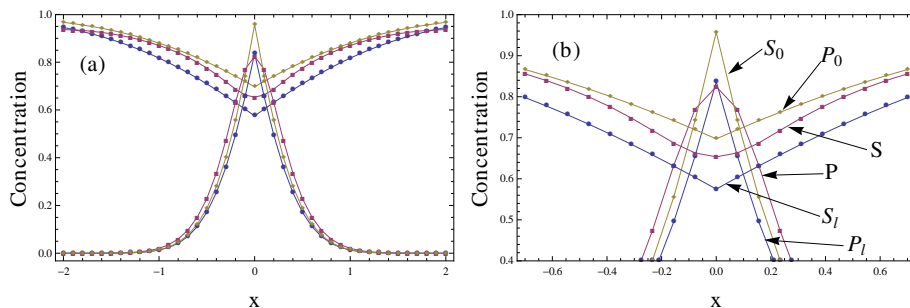


Figure 3.2: (a) Concentrations: Numerical solution S, P , solution without exclusion ($\epsilon = 0$) S_0, P_0 and solutions of the simplified linear equation S_l, P_l , (b) Concentrations close to the defect at the origin.

3.3 Trapping reaction with self-exclusion

To understand the effect of self-exclusion we consider a single diffusing species with a trap at the origin. We assume that particles interact among themselves, so we introduce a self-exclusion term proportional to the density gradient as we have done in the previous section. When a particle reaches the trap site it gets trapped with a time-independent rate constant κ . The reaction diffusion equation for the problem is then

$$\partial_t u(x, t) = \partial_x (D_0 \partial_x u(x, t) + \epsilon u(x, t) \partial_x u(x, t)) - \kappa \delta(x) u(x, t). \quad (3.23)$$

We use the initial condition $u(x, 0) = 1$ along with appropriate boundary conditions [128]. By rearranging terms in Eq. (3.23) the term due to exclusion can simply be absorbed in a concentration dependent diffusion coefficient, $D(u) = D_0(1 + \epsilon u)$ (here ϵ is redefined as $\epsilon = \epsilon/D_0$). We note that with self-exclusion the current due to diffusion and drift are in the same direction as this can be seen from the expression for the current $j(u) = -D(u)\partial_x u$. For $\epsilon = 0$, Eq. (3.23) has an exact solution [21]. Let us consider the case of a small reaction rate $\kappa \ll 1$ and $\epsilon \neq 0$.

With no loss of generality, setting $D_0 = 1$ we expand Eq. (3.23) in terms of perturbation series in κ [127].

$$u = u_0 + \kappa u_1 + \kappa^2 u_2 + O(\kappa^3). \quad (3.24)$$

The solution $u_0 = 1$ satisfy the zeroth order equation. The equations for u_1 and u_2 are given by

$$\partial_t u_1 = (1 + \epsilon) \partial_x^2 u_1 - \delta(x), \quad u_1(x, 0) = 0, \quad (3.25)$$

$$\partial_t u_2 = (1 + \epsilon) \partial_x^2 u_2 - \delta(x) u_1 + \epsilon \partial_x (u_1 \partial_x u_1), \quad u_2(x, 0) = 0. \quad (3.26)$$

Equation (3.25) describe diffusion with an external flux which for this case is a negative point flux at the origin. In Eq. (3.26) the expression $\epsilon \partial_x(u_1 \partial_x u_1)$ albeit exactly known is quite complicated. It is maximum at the origin and monotonically decreases with increasing values of $|x|$ and vanishes at infinity. Inasmuch as we are interested in the behavior of the solution at a finite time, we can replace this term by a point flux at the origin without compromising the basic physics. This assumption is valid only for small t . We have

$$\partial_x(u_1 \partial_x u_1) \simeq j_0 \delta(x), \quad (3.27)$$

where $j_0 = \lim_{x \rightarrow 0} \partial_x(u_1 \partial_x u_1) = (\pi + 2)/(4\pi(1 + \epsilon)^2)$. Substituting Eq. (3.27) in Eq. (3.26) and solving Eq. (3.25) and (3.26) we have

$$\begin{aligned} u(x, t) = & 1 - \frac{\kappa - \epsilon \kappa^2 j_0}{2\sqrt{1 + \epsilon}} \left[2\sqrt{\frac{t}{\pi}} \exp\left(\frac{-x^2}{4(1 + \epsilon)t}\right) - \frac{|x|}{\sqrt{1 + \epsilon}} \operatorname{erfc}\left(\frac{|x|}{2\sqrt{(1 + \epsilon)t}}\right) \right] \\ & + \frac{\kappa^2}{4(1 + \epsilon)} \left[\left(\frac{x^2}{2(1 + \epsilon)} + t\right) \operatorname{erfc}\left(\frac{|x|}{2\sqrt{(1 + \epsilon)t}}\right) \right. \\ & \left. - |x| \sqrt{\frac{t}{\pi}} \exp\left(\frac{-x^2}{4(1 + \epsilon)t}\right) \right] + O(\kappa^3). \end{aligned} \quad (3.28)$$

Let $\tilde{u}(x, t) = \lim_{\epsilon \rightarrow 0} u(x, t)$ be the concentration when there is no self-exclusion. Define by $\Delta u = u(x, t) - \tilde{u}(x, t)$, the difference in the concentration. From Eq. (3.28) we note that the concentration at the origin has increased due to the flux term j_0 and we have $\Delta u \simeq (1 - 1/\sqrt{1 + \epsilon})\kappa\sqrt{t/\pi} + \kappa^2 \epsilon j_0 \sqrt{t/(\pi(1 + \epsilon))} - (1 - 1/(1 + \epsilon))\kappa^2 t/4$. For $\epsilon = 0.5$, $\kappa = 0.2$ at $t = 1.0$ we have $\Delta u = 0.019$ and the corresponding numerical solutions give $\Delta u_{numerical} = 0.0154$ see Fig. (3.3). We see that in this case the effect is exactly the opposite (compare Fig. 3.2 for the multispecies case). Furthermore, the width of the depletion zone has increased due to the increase in the diffusion coefficient by ϵ .

3.3.1 Survival probability

In chapter 1 we discussed the survival probability for the “trapping reaction-diffusion” problem in one dimension. We observed that the survival probability decays slower than exponential decay. Here, we shall discuss the effect of self-exclusion on survival probability. We recall from Eq. (1.43) that, for the case of perfect traps i.e. limit $\kappa \rightarrow \infty$ the problem reduces to solving the diffusion equation in a finite domain $[-a, a]$ with absorbing boundary condition.

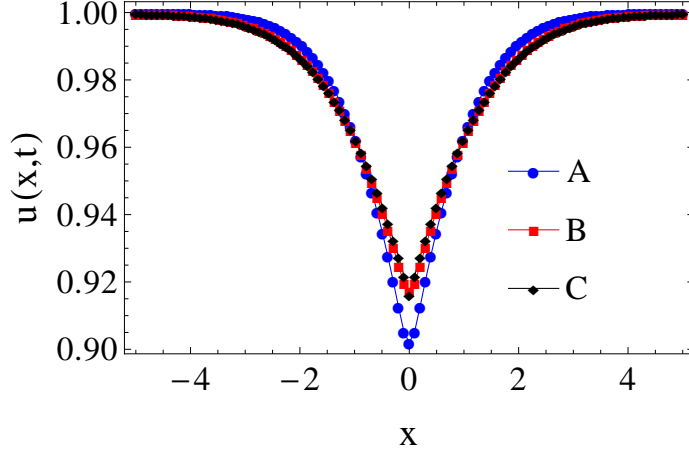


Figure 3.3: Concentration $u(x, t)$ numerical solution (A) without exclusion $\epsilon = 0.0$ and with exclusion $\epsilon = 0.5$ (B) numerical solution, (C) analytical solution (3.28) for $\kappa = 0.2$ and time $t = 1.0$. The difference between (A) and (C) at $x = 0$ is Δu .

With self-exclusion we have

$$\partial_t u = \partial_x((1 + \epsilon u)\partial_x u), \quad x \in [-a, a], t > 0. \quad (3.29)$$

The initial concentration $u(x, 0) = 1$ and the absorbing boundary condition is $u(\pm a, t) = 0$.

Let us consider the following eigenvalue problem

$$\partial_x((1 + \epsilon\psi)\partial_x\psi) + \lambda\psi = 0, \quad x \in [-a, a]. \quad (3.30)$$

To understand the behavior of the survival probability for we need to know how the eigenvalue λ get modified for nonzero ϵ . For small ϵ we can write [127]

$$\begin{aligned} \psi &= \psi_0 + \epsilon\psi_1 + \epsilon^2\psi_2 + \dots, \\ \lambda &= \lambda_0 + \epsilon\lambda_1 + \epsilon^2\lambda_2 + \dots \end{aligned} \quad (3.31)$$

Substituting Eq. (3.31) in Eq. (3.30) we obtain

$$O(1) : \quad \partial_x^2\psi_0 + \lambda_0\psi_0 = 0, \quad (3.32a)$$

$$O(\epsilon) : \quad \partial_x^2\psi_1 + \lambda_0\psi_1 = -\lambda_1\psi_0 - \partial_x(\psi_0\partial_x\psi_0), \quad (3.32b)$$

$$O(\epsilon^2) : \quad \partial_x^2\psi_2 + \lambda_0\psi_2 = -\lambda_1\psi_1 - \lambda_2\psi_0 - \partial_x(\psi_1\partial_x\psi_0 + \psi_0\partial_x\psi_1). \quad (3.32c)$$

The above set of linear equation can be solved with the absorbing boundary conditions $\psi_m(\pm a) =$

0, $m = 0, 1, 2, \dots$. The eigenvalues and the eigenfunctions of Eq. (3.32a) are given by

$$\psi_0^{(n)}(x) = \frac{1}{\sqrt{a}} \begin{cases} \cos(n\pi x/2a), & \text{if } n \text{ is odd,} \\ \sin(n\pi x/2a), & \text{if } n \text{ is even,} \end{cases} \quad (3.33)$$

$$\lambda_0^{(n)} = \frac{n^2\pi^2}{4a^2} \text{ for } n = 1, 2, \dots \quad (3.34)$$

Similarly, from Eq. (3.32b) after setting $\lambda_0 = \lambda_0^{(n)}$ and $\psi_0 = \psi_0^{(n)}$ we have

$$\partial_x^2 \psi_1 + \lambda_0^{(n)} \psi_1 = -\lambda_1 \psi_0^{(n)} - \partial_x(\psi_0^{(n)} \partial_x \psi_0^{(n)}). \quad (3.35)$$

Let ψ_1 be written as the sum $\psi_1 = \sum_m A_m \psi_0^{(m)}$ which satisfies the boundary condition. From Eq. (3.35) we obtain

$$A_m(\lambda_0^{(n)} - \lambda_0^{(m)}) = -\lambda_1 \delta_{m,n} - \int_{-a}^{+a} \partial_x(\psi_0^{(n)} \partial_x \psi_0^{(n)}) \psi_0^{(m)} dx \quad (3.36)$$

Using Eq. (3.33), Eq. (3.34) and Eq. (3.36) we can write for odd n

$$\int_{-a}^{+a} \partial_x(\psi_0^{(n)} \partial_x \psi_0^{(n)}) \psi_0^{(m)} dx = -\frac{\lambda_0^{(n)}}{\sqrt{a}} \mu_{n,m} \quad (3.37)$$

where $\mu_{n,m} = (4m \cos(n\pi) \sin(m\pi/2) - 8n \cos(m\pi/2) \sin(n\pi)) / (\pi(m^2 - 4n^2))$ for m odd otherwise $\mu_{n,m} = 0$. Similarly for even n we can calculate $\mu_{n,m}$. Here we will not require to calculate beyond $\mu_{1,1}$ since we only need $\lambda^{(1)} = \lambda_0^{(1)} + \epsilon \lambda_1^{(1)}$ to determine the behavior of the asymptotic survival probability. The eigenfunctions and the eigenvalues for $n = 1$ can be written as

$$\begin{aligned} \psi^{(1)} &= \psi_0^{(1)} + \frac{\epsilon}{\sqrt{a}} \sum_{m=1}^{\infty} \mu_{1,m} \frac{\lambda_0^{(1)}}{\lambda_0^{(1)} - \lambda_0^{(m)}} \psi_0^{(m)}, \\ \lambda^{(1)} &= \lambda_0^{(1)} \left(1 + \frac{\epsilon \mu_{1,1}}{\sqrt{a}} \right). \end{aligned} \quad (3.38)$$

In Sec. 1.4.2 we obtained the stretched exponential behavior by taking into account $n = 1$ case only. The behavior of the survival probability can therefore be found from (cf. Eq. (1.45) and Eq. (1.46))

$$P(t) \sim \int_0^{\infty} \exp(-\lambda^{(1)}(x)t) \rho^2 4x e^{-2\rho x} dx \quad (3.39)$$

We will use the Laplace method to evaluate Eq. (3.39) as done by Balagurov and Vaks [96]. The exponent in Eq. (3.39) can be explicitly written as

$$f(x) = -\frac{\pi^2}{x^2} \left(1 + \frac{\sqrt{2}\epsilon \mu_{1,1}}{\sqrt{x}} \right) t - \rho x. \quad (3.40)$$

The function $f(x)$ attains maximum at

$$\tilde{x} \simeq x^* + \epsilon \frac{5\mu_{1,1}}{6\sqrt{2}} \sqrt{x^*} \quad (3.41)$$

where $x^* = (2\pi^2 t / \rho)^{1/3}$. The integral Eq. (3.39) becomes

$$\begin{aligned} P(t) &\sim c \exp(f(\tilde{x})), \\ &= c \exp\left(\frac{-3(\rho^2 \pi^2 t)^{1/3}}{2^{2/3}} - \epsilon \mu_{1,1} \left(\frac{\pi}{2}\right)^{1/3} \rho^{5/6} t^{1/6}\right) \end{aligned} \quad (3.42)$$

where $c = \left(\frac{\pi}{2f''(\tilde{x})}\right)^{1/2} \tilde{x}$, $\mu_{1,1} = 4/3\pi$. The derivation of the result Eq. (3.42) is based on the fact that the eigenvalues get modified due to exclusion which affects the exponent on averaging over disorder. We note that an extra correction term $\sim t^{1/6}$ appear in the exponent. It would be interesting to calculate the survival probability in arbitrary dimension in a more rigorous manner so that all modes contribute to the survival probability.

3.4 Numerical results

The well known finite difference method [129] is used to compute the solution of Eq. (3.1) and Eq. (3.2) numerically. In one dimension we will first examine the effect of exclusion and nonlinearity on the shape of the concentration profile with a reaction center at the origin. The parameters used are $D_s = 1.0$, $D_p = 0.25$, $k_f = 1.0$ and $k_b = 0.1$. In Fig. 3.4 (a) and 3.4(b) we have plotted concentration $S(x, t)$ for $\eta = 1, 2$ and 3 at $\epsilon = 0.2$ and time $t = 1.0$. The concentration of S is decreases with increase in η . The variation of concentrations with different values of the exclusion parameter $\epsilon = 0.0, 0.1, 0.2$ and 0.3 are shown in Fig. 3.4 (c) and 3.4 (d). Here as we increase ϵ , the concentration $S(x, t)$ decreases. It has already been discussed in our study of the modified linear equations (see Eq. (3.11) and (3.12)). It is shown that exclusion effect modifies the reaction rate at the reaction center and consequently the concentration decreases. We also note that change in concentration $P(x, t)$ with ϵ is negligible for $\epsilon \ll 1$. This is also due to the fact that change in $P(x, t)$ due to exclusion is not first order in ϵ . We have also found that the width of the concentration profile of P reduces as the parameter ϵ is increased. In Fig. (3.5) we have calculated the FWHM for the concentration $P(x, t)$ for different values of η . This clearly indicates that exclusion or/and nonlinearity suppress the formation of clusters. In Fig. 3.6 we have plotted the concentration profile of P in two dimensions. Here we have used the same set of parameters as in the one dimension case. The number of defects

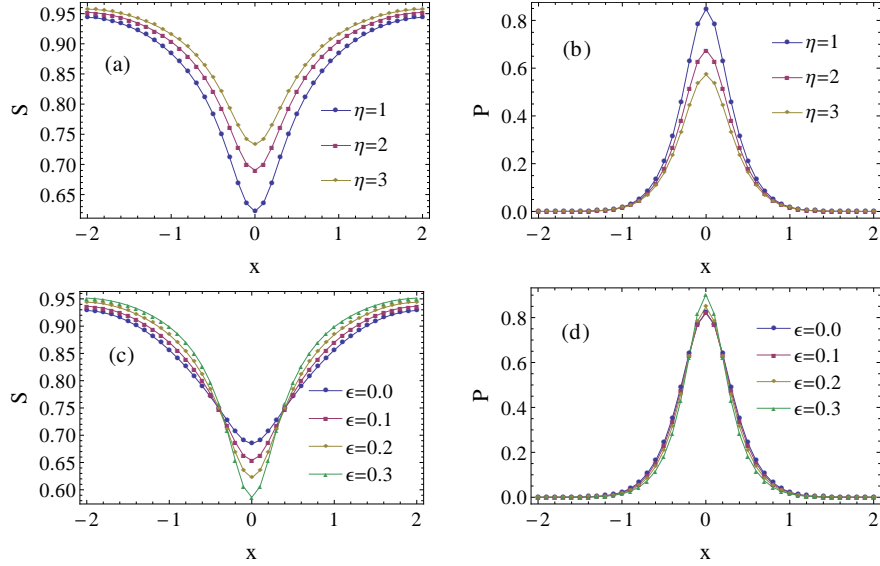


Figure 3.4: Variation of concentration with exclusion and nonlinearity. (a) and (b) $\epsilon = 0.2$ and $\eta = 1, 2, 3$, (c) and (d) $\eta = 1$, $\epsilon = 0.0, 0.1, 0.2, 0.3$. The parameters are $D_s = 1.0$, $D_p = 0.25$, $k_f = 1.0$ and $k_b = 0.1$ and $t = 1.0$.

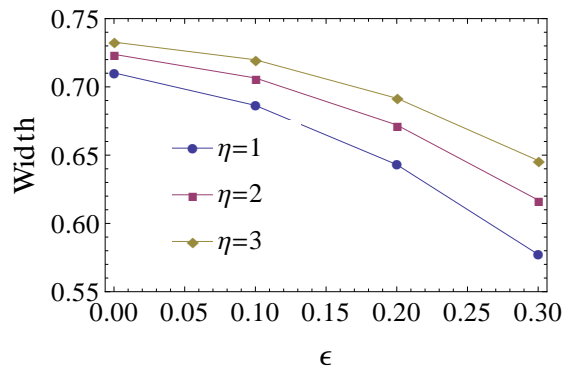


Figure 3.5: Width of concentration $P(x, t)$ for $D_s = 1.0$, $D_p = 0.25$, $k_f = 1.0$ and $k_b = 0.1$ and $t = 1.0$, $\eta = 1, 2, 3$.

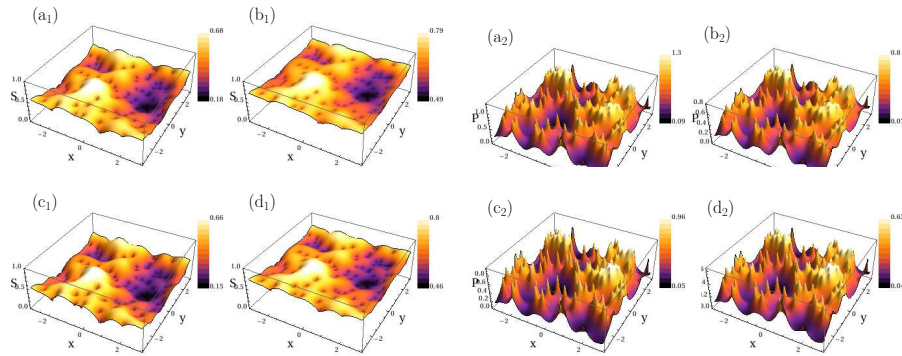


Figure 3.6: Formation of clusters in the presence of exclusion. (a_{1,2}) $\epsilon = 0$, $\eta = 1$, (b_{1,2}) $\epsilon = 0$, $\eta = 3$, (c_{1,2}) $\epsilon = 0.2$, $\eta = 1$, (d_{1,2}) $\epsilon = 0.2$, $\eta = 3$ for $D_s = 1.0$, $D_p = 0.25$, $k_f = 1.0$ and $k_b = 0.1$ and $t = 1.0$.

is 100 which is uniformly distributed in the region $-3 \leq x \leq 3$ and $-3 \leq y \leq 3$. For a given randomly distributed defects we have plotted concentration $P(x, y, t)$. Here also we see that as we go from $\epsilon = 0$ to $\epsilon = 0.2$ keeping $\eta = 1$ fixed the concentration decreases. The concentration is also found to decrease as we increase the nonlinearity from $\eta = 1$ to $\eta = 3$. In Fig. 3.7 we have calculated the mean concentration averaged over the randomness of defect distribution. The decay of concentration S monotonically decreases with time and the rate of its decay slows down as η is increased. Similarly for P its mean concentration increases with time and its concentration for any given time t increases with increase in η . We also note that the mean concentration for both S and P decreases with increasing ϵ . This clearly suggests that both exclusion and nonlinearity suppress the formation of cluster and the effect of both is additive.

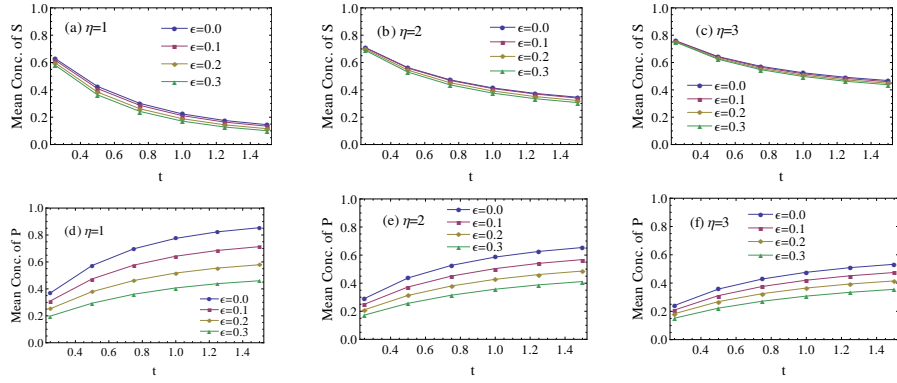


Figure 3.7: Mean concentrations of adatoms S for (a) $\eta = 1$, (b) $\eta = 2$, (c) $\eta = 3$ and cluster P for (d) $\eta = 1$, (e) $\eta = 2$, (f) $\eta = 3$ and $D_s = 1.0$, $D_p = 0.25$, $k_f = 1.0$ and $k_b = 0.1$ and $0.25 \leq t \leq 1.5$.

Chapter 4

Conclusion

The presence of randomness is ubiquitous in nature. The aim of our study was to explain the formation of random clusters that we observed in our experiments. We found that these patterns can be explained by simple reaction diffusion models in which disorder play a very important role. Our results gives a qualitative understanding of the cluster formation processes.

In our linear models we presented a simple model which captures the essential features of reaction-diffusion processes on surfaces having defects. The solution to the problem was obtained by the method of Green's functions. The reaction part of the equation was used as perturbation which was found to be exactly summable. Our model describes qualitatively the observed features of pattern formation in Ge clustering on clean Si(111)-(7 × 7) and oxidized Si(111)-(7 × 7) surfaces. First we had shown the formation of patterns in the ring model with four ring defects. The point model was discussed in detail. The time evolution of the reaction diffusion process was explored numerically from the solutions obtained for a case of eight defects distributed uniformly inside the domain.

We used further Monte Carlo simulations to study the point model case for a large number of defects. The first passage time statistics was also studied and obtained empirically the first passage time probability density. These models presented here are real time analysis of the deposition-diffusion-reaction process. It would be very interesting if a thorough time analysis of the formation of patterns is carried out experimentally in future. Finally we note that in this model the product P describes n-mers, $n = 2, 3, \dots$ we assume that all n-mers have the same diffusion coefficient. However, we believe, this assumption does not seriously affect the result obtained here. In earlier studies on fractal patterns formed in diffusion limited cluster aggregation, the fractal pattern and the fractal dimension were found to be practically the same for the two cases where (i) all clusters have been assumed to have the same diffusion coefficient

and (ii) diffusion coefficient was assumed to be inversely proportional to the cluster mass [130]. Definitely, there will be some optimum size of the cluster with dispersion. So, an improved model must include a sequence of reactions forming clusters.

Furthermore, we studied the effect of exclusion on the formation of cluster in the presence of surface defects. In our reaction diffusion model we have introduced exclusion through a repulsive interaction between the particles of dissimilar nature. This repulsive force is taken to be proportional to the gradient of concentration and a set of coupled Smoluchowsky equations is obtained. In the perturbative regime a set of modified linear reaction-diffusion equation as an approximation to the actual process is considered and this gave us important understanding of the effect of exclusion on the formation of clusters in the reaction diffusion processes. The solutions to these equation are obtained using Green's function method [131]. The most important conclusion of this work is that, both exclusion and nonlinear reaction processes considered here suppress the formation of cluster. The effect of self-exclusion on diffusion in one dimension with a trapping reaction at the origin is studied. It is found that self-exclusion can give rise to a concentration dependent diffusion coefficient as obtained in earlier works [121]. The width of the depletion zone is found to increase by ϵ (strength of exclusion). Our numerical studies in one dimension showed that the width of the cluster concentration profile decreases with increasing ϵ . We investigated how exclusion affects the survival probability for trapping reaction. In two dimensions we calculated the mean concentrations averaged over the surface disorder are calculated. It is found that the mean concentration of adatoms S decreases monotonically where as the mean concentration of P increases monotonically in time respectively. However, for higher exclusion and nonlinearity these mean concentrations are found to decrease with the increase in exclusion and nonlinearity in the reaction scheme.

There can be quite a few extension of the present work. For example, in this model, the repulsive potential is considered to be simple linear function of concentration. But, it is indeed possible for this potential to depend nonlinearly on concentration. This needs to be explored. Furthermore, we have considered here a simple algebraic nonlinearity in the reaction scheme. This is due to the lack of sufficient knowledge of the reaction scheme for the formation of Ge-clusters on Si surfaces. As this model can be used in other physical situations, different types of nonlinear exclusion potential and reaction scheme can be studied.

Appendix A

Green's function

A.1 Green's functions-I

The Green's function appearing in Eq. (2.3) are given by

$$G_s^{(1)}(r, \theta|r', \theta') = \sum_{n=0}^{\infty} \left(g_n(r|r') - \frac{g_n(r|R)g_n(R|r')}{g_n(R|R)} \right) \cos(n(\theta - \theta')),$$

$$G_p^{(0)}(r, \theta|r', \theta') = \sum_{n=0}^{\infty} h_n(r|r') \cos(n(\theta - \theta')), \quad (\text{A.1})$$

$$\text{where } g_n(r|r') = \begin{cases} \epsilon_n I_n(\sqrt{s/D_s}r) K_n(\sqrt{s/D_s}r') & \text{if } r \leq r', \\ \epsilon_n I_n(\sqrt{s/D_s}r') K_n(\sqrt{s/D_s}r) & \text{if } r > r'. \end{cases} \quad (\text{A.2})$$

$$h_n(r|r') = \begin{cases} \epsilon_n I_n(\sqrt{s/D_p}r) K_n(\sqrt{s/D_p}r') & \text{if } r \leq r', \\ \epsilon_n I_n(\sqrt{s/D_p}r') K_n(\sqrt{s/D_p}r) & \text{if } r > r'. \end{cases} \quad (\text{A.3})$$

with $\epsilon_0 = 1$ and $\epsilon_n = 2$ for all $n = 1, 2, \dots$

A.2 Green's functions-II

The Green's function in (3.15) and (3.16) has the following form

$$G_\alpha(s) = [s - D_\alpha \partial_x^2 + v_\alpha \text{sgn}(x) \partial_x]^{-1} \quad (\text{A.4})$$

$$G_\alpha(x|x') = \begin{cases} \exp(-\rho_\alpha(x - x')) A_\alpha(x, x') & \text{if } x < x' < 0 \\ \exp(-\rho_\alpha(x - x')) A_\alpha(x', x) & \text{if } x' < x < 0, \\ \frac{1}{2D_\alpha(-\rho_\alpha + \gamma_\alpha)} \exp(\rho_\alpha(x + x') - \gamma_\alpha(x - x')) & \text{if } x' < 0 < x, \end{cases} \quad (\text{A.5})$$

and

$$G_\alpha(x|x') = \begin{cases} \frac{1}{2D_\alpha(-\rho_\alpha + \gamma_\alpha)} \exp(-\rho_\alpha(x + x') - \gamma_\alpha(x' - x)) & \text{if } x < 0 < x', \\ \exp(\rho_\alpha(x - x')) B_\alpha(x, x') & \text{if } 0 < x < x' \\ \exp(\rho_\alpha(x - x')) B_\alpha(x', x) & \text{if } 0 < x' < x, \end{cases} \quad (\text{A.6})$$

where $A_\alpha(x, x') = \frac{1}{2D_\alpha\gamma_\alpha} \left(\exp(\gamma_\alpha(x - x')) - \frac{\rho_\alpha}{\rho_\alpha - \gamma_\alpha} \exp(\gamma_\alpha(x + x')) \right)$ and
 $B_\alpha(x, x') = \frac{1}{2D_\alpha\gamma_\alpha} \left(\exp(\gamma_\alpha(x - x')) - \frac{\rho_\alpha}{\rho_\alpha - \gamma_\alpha} \exp(-\gamma_\alpha(x + x')) \right)$. Here $\rho_\alpha = v_\alpha/(2D_\alpha)$ and
 $\gamma_\alpha = \sqrt{\rho_\alpha^2 + s/D_\alpha}$ are constants.

Appendix B

The Talbot Method

We describe the fixed Talbot algorithm to compute the Inverse Laplace transform of a function $\hat{f}(s)$. The Inverse Laplace transform of $\hat{f}(s)$ is given by

$$f(t) = \frac{1}{2\pi i} \int_B \exp(st) \hat{f}(s) ds, \quad (\text{B.1})$$

where B denotes the Bromwich contour defined by the vertical line $s = r + iy$, $-\infty < y < \infty$ and a curve joining the endpoints at infinity such that all branch points remains outside the contour. The Talbot algorithms computes the inverse Laplace transform by deforming the contour B . The deformed contour is (cf. Fig. (B.1))

$$s(\theta) = r\theta(\cot \theta + i), \quad -\pi < \theta < \pi. \quad (\text{B.2})$$

The expression in Eq. (1) thus becomes

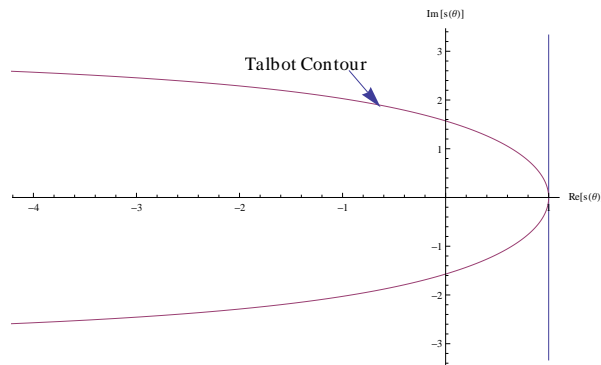


Figure B.1: The Talbot contour Eq. (B.2) and vertical line $s = r + iy$, $-\infty < y < \infty$. Parameter $r = 1$.

$$f(t) = \frac{1}{2\pi i} \int_{-\pi}^{\pi} \exp(s(\theta)t) \hat{f}(s(\theta)) s'(\theta) d\theta, \quad (\text{B.3})$$

where $s'(\theta) = ir(1 + i\sigma(\theta))$ with $\sigma(\theta) = \theta + (\theta \cot \theta - 1) \cot \theta$. So Eq. (3) can now be written as

$$f(t) = \frac{r}{\pi} \int_0^{\pi} \mathbf{Re} \left[\exp(s(\theta)t) \hat{f}(s(\theta)) (1 + i\sigma(\theta)) \right] d\theta, \quad (\text{B.4})$$

Since the above integral is evaluated over a finite range 0 to π we adopt a trapezoidal integration of Eq() as given in Ref. [32]

$$f(t) = \frac{r}{M} \left(\frac{1}{2} \hat{f}(r) e^{rt} + \sum_{k=1}^{M-1} \mathbf{Re} \left[\exp(s(\theta_k)t) \hat{f}(s(\theta_k)) (1 + i\sigma(\theta_k)) \right] \right), \quad (\text{B.5})$$

where $\theta_k = k\pi/M$ for all $k = 1, 2, \dots, M - 1$ and $r = 2M/5t$. So finally there is only a single free parameter M which can be varied to obtain results at desired precession.

Appendix C

Derivation of the kinetic equations

C.1 Kinetic equation for linear model

We denote by S_n a cluster of $n = 2, 3, \dots, N$ Ge atoms. Various possible one step reactions may occur at a reaction center in which cluster of size n could break to form a cluster of size $n - 1$ or an adatom S could coalesce to form a cluster of size $n + 1$ (see Fig. C.1). The rate equation are given by

$$\begin{aligned} \frac{dS_n}{dt} &= -(k_{-(n-1)} + k_n S) S_n \\ &\quad + (k_{n-1} S S_{n-1} + k_n S_{n+1}), \end{aligned} \quad (\text{C.1})$$

$$\frac{dS_N}{dt} = k_{N-1} S S_{N-1} - k_{-(N-1)} S_N, \quad (\text{C.2})$$

where $2 \leq n \leq N - 1$.

$$\frac{d}{dt} \sum_{n=2}^N S_n = (k_1 S) S - k_{-1} S_2. \quad (\text{C.3})$$

We now make the following assumptions (i) All clusters, S_2 to S_N have comparable diffusion coefficients. So, in the first approximation, these can be taken equal. (ii) If $P = \sum_{n=2}^N S_n$, we assume that formation of larger clusters at the reaction centers is a very slow process and P is dominated by S_2 . So, we replace S_2 by $\sum_{n=2}^N S_n$. This need arises for two considerations.

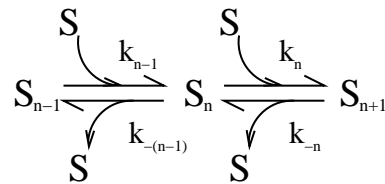


Figure C.1: Reaction scheme.

Firstly we have no knowledge of N , though it will not be very large. Secondly, since we want a minimal model which is able to capture the basic physics, we make this approximation to close the equation. So, the assumption is made that the clusters are predominantly of two Ge-atoms. (iii) Even though the formation process is a second order rate process in S , we replace $k_1 S$ by k_f which we call intrinsic clusterization rate of each available reaction center. The rate k_{-1} is redefined as k_b .

Albeit the assumptions incorporated in our model for cluster formation on Si surfaces, appears too simplistic, we are strongly of the opinion that inclusion of all the processes in the clusterization will not significantly change the overall result. On the other hand as we are solving this problem numerically, inclusion of all possible processes of clusterization will increase the time and cost significantly without gaining much in physics. We consider in a separate analysis a reaction scheme in which the cluster formation is second order in substrate S .

C.2 Kinetic equations for nonlinear model

The reaction scheme is described in Fig C.2. We have

$$\frac{d[S_N]}{dt} = k_{N-1}[S][S_{N-1}] - k_N[S_N]. \quad (\text{C.4})$$

and

$$\frac{d[S_n]}{dt} = k_{n-1}[S][S_{n-1}] - (k_{-(n-1)} + k_n[S])[S_n] + k_{-n}[S_{n+1}], \quad n = 2, \dots, (N-1). \quad (\text{C.5})$$

We us assume that all intermediate states are in equilibrium. This assumption implies that intermediate reactions are very fast. With this assumption we get

$$k_{(n-1)}[S][S_{(n-1)}] - k_{-(n-1)}[S_n] = 0, \quad n = 2, \dots, N-2, \quad (\text{C.6})$$

$$[S_n] = \frac{k_{n-1}}{k_{-(n-1)}}[S][S_{n-1}] = K_n[S][S_{n-1}], \quad n = 2, 3, \dots, N-2 \quad (\text{C.7})$$

where $K_n = k_n/k_{-n}$.

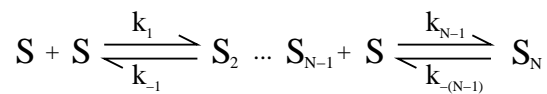


Figure C.2: Reaction scheme.

Using (C.7) and (C.8) we obtain

$$\frac{d[S_N]}{dt} = k_{clus.}[S]^N - k_N[S_N]. \quad (\text{C.8})$$

In another approximation we replace $[S_N]$ by $\sum_{n=2}^N S_n = P$ to get the equation.

Appendix D

Derivation of exclusion term from master equation

The diffusion and the exclusion terms in (3.1) and (3.2) from the master equation are derived in the following way. Let us discretize the continuous space into cells of size Δx and denote by $n_i \geq 0$ and $m_i \geq 0$ for all $i = 1, 2, \dots, N$ the number of S and P particles in the i -th cell. The configuration of the system can be described by the N-vectors $\mathbf{n} = (n_1, n_2, \dots, n_N)$ and $\mathbf{m} = (m_1, m_2, \dots, m_N)$. Let \mathbb{N} be the set of natural numbers, we define the operator $H_i^\pm : \mathbb{N}^N \rightarrow \mathbb{N}^N$ by

$$\begin{aligned} H_i^+(n_1, \dots, n_{i-1}, n_i, n_{i+1}, \dots, n_N) &= (n_1, \dots, n_{i-1}, n_i - 1, n_{i+1} + 1, \dots, n_N), \\ H_i^-(n_1, \dots, n_{i-1}, n_i, n_{i+1}, \dots, n_N) &= (n_1, \dots, n_{i-1} + 1, n_i - 1, n_{i+1}, \dots, n_N), \end{aligned} \tag{D.1}$$

for all $i = 1, 2, \dots, N$. Note that for $i = 1, N$ we use periodic boundary condition [126].

We define density dependent hopping rates $W_s^\pm(i)$ and $W_p^\pm(i)$ of a particle at the i th site for S and P respectively by

$$\begin{aligned} W_s^\pm(i) &= w_s(1 - \mu_s(m_{i\pm 1} - m_i)), \\ W_p^\pm(i) &= w_p(1 - \mu_p(n_{i\pm 1} - n_i)), \end{aligned} \tag{D.2}$$

where w_s, w_p, μ_s and μ_p are constants and the superscript \pm denotes hopping to the site $i \pm 1$. Here we note that a particle S (say) at cell i has lower hopping rate if the cell $i \pm 1$ contains more number of particles P than that in the cell i . Similarly for P this is exactly what should be happening when there is an effect of exclusion. Let $p(\mathbf{n}, \mathbf{m}, t)$ be the probability of finding the

system in the configuration \mathbf{n}, \mathbf{m} , at time t The master equation is given by [125, 126]

$$\begin{aligned} \partial_t p(\mathbf{n}, \mathbf{m}, t) = & \sum_{j=1}^N (n_j + 1) [W_s^-(j)p(H_{j-1}^+ \mathbf{n}, \mathbf{m}, t) + W_s^+(j)p(H_{j+1}^- \mathbf{n}, \mathbf{m}, t)] \\ & + (m_j + 1) [W_p^-(j)p(\mathbf{n}, H_{j-1}^+ \mathbf{m}, t) + W_p^+(j)p(\mathbf{n}, H_{j+1}^- \mathbf{m}, t)] \\ & - (n_j [W_s^-(j) + W_s^+(j)] + m_j [W_p^-(j) + W_p^+(j)]) p(\mathbf{n}, \mathbf{m}, t) \end{aligned} \quad (\text{D.3})$$

Let $S_i = \sum_{\Omega} n_i p(\mathbf{n}, \mathbf{m}, t)$ and $P_i = \sum_{\Omega} m_i p(\mathbf{n}, \mathbf{m}, t)$ where \sum_{Ω} represents sum over all configurations having $n_1, \dots, n_N, m_1, \dots, m_N$, be the mean number of particles in the i th cell. Let us assume that there are no correlation between particles so that we can write $\sum_{\Omega} n_i n_j p(\mathbf{n}, \mathbf{m}, t) = S_i S_j$, $\sum_{\Omega} m_i m_j p(\mathbf{n}, \mathbf{m}, t) = P_i P_j$ and $\sum_{\Omega} n_i m_j p(\mathbf{n}, \mathbf{m}, t) = S_i P_j$. Multiplying n_i through (D.3) and summing over all configurations we obtain

$$\begin{aligned} \partial_t S_i = & w_s (S_{i+1} + S_{i-1} - 2S_i) - w_s \mu_s [S_{i+1}(P_i - P_{i+1}) + S_{i-1}(P_i - P_{i-1}) \\ & - S_i(P_{i+1} + P_{i-1} - 2P_i)] \end{aligned} \quad (\text{D.4})$$

Now we can substitute $S_i = S(x, t)$, $P_i = P(x, t)$ and expand $S_{i\pm 1}$ and $P_{i\pm 1}$ in Taylor series

$$\begin{aligned} S_{i\pm 1} & \simeq S(x, t) \pm \Delta x \partial_x S(x, t) + \Delta x^2 \partial_x^2 S(x, t), \\ P_{i\pm 1} & \simeq P(x, t) \pm \Delta x \partial_x P(x, t) + \Delta x^2 \partial_x^2 P(x, t), \end{aligned} \quad (\text{D.5})$$

and ignoring $O(\Delta x^3)$ and higher order terms, we obtain from (D.4)

$$\begin{aligned} \partial_t S(x, t) = & w_s \Delta x^2 \partial_x^2 S(x, t) - w_s \mu_s \Delta x^2 [- (2\partial_x S(x, t) \partial_x P(x, t) \\ & + S(x, t) \partial_x^2 P(x, t)) - S(x, t) \partial_x^2 P(x, t)] \end{aligned} \quad (\text{D.6})$$

Now rearranging terms in (D.6) we obtain

$$\partial_t S(x, t) = D_s \partial_x^2 S(x, t) + \epsilon_s (\partial_x S(x, t) \partial_x P(x, t) + S(x, t) \partial_x^2 P(x, t)), \quad (\text{D.7})$$

where $D_s = w_s \Delta x^2$ and $\epsilon_s = 2w_s \mu_s \Delta x^2$. Similarly multiplying m_i through (D.3) and summing over all configurations we obtain the equation for $P(x, t)$. A point to note here is that $0 < \mu_{s,p} \ll 1$, and for simplicity we have taken $\epsilon_s = \epsilon_p = \epsilon$. Using expression (D.7), the general expression in arbitrary dimension can be written as

$$\partial_t S(\mathbf{x}, t) = \partial_{\mathbf{x}} [D_s \partial_{\mathbf{x}} S(\mathbf{x}, t) + \epsilon_s S(\mathbf{x}, t) \partial_{\mathbf{x}} P(\mathbf{x}, t)]. \quad (\text{D.8})$$

Appendix E

Monte Carlo Algorithm

E.1 Stochastic simulation algorithm based on Smoluchowski equation:

Let $\Omega \subset \mathbb{R}^2$ be the domain of computation. In our model the domain boundary is assumed as a circle of radius R . Inside the domain, let there be N_D reaction centers of radius a . The reaction centers are uniformly distributed with centers at $\mathbf{r}_1, \mathbf{r}_2, \dots, \mathbf{r}_{N_D}$. The reaction centers are given by the sets $\omega_j = \{\mathbf{r} \in \mathbb{R}^2 : |\mathbf{r} - \mathbf{r}_j| \leq a\}$ for all $j = 1, 2, \dots, N_D$. The setting is described in Fig. (E.1).

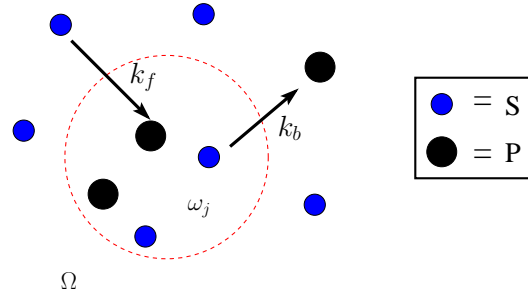


Figure E.1: Schematic diagram for the $S \rightleftharpoons P$ in Ω . The small blue filled circle denotes atoms S and the larger black filled circle denotes the cluster. The region enclosed inside the circle ω_j denotes the reaction center. The ratio a/R should be less than the minimum diffusion length.

Let $D^{(i)} \in \{D_s, D_p\}$ be the diffusion coefficient of the i th particle. Similarly depending on the current position of the particle it can undergo a reaction with reaction rate $k^{(i)} \in \{k_f, k_b\}$. Let $\xi(t)$ be a Gaussian random number with zero mean and unit variance. The algorithm we follow is described in Ref. [115, 126] for the case of homogeneous reaction-diffusion processes.

The stochastic simulation Algorithm:

1. If $t \leq T$ GOTO Step (2),
else GOTO Step (6).
2. Drop an adatom S at a random position \mathbf{r}_k , $k > 0$ inside the domain at every $kM\delta t$ time step.
The number M can be varied to obtain the desired flux i.e. $1/(\pi R^2 M \delta t)$ adatoms per unit time per unit area.
3. For each particle $i = 1, \dots, k$ compute the diffusive step
 $\mathbf{r}_{i,t+\delta t} = \mathbf{r}_{i,t} + \sqrt{2D^{(i)}\delta t} \xi(t)$.
4. For each particle $i = 1, \dots, k$ generate random no. ρ
if $\rho < 1 - \exp(-k^{(i)}\delta t)$ and $\mathbf{r}_{i,t+\delta t} \in \omega_j \forall 1 < j < N_D$
perform reaction step.
5. Increase time by δt
 $t \rightarrow t + \delta t$
GOTO Step (1)
6. STOP.

Note that for the computation of the first passage time probability distribution the adatom is dropped at the center of the domain as in Step (2). The particle undergoes the reaction-diffusion processes. When ever the particle reaches the domain boundary $|\mathbf{r}| = R$ the time t_k registered and program is terminated. This process is repeated a number of times.

Appendix F

Numerical Codes

Here we provide some of the computer programs that has been used in our calculations.

F.1 Numerical solution of the trapping problem

```
(*FINITE DIFFERENCE SOLUTION OF THE TRAPPING PROBLEM IN 1D*)
(*AUTHOR: TRILOCHAN BAGARTI, IOP, BHUBANESWAR, INDIA.*)
(*YEAR: 2012*)

(*
Parameters: (-Nl*h, Nl*h) domain of computation,
           κ = trapping rate,
           ε = strength of exclusion,
           defN = # of traps
           h = step size.
*)
Nl = 100; h = 0.1; κ = 0.1;
r1 = 1.0/h^2;
defN = 40;
Do[{X[i] = RandomInteger[{-Nl, Nl}] * h}, {i, 1, defN}];
σ = 0.5 h;
(*Reaction function; Gaussian is used for the Dirac delta functions*)
Kfunc[x_] := Sum[
$$\frac{1}{\sqrt{2\pi}\sigma} \text{Exp}\left[\frac{-(x - X[i])^2}{2\sigma^2}\right], \{i, 1, \text{defN}\}];$$

(*Module to solve the differential equation*)
DiffSolve[vare_, varT_] := Module[{ε = vare, T = varT},
  n = 1;
  ClearAll[eq];

  e1 = ε / (4 h^2);

  Do[{eq[n] = D[S[x, t], t] == r1 * (1.0 + ε S[x, t]) * (S[x + 1, t] + S[x - 1, t] - 2 S[x, t]) +
    e1 * (S[x + 1, t] - S[x - 1, t])^2 - κ * Kfunc[x * h] * S[x, t]; n = n + 1;}, {x, -Nl, Nl}];
```

```

(*Boundary conditions*)
eq[n] = S[Nl + 1, t] == S[Nl - 1, t]; n = n + 1;
eq[n] = S[-Nl - 1, t] == S[-Nl + 1, t]; n = n + 1;
(*Initial condition*)
Do[
$$\left\{ \text{eq}[n] = S[x, 0.0] = \frac{1}{\sqrt{2\pi}\sigma} \text{Exp}\left[\frac{-x^2}{2\sigma^2}\right] + 0.00000001; n = n + 1; \right\}, \{x, -Nl, Nl\}];$$

pde = Table[eq[m], {m, 1, n - 1}];

sol = Table[S[x, t], {x, -Nl - 1, Nl + 1}];
pdsol = NDSolve[pde, sol, {t, 0.0, T}];

(*ClearAll[ex];*)
T = 20.0; Nk = 100;
Do[
  Do[{
    Do[{X[i] = RandomInteger[{-Nl, Nl}] * h}, {i, 1, defN}];
    Do[If[X[i] == X[j] && i ≠ j, X[j] = RandomInteger[{-Nl, Nl}] * h], {i, 1, defN}, {j, 1, defN}];
    DiffSolve[0.0, T];
    ex[k, m] = Evaluate[sol /. pdsol /. t → m T / 10];
    If[Mod[k, 50] == 0, Print["ENSB=", k, " T =", m T / 10]]
  }, {m, 1, 1}]
, {k, 1, Nk}]

ClearAll[t];
T = 2.0;
Do[{X[i] = RandomInteger[{-Nl, Nl}] * h}, {i, 1, defN}];
Do[If[X[i] == X[j] && i ≠ j, X[j] = RandomInteger[{-Nl, Nl}] * h], {i, 1, defN}, {j, 1, defN}];
DiffSolve[0.0, T];
ex1 = Evaluate[sol /. pdsol /. t → T];

gauss[x_, t_] := 
$$\frac{1}{\sqrt{4\pi t}} \text{Exp}\left[\frac{-x^2}{4t}\right];$$

anylU[x_, t_] := 
$$\frac{1}{\sqrt{4\pi t}} \text{Exp}\left[\frac{-x^2}{4t}\right] - \frac{\kappa}{4} \text{Sum}\left[\text{Exp}\left[\left(\text{Abs}[x - X[i]] + \text{Abs}[X[i]]\right) \kappa / 2 + \kappa^2 t / 4\right]\right.$$


$$\left. \text{Erfc}\left[\frac{\text{Abs}[x - X[i]] + \text{Abs}[X[i]]}{2\sqrt{t}} + \frac{\kappa\sqrt{t}}{2}\right], \{i, 1, \text{defN}\}\right];$$

tb = Table[anylU[x * h, T], {x, -Nl, Nl}];
gtb = Table[gauss[x * h, T], {x, -Nl, Nl}];
p1 = ListLinePlot[tb, Frame → True,
  DataRange → {-Nl * h, Nl * h}, Axes → None, PlotStyle → Red, PlotRange → All];
p2 = ListLinePlot[ex1[[1]], Frame → True, DataRange → {-Nl * h, Nl * h},
  Axes → None, PlotStyle → Black, PlotRange → All];
p3 = ListLinePlot[gtb, Frame → True, DataRange → {-Nl * h, Nl * h},
  Axes → None, PlotStyle → Blue, PlotRange → All];
Show[p1, p2, p3]

```

F.2 Numerical solution of the ring defect model

```
(*PROGRAM: CALCULATION OF CONCENTRATION S, P FOR RING DEFECT CASE*)
(*AUTHOR: TRILOCHAN BAGARTI, INST. OF PHYS. BHUBANESWAR, INDIA*)
(*DATE: JUN 26 2010*)
nPointDef = 4; (*# of defect*)
rndPts = {0.1, 0.3, 0.6, 0.7}; (* position of defects*)

Do[r[i] = rndPts[[i]], {i, 1, nPointDef}];
(*Green's functions*)
Gs0[r_, rp_, s_] := If[r < rp, BesselI[0, Sqrt[s/Ds] r] BesselK[0, Sqrt[s/Ds] rp] / (2 Pi),
  BesselI[0, Sqrt[s/Ds] rp] BesselK[0, Sqrt[s/Ds] r] / (2 Pi)];
Gp0[r_, rp_, s_] := If[r < rp, BesselI[0, Sqrt[s/Dp] r] BesselK[0, Sqrt[s/Dp] rp] / (2 Pi),
  BesselI[0, Sqrt[s/Dp] rp] BesselK[0, Sqrt[s/Dp] r] / (2 Pi)];
Gs1[r_, rp_, s_] := If[r < rp, (BesselI[0, Sqrt[s/Ds] r] BesselK[0, Sqrt[s/Ds] rp] - BesselI[0,
  Sqrt[s/Ds] r] BesselI[0, Sqrt[s/Ds] rp] BesselK[0, Sqrt[s/Ds] R] / BesselI[0, Sqrt[s/Ds] R]) /
  (2 Pi), (BesselI[0, Sqrt[s/Ds] rp] BesselK[0, Sqrt[s/Ds] r] - BesselI[0, Sqrt[s/Ds] r]
  BesselI[0, Sqrt[s/Ds] rp] BesselK[0, Sqrt[s/Ds] R] / BesselI[0, Sqrt[s/Ds] R]) / (2 Pi)];
Q[r_, s_] :=  $\left(\frac{2 \text{ Pi}}{\text{Ds}}\right) \text{NIntegrate}\left[\text{Gs1}[r, rp, s] \frac{\text{Exp}[-\lambda rp] rp}{s}, \{rp, 10^{(-6)}, R\}\right];$ 

f[r0_, s0_] := Module[{sVar = s0, rVar = r0},
  Do[{GS1[i, j] = Gs1[r[i], r[j], sVar]; GP0[i, j] = Gp0[r[i], r[j], sVar];},
    {i, 1, nPointDef}, {j, 1, nPointDef}];

  matGS1 = Table[Table[GS1[i, j], {j, 1, nPointDef}], {i, 1, nPointDef}];
  matGP0 = Table[Table[GP0[i, j], {j, 1, nPointDef}], {i, 1, nPointDef}];

  invGP0 = Inverse[IdentityMatrix[nPointDef] + (kp/Dp) matGP0];
  mat = IdentityMatrix[nPointDef] + (kf/Ds) matGS1 - kap matGS1.invGP0.matGP0;

  Qf = Table[Q[r[i], sVar], {i, 1, nPointDef}];
  PHI = Inverse[mat].Qf;
  PSI = (kf/Dp) * invGP0.matGP0.PHI;
  y = {Q[rVar, sVar] +
    Sum[GS1[rVar, r[kk], sVar] * (-kf * PHI[[kk]] + kp * PSI[[kk]]) / Ds, {kk, 1, nPointDef}},
    Sum[Gp0[rVar, r[kk], sVar] * (kf * PHI[[kk]] - kp * PSI[[kk]]) / Dp, {kk, 1, nPointDef}]];
];
Ds = 0.1; (*Diffusion constant of S*)
Dp = 0.01; (*Diffusion constant of P*)
kf = 1.0; (* Forward reaction rate*)
kp = 0.1; (*Backward reaction rate*)
kap = kf * kp / (Ds * Dp);
R = 1;
λ = 1.0;
```

```

(*Talbot method*)
Mu = 50;
t = 1.0;

Do[{
  rho = 2*Mu / (5*t);
  rc = xc;
  If[rc == 0, rc = 10^-6];
  f[rc, rho];
  sum1 = 0.5*y[[1]] * Exp[rho*t];
  sum2 = 0.5*y[[2]] * Exp[rho*t];
  Do[{
    theta = k*Pi / Mu;
    sf[k] = rho*theta * (Cot[theta] + i);
    sigma[k] = theta + (theta*Cot[theta] - 1) * Cot[theta];
    f[rc, sf[k]];
    sum1 = sum1 + Re[Exp[sf[k]*t] * y[[1]] * (1 + i*sigma[k])];
    sum2 = sum2 + Re[Exp[sf[k]*t] * y[[2]] * (1 + i*sigma[k])];}, {k, 1, Mu - 1}];

  sum1 = sum1 * rho / Mu;
  sum2 = sum2 * rho / Mu;
  phi[xc] = Chop[sum1];
  psi[xc] = Chop[sum2];
  Print[N[xc], " ", Chop[sum1], " ", Chop[sum2]];}, {xc, 0, 1, 1/20}]
(*****)

```

F.3 Numerical solution of the point defect model

```
(*PROGRAM : CALCULATION OF CONCENTRATIONS S,P FOR THE POINT DEFECT CASE*)
(*AUTHOR : TRILLOCHAN BAGARTI, INST. OF PHYS. BHUBANESWAR, INDIA*)
(*DATE : DEC 14 2010 *)
(*)
nPointDef = # of point defects, rndPts = pos vec of defect, Ds, Dp = diffusion const of S, P,
kf,kb= forward, backward reaction rates, bessOrd = highest order Bessel func used in the series,
R = radius of domain, lambda = input flux strength, Gs1,Gp0 = Green's functions
*)
nPointDef = 8;
rndPts = {{0.5, 0.4}, {0.3, 0.1}, {-0.7, -0.4},
          {0.1, 0.4}, {-0.5, 0.6}, {-0.4, 0.0}, {0.0, -0.3}, {0.4, -0.3}};
(*Position of random reaction centers*)

Do[{r[i] = Norm[rndPts[[i]]], th[i] = ArcTan[rndPts[[i]][[1]], rndPts[[i]][[2]]]},
  {i, 1, nPointDef}]
Ds = 1.0;
Dp = 0.1;
kf = 1.0;
kp = 0.1;
kap = kf * kp / (Ds * Dp);
bessOrd = 10;
R = 1;
lambda = 1.0;
g[n_, r_, rp_, s_] := If[r < rp, BesselI[n, r Sqrt[s/Ds]] BesselK[n, rp Sqrt[s/Ds]],
  BesselI[n, rp Sqrt[s/Ds]] BesselK[n, r Sqrt[s/Ds]]
];
h[n_, r_, rp_, s_] := If[r < rp, BesselI[n, r Sqrt[s/Dp]] BesselK[n, rp Sqrt[s/Dp]],
  BesselI[n, rp Sqrt[s/Dp]] BesselK[n, r Sqrt[s/Dp]]
];
e[0] = 1;
Do[e[m] = 2, {m, 1, bessOrd}];
Gs1[r_, th_, rp_, thp_, s_] := Sum[e[m]
  (g[m, r, rp, s] - g[m, r, R, s] g[m, R, rp, s] / g[m, R, R, s]) Cos[m (th - thp)], {m, 0, bessOrd}];
Gp0[r_, th_, rp_, thp_, s_] := Sum[e[m] h[m, r, rp, s] Cos[m (th - thp)], {m, 0, bessOrd}];

q[r_, s_] := 2 Pi * NIntegrate[
  (g[0, r, rp, s] - (g[0, r, R, s] g[0, R, rp, s]) / g[0, R, R, s]) Exp[-lambda * rp] rp, {rp, 10^-5, R}] / (s Ds);

(*j0=1
  module f[r,theta,s] calculates phi(r,theta,s) and psi(r,theta,s) for each (r,theta,s), the
  values are return by the variable y
*)
f[r0_, th0_, s0_] :=
Module[{sVar = s0, rVar = r0, thVar = th0}, Do[{Gs1[i, j] = Gs1[r[i], th[i], r[j], th[j], sVar];
  Gp0[i, j] = Gp0[r[i], th[i], r[j], th[j], sVar];}, {i, 1, nPointDef}, {j, 1, nPointDef}];
matGS1 = Table[Table[GS1[i, j], {j, 1, nPointDef}], {i, 1, nPointDef}];
matGP0 = Table[Table[GP0[i, j], {j, 1, nPointDef}], {i, 1, nPointDef}];
invGP0 = Inverse[IdentityMatrix[nPointDef] + (kp/Dp) matGP0];
mat = IdentityMatrix[nPointDef] + (kf/Ds) matGS1 - kap matGS1.invGP0.matGP0;
Qf = Table[q[r[i], sVar], {i, 1, nPointDef}];
PHI = Inverse[mat].Qf;
PSI = (kf/Dp) * invGP0.matGP0.PHI;
y =
  (q[rVar, sVar] + Sum[Gs1[rVar, thVar, r[kk], th[kk], sVar] * (-kf * PHI[[kk]] + kp * PSI[[kk]]) / Ds,
    {kk, 1, nPointDef}), Sum[Gp0[rVar, thVar, r[kk], th[kk], sVar] *
    (kf * PHI[[kk]] - kp * PSI[[kk]]) / Dp, {kk, 1, nPointDef}]]];
```

```

Mu = 20;
t = 0.5;
(*
Numerical evaluation of Inverse Laplace transformation
by fixed Talbot method
*)
Do[{
  rho = 2*Mu / (5*t);
  rc = Sqrt[xc^2 + yc^2];
  If[xc == 0, xc = xc + Sign[xc] * 10^-6];
  thc = N[ArcTan[xc, yc]];
  f[rc, thc, rho];
  sum1 = 0.5*y[[1]] * Exp[rho*t];
  sum2 = 0.5*y[[2]] * Exp[rho*t];
  Do[{
    theta = k*Pi / Mu;
    sf[k] = rho*theta * (Cot[theta] + i);
    sigma[k] = theta + (theta*Cot[theta] - 1) * Cot[theta];
    f[rc, thc, sf[k]];
    sum1 = sum1 + Re[Exp[sf[k]*t] * y[[1]] * (1 + i*sigma[k])];
    sum2 = sum2 + Re[Exp[sf[k]*t] * y[[2]] * (1 + i*sigma[k])];}, {k, 1, Mu - 1}];

  sum1 = sum1 * rho / Mu;
  sum2 = sum2 * rho / Mu;
  phi[xc, yc] = Chop[sum1];
  psi[xc, yc] = Chop[sum2];
  (*tmp=PrintTemporary[{Chop[xc],Chop[yc],Chop[sum1],Chop[sum2]}];
  Pause[1];
  NotebookDelete[tmp];*)
  Print[{Chop[xc], Chop[yc], Chop[sum1], Chop[sum2]}];
}, {xc, -1.0, 1.0, 0.1}, {yc, -1.0, 1.0, 0.1}];

(*****

```

Bibliography

- [1] K. Brunner, Rep. Prog. Phys. **65**, 27 (2002).
- [2] D. Petrovykh and F. Himpsel, Self-assembled nanostructures at silicon surfaces, in *Encyclopedia of Nanoscience and Nanotechnology*, edited by H. Nalwa, volume 9, page 497, American Scientific Publishers, California, 2004.
- [3] B. Voigtlander, M. Kawamura, and V. C. N. Paul, J. Phys.: Cond. Mat. **16**, 31535 (2004).
- [4] A. Hirai and K. M. Itoh, Physica E **23**, 248 (2004).
- [5] H. Omi and T. Ogino, Thin Solid Films **369**, 88 (2000).
- [6] A. Sgarlata, P. Szkutnik, A. Balzarotti, and F. R. N. Motta, Appl. Phys. Lett. **83**, 4002 (2003).
- [7] H. J. Kim, Z. M. Zhao, and Y. H. Xie, Phys. Rev. B **68**, 205312 (2003).
- [8] Y. Xie, S. Samavedam, M. Bulsara, T. Langdo, and E. Fitzgerald, Appl. Phys. Lett. **71**, 3567 (1997).
- [9] H. Kim, J. Chang, and Y. Xie, J. Cryst. Growth **247**, 251 (2003).
- [10] A. Das, J. Kamila, B. Dev, B. Sundaravel, and G. Kuri, Appl. Phys. Lett. **77**, 951 (2000).
- [11] T. Schmidt et al., Phys. Rev. Lett. **98**, 066104 (2007).
- [12] T. Schmidt et al., New J. Phys. **7**, 193 (2005).
- [13] A. Roy, T. Bagarti, K. Bhattacharjee, K. Kundu, and B. N. Dev, Surf. Sc. **606**, 777 (2012).
- [14] M. C. Cross and P. C. Hohenberg, Rev. Mod. Phys. **65**, 851 (1993).

- [15] A. Turing, *Phil. Trans. R. Soc. Lond. B* **237**, 37 (1952).
- [16] S. Havlin and D. ben Avraham, *Adv. Phys.* **36**, 695 (1987).
- [17] H. Taitelbaum and Z. Koza, *Physica A* **285**, 166 (2000).
- [18] P. K. Datta and A. M. Jayannavar, *Pramana-J. Phys.* **38**, 257 (1992).
- [19] P. Grassberger and I. Procaccia, *J. Chem. Phys.* **77**, 6281 (1982).
- [20] T. M. Nieuwenhuizen and H. Brand, *J. Stat. Phys.* **59**, 53 (1990).
- [21] G. Abramson and H. S. Wio, *Chaos Soliton and Fract.* **6**, 1 (1995).
- [22] C. Mandache and D. ben Avraham, *J. Chem. Phys.* **112**, 7735 (2000).
- [23] H. Taitelbaum, R. Kopelman, G. H. Weiss, and S. Havlin, *Phys. Rev. A* **41**, 3116 (1990).
- [24] R. Kopelman, *J. Stat. Phys.* **42**, 185 (1986).
- [25] J. C. Rasaiah, J. B. Hubbard, R. J. Rubin, and S. H. Lee, *J. Phys. Chem.* **94**, 652 (1990).
- [26] A. Missel and K. A. Dahem, *Phys. Rev. E* **79**, 021126 (2009).
- [27] M. Vald, D. Rothman, and J. Ross, *Physica D* **239**, 739 (2010).
- [28] J. P. Bouchaud and A. Georges, *Phys. Rep.* **195**, 127 (1990).
- [29] P. M. Morse and H. Feshbach, *Methods of Theoretical Physics, Part I*, McGraw-Hill, 1953.
- [30] E. Economou, *Green's Functions in Quantum Physics*, third ed., Springer, Berlin Heidelberg, 2006.
- [31] W. Rudin, *Functional Analysis*, Tata Mc Graw-Hill, 1973.
- [32] J. Abate and P. Valko, *Int. J. Numerical Meth. Engng.* **60**, 979 (2004).
- [33] N. Kumar and W. Horsthemke, *Phys. Rev. E* **83**, 036105 (2011).
- [34] N. Kumar and V. M. Kenkre, *PNAS* **105**, 18752 (2008).
- [35] K. Yagi, H. Minoda, and M. Degawa, *Surf. Sci. Rep.* **43**, 45 (2001).

- [36] B. Voigtlander, A. Zinner, T. Weber, and H. Bonzel, *Phys. Rev. B* **51**, 7583 (1995).
- [37] H. Omi and T. Ogino, *Thin Solid Films* **369**, 88 (2000).
- [38] T. Ogino et al., *Acc. Chem. Res.* **32**, 447 (1999).
- [39] Y. Xie, S. Samavedam, M. Bulsara, T. Langdo, and E. Fitzgerald, *Appl. Phys. Lett.* **71**, 3567 (1997).
- [40] H. Kim, J. Chang, and Y. Xie, *J. Cryst. Growth* **247**, 251 (2003).
- [41] A. Das, J. Kamila, B. Dev, B. Sundaravel, and G. Kuri, *Appl. Phys. Lett.* **77**, 951 (2000).
- [42] T. Schmidt et al., *New J. Phys.* **7**, 193 (2005).
- [43] E. Bauer and J. van der Merwe, *Phys. Rev. B* **33**, 3657 (1986).
- [44] Aspects of self-assembled nanostructures grown by molecular beam epitaxy on pristine ion-beam modified and oxidized silicon surface, 2011, The experimental work was carried out by the group of Prof. B.N. Dev. of IACS, Kolkata. The experimental work in Ref. [13] is a part of the thesis of Dr. A. Roy.
- [45] G. Fisanick, H. Gossmann, and P. Kuo, *Res. Soc. Symp. Proc.* **102**, 25 (1988).
- [46] Y.-W. Mo, J. Kleiner, M. Webb, and M. Lagally, *Surf. Sci.* **268**, 275 (1992).
- [47] R. Becker, J. Golovchenko, G. Higashi, and B. Swartzentruber, *Phys. Rev. Lett.* **57**, 1020 (1986).
- [48] M. Hadley and S. Tear, *Surf. Sci. Lett.* **247**, L221 (1991).
- [49] Q. Gu et al., *Surf. Sci.* **327**, 241 (1995).
- [50] J. Demuth, R. Hamers, R. Tromp, and M. Welland, *J. Vac. Sci. Technol. A* **3**, 1320 (1986).
- [51] H. Yang, J. Gao, Y. Zhao, Z. Xue, and S. Pang, *Surf. Sci.* **406**, 229 (1998).
- [52] M. Hoshino, Y. Shigeta, K. Ogawa, and Y. Homma, *Surf. Sci.* **365**, 29 (1996).
- [53] H. Tanaka et al., *Ultramicroscopy* **42-44**, 864 (1994).

- [54] T. Berghaus, A. Brodde, H. Neddermeyer, and S. Tosch, *Surf. Sci.* **193**, 235 (1988).
- [55] K. Bhattacharjee et al., *J. Nanosci. Nanotechnol.* .
- [56] U. Kohler, O. Jusko, G. Pietsch, B. Mueller, and M. Henzler, *Surf. Sc.* **248**, 321 (1991).
- [57] S. Teys, A. Talochkin, and B. Olshanetsky, *J. Crys. Growth* **311**, 3898 (2009).
- [58] Y. Homma, H. Hibino, and N. Aizawa, *Surf. Sci.* **324**, L333 (1995).
- [59] E. L. Koschmieder, *Bénard Cells and Taylor Vortices*, Cambridge University Press, Cambridge, England, 1993.
- [60] H. wen Xi and J. D. Gunton, *Phys. Rev. E* **47**, R2987 (1993).
- [61] M. Assenheimer and V. Steinberg, *Phys. Rev. Lett.* **70**, 3888 (1993).
- [62] M. Assenheimer and V. Steinberg, *Nature* **367**, 345 (1994).
- [63] H. Tennekes and J. L. Lumley, *A first course in turbulence*, MIT Press, 1972.
- [64] J. S. langer, *Rev. Mod. Phys.* **52**, 1 (1980).
- [65] T. A. Witten and L. M. Sander, *Phys. Rev. Lett.* **47**, 1400 (1981).
- [66] M. Matsushita, M. S. Y. Hayakawa, H. Honjo, and Y. Sawada, *Phys. Rev. Lett.* **53**, 286 (1984).
- [67] R. M. Brady and R. C. Ball, *Nature* **309**, 225 (1984).
- [68] E. Ben-Jacob et al., *Phys. Rev. Lett.* **55**, 1315 (1985).
- [69] J. Nittmann, G. Daccord, and H. E. Stanley, *Nature* **314**, 141 (1985).
- [70] M. Matsushita and H. Fujikawa, *Physica A* **168**, 498 (1990).
- [71] W. W. Mullin and R. F. Sekerka, *J. Appl. Phys.* **34**, 323 (1963).
- [72] T. A. Witten and L. M. Sander, *Phys. Rev. B* **27**, 5686 (1983).
- [73] T. Vicsek, *Phys. Rev. Lett.* **52**, 2281 (1984).
- [74] A. Gierer and H. Meinhardt, *Kybernetik* **12**, 30 (1972).

- [75] J. D. Murray, *Mathematical Biology II: Spatial Models and Biomedical Applications*, 3rd ed., Springer, 2004.
- [76] R. Satnoianu, M. Menzinger, and P. Maini, *J. Math. Biol.* **41**, 493 (2000).
- [77] J. E. Pearson and W. Horsthemke, *J. Chem. Phys.* **90**, 1588 (1989).
- [78] V. Ambegaokar, B. I. Halperin, and J. S. Langer, *Phys. Rev. B*, **4**, 2612 (1971).
- [79] J. Haus and K. Kehr, *Phys. Rep.* **150**, 263 (1987).
- [80] R. A. Guyer, *Phys. Rev. E* **29**, 2751 (1984).
- [81] J. Bernasconi, S. Alexander, and R. Orbach, *Phys. Rev. Lett.* **41**, 185 (1978).
- [82] M. Sahimi, B. D. Huges, L. E. Scriven, and H. T. Davis, *J. Chem. Phys.* **78**, 6849 (1983).
- [83] S. Alexander, J. Bernasconi, W. R. Schneider, and R. Orbach, *Rev. Mod. Phys.* **53**, 175 (1981).
- [84] G. H. Weiss and S. Havlin, *Physica A* **134**, 474 (1986).
- [85] R. C. Ball and B. Huberman, *J. Phys. A* **20**, 4995 (1987).
- [86] S. Alexander, *Phys. Rev. B* **23**, 2951 (1981).
- [87] K. Kundu, D. Izzo, and P. Phillips, *J. Chem. Phys.* **88**, 2692 (1988).
- [88] K. Kundu, P. E. Parris, and P. Phillips, *Phys. Rev. B* **35**, 3468 (1987).
- [89] K. Kundu and P. Phillips, *Phys. Rev. A* **35**, 857 (1987).
- [90] J. Machta, *Phys. Rev. B*, **24**, 5260 (1981).
- [91] D. S. Novikov, E. Fieremans, J. H. Jensen, and J. A. Helpert, *Nature Physics* **7**, 508 (2011).
- [92] D. ben Avraham, S. Redner, and Z. Cheng, *J. Stat. Phys.* **56**, 437 (1987).
- [93] M. V. Smoluchowski, *Phys. Z.* **17**, 557 (1916).
- [94] G. H. Weiss, R. Kopelman, and S. Havlin, *Phys. Rev. A* **39**, 446 (1989).

- [95] M. Bixon and R. Zwanzig, *J. Chem. Phys.* **75**, 2345 (1981).
- [96] B. Y. Balagurov and V. G. Vaks, *Sov. Phys. JETP* **38**, 968 (1974).
- [97] M. D. Donsker and S. R. S. Varadhan, *Commun. Pure Appl. Math.* **32**, 721 (1979).
- [98] M. Bramson and J. L. Lebowitz, *Phys. Rev. Lett.* **61**, 2397 (1988).
- [99] M. Bramson and J. L. Lebowitz, *J. Stat. Phys.* **62**, 297 (1991).
- [100] A. J. Bray and J. Bray, *Phys. Rev. Lett.* **89**, 150601 (2002).
- [101] R. A. Blythe and J. Bray, *Phys. Rev. E* **67**, 041101 (2003).
- [102] S. B. Yuste, G. Oshanin, K. Lindenberg, O. Bnichou, and J. Klafter, *Phys. Rev. E* **78**, 021105 (2008).
- [103] R. Borrego, E. Abad, and S. B. Yuste, *Phys. Rev. E* **80**, 061121 (2009).
- [104] P. M. Chaikin and T. C. Lubensky, *Principles of condensed matter physics*, first ed., Cambridge University Press, Cambridge, 1998.
- [105] T. Ala-Nissila, R. Ferrando, and S. C. Ying, *Adv. Phys.* **51**, 949 (2002).
- [106] F. Oberhettinger and L. Badii, *Table of Laplace Transform*, Springer-Verlag, Berlin Heidelberg, 1973.
- [107] I. S. Gradshteyn and I. M. Ryzhik, *Tables of Integrals, Series, and Products*, 6th ed., Academic Press, San Diego, CA, 2000.
- [108] S. Redner, *A guide to first-passage processes*, Cambridge University Press, Cambridge, 2001.
- [109] T. Ogino et al., *Acc. Chem. Res.* **32**, 447 (1999).
- [110] T. Schmidt et al., *Phys. Rev. Lett.* **98**, 066104 (2007).
- [111] T. Bagarti, A. Roy, K. Kundu, and B. N. Dev, *Proceeding of Third National Conference on Mathematical Techniques Emerging Paradigms for Electronics and IT Industries*, University of Delhi, New Delhi, pp. ts (Jan 30-31, 2010).

- [112] T. Bagarti, A. Roy, K. Kundu, and B. N. Dev, *AIP Advances* **2**, 042101 (2012).
- [113] M. Abramowitz and I. Stegun, *Handbook of Mathematical Functions*, Dover Publications Inc., New York, 1972.
- [114] H. Carslaw and J. Jaeger, *Conduction of Heat in Solids*, second ed., Oxford University Press, New York, 1959.
- [115] S. S. Andrews and D. Bray, *Phys. Biol.* **1**, 137 (2004).
- [116] A. E. Fernando, K. A. Landman, and M. J. Simpson, *Phys. Rev. E* **81**, 011903 (2010).
- [117] S. Kwon and Y. Kim, *Phys. Rev. E* **84**, 041103 (2011).
- [118] M. Küntz and P. Lavallée, *J. Phys. D: Appl. Phys.* **36**, 1135 (2003).
- [119] M. Küntz and P. Lavallée, *J. Phys. D: Appl. Phys.* **37**, L5 (2004).
- [120] T. D. Frank, *Phys. Lett. A* **305**, 150 (2002).
- [121] T. D. Frank, *Nonlinear FokkerPlanck Equations*, Springer, Berlin, 2005.
- [122] L. Borland, *Phys. Rev. E* **57**, 6634 (1998).
- [123] L. Borland, F. Pennini, A. R. Plastino, and A. Plastino, *Eur. Phys. J. B* **12**, 285 (1999).
- [124] S. Martinez, R. A. Plastino, and A. Plastino, *Physica A* **259**, 183 (1998).
- [125] N. G. van Kampen, *Stochastic Processes in Physics and Chemistry*, first ed., North-Holland, Amsterdam, 1981.
- [126] R. Erban, S. J. Chapman, and P. Maini, A practical guide to stochastic simulations of reaction-diffusion processes, 2007, available as <http://arxiv.org/abs/0704.1908>.
- [127] A. H. Nayfeh, *Perturbation Methods*, John Wiley & Sons Inc, New York, 1973.
- [128] A length L is introduced which defines the domain of integration which is taken much larger than the diffusion length. Neumann boundary condition at the boundaries will not affect the short time solution.
- [129] W. F. Ames, *Numerical Methods for Partial Differential Equations*, second ed., Academic Press Inc., New York, 1977.

[130] P. Meakin, *Phys. Rev. Lett.* **51**, 1119 (1983).

[131] F. B. Hildebrand, *Methods of Applied Mathematics*, second ed., Prentice-Hall, New Jersey, 1965.